2019年度

博士学位論文

ハダカイワシDiaphus watasei における発光器の反射組織に関する研究：カウンターイルミネーション効果を発揮するその機能形態学的特性について

Reflector in body photophores of lanternfish *Diaphus watasei*: functional structure and ecological role for successful counterillumination

Supervised by:

大場裕一

長谷川浩一

武井史郎

中部大学

大学院 応用生物学研究科 応用生物学専攻

José Paitio

Declaration of authorship

I hereby declare the content of this thesis from my entirely authorship, all references identified, adequately and clearly cited. No plagiarism of any kind is present in the published manuscripts of any means, neither digital nor handwritten of any academic studies.

Quem não é para elas, não se mete nelas

Portuguese traditional saying

Who is not up to it, do not go for it

Abstract

AIM: Bioluminescent mesopelagic fishes have pigmented filters on ventral body photophores to match downwelling sunlight at these depths and generally migrate to shallower waters to feed at night. Lanternfishes photophores have exceptional colourless lenses and specular blue-green reflector. Reflector has an unique "honeycomb-like" pattern of hexagon iridophores composed by guanine-like platelets.

The aim of this thesis was to analyse the reflector in lanternfish *Diaphus watasei* and explain the mechanisms to project a successful counterillumination.

METHODS: Iridophores platelets were observed under light microscope for morphological analyses. Reflector shape was estimated from histological sections. Extracts of photophores purified luciferase was mixed in a spectrometer with commercial coelenterazine to determine the reaction spectra. Reflection spectra of fresh fishes photophore reflectors was measured under light microscope linked to a spectrometer. Osmoregulation modulation on defrosted photophores was investigated submerging photophores on hypertonic, isotonic and hypotonic solutions.

RESULTS: Regular hexagonal shape of iridophores on body photophores was found to be statistically different ($p < 0.01$, n=50) from all other reflective tissues. Approximated quadratic curves (R^2=0.95 - 1.00) and eccentricity close to 1 (e= 0.98 – 1.02) revealed a parabola-like shape of reflector with focus points on photocytes. *Diaphus* luciferin-luciferase reaction was found to emit λmax= 454 nm. Reflector spectra of fresh photophores revealed variation between 460 – 470 nm. On defrosted photophores, reflection spectra is isotonic media (499 – 532 nm) were found to be modified to shorter wavelengths on hypertonic media (479 – 483 nm).

DISCUSSION: Unique regular hexagon allows simultaneous light reflection from all iridophores on the same angle while minimizing gaps and, consequently, light losses. Parabola-like shape of reflector with focus point located on photocytes ensures all the light from photogenic cells is reflected ventrally. Angle of light emission from body photophores in *D. watasei* matches the vertical angle of downwelling light on mesopelagic depths. Reflector alters luciferin-luciferase reaction spectra to match downwelling sunlight (Paitio *et al.,* 2019). Iridophores are tunable by osmoregulation suggesting reflectors to match light spectra during vertical migrations from dusk to dawn. (Paitio *et al.*, in preparation). In summary, it was found that that *Diaphus* body photophores achieve successful counterillumination by matching the angle of downwelling light and adapt spectra during vertical migrations.

Acknowledgements

I would like to start by thanking to all my supervisors for all the teaching, advising and friendship support that made possible this adventure.

First, to 大場裕一先生 for accepting me as his student, believing in my potential and tireless providing all the academic and personal guidance even before the first day I arrived in Japan. For all, between a supervisor and an "adoptive father", there is no words to express my gratitude. To 武井史郎先生 for accepting being my supervisor, for all his kind support and teaching of new methodologies crucial to achieve the results of this thesis. To 長谷川浩一先生 for accepting me as a student and his essential help in the application for the enrolment of the doctoral graduation program in 中部大学 and all his kind support since my arrival. To 宗宮先生 for the acceptance as supervisor and supporting my first year of doctoral research before his retirement. To Professor Meyer-Rochow for all his fundamental help and support since the reply to my e-mail that would become the starting point of coming to Japan to study. To 岩坂正和先生 (広島大学), 浅田裕法先生 (山口大学) and all the team members of JST CREST for all the support and collaboration on a research field completely unknown to me a couple of years ago. To 遠藤広光先生 (高知大学), 吉岡伸也先生 (東京理科大学), 伊**澤和義先生** (中部大学), 大塚攻先生(広島大学), for their collaboration and expertise knowledge that allowed the methodological achievements for this work.

I would not be able to came all this way without all my previous professors and colleagues that taught me and guided me, a big thanks for all of them. To my colleagues and friends in 中部大学 and the rest of Japan for their support and friendship since the first day I arrived in here, namely, 蟹江さん, 別所さん, 内藤さん, 金さん, 小西さん, 矢野さん.

Last but definitely not least, thanks to all my friends back in Portugal for all the friendship and support, always. Above all, thanks to my family, the three most important persons on my life, without all their love and support nothing of this would be possible.

Table of contents

List of figures

Chapter 1

Chapter 2

Chapter 3

Chapter 4

Chapter 5

Chapter 6

Chapter 7

Supplements

List of tables

Supplements

List of abbreviations

λmax	Wavelength maximum
A	Anterior
Ant	Antorbital organ
AS	Artifact space from detachment of photophore from supportive connective tissue
Av	Average
Ba	Bottom area
BP	Body photophores
BP.L	Lateral body photophore
BP.V	Ventral body photophore
BP.R	Inner reflector of body photophore
Br	Branchiostegal organ
BSE	Backscattered electrons
CCD	Charge-coupled device
CL	Cartilage lens
CoPL	Primary collagen layer
CoSL	Secondary collagen layer
Cp	Cup
CT	Connective tissue
D	Dorsal
Dn	Dorsonasal organ
DS	*Diaphus* sp.
DVMs	Diel vertical migrations

DW	*Diaphus watasei*
E	Eye
Ea	Emission area;
EMa	Emission-median area
EPa	Emission-peripheral area
Es	Emission side
FTIR	Fourier-transform infrared spectroscopy
HP	Head photophores
HP.R	Inner reflector of head photophore
Hyper	Hypertonic
I	Iris
IA	Inter-tissue artifact space between cup and reflector
Ir	Iridophore
IS	Inter-tissue space between cup and inner reflector
ISp	Inter-tissue space between photocytes and inner reflector
Iso	Isotonic
L	Lateral
Lat	Latitude
Le	Lens
LI	Light intensity
LL	Luciferin-luciferase reaction
~~LO~~	Fibre optic light source off
LO	Fibre optic light source on
Long	Longitude

LR	Lens reflector
LRa	Lens reflector area
LRs	Lens reflector side
L/W	Length/width
Max	Maximum
Me	Melanophores
Min	Minimum
MO	Microscope objective
N	North
No	Nostril
n.a.	Not applicable
n.d.	No data
P	Photocytes
PB	Phosphate buffer
PL	Pigment layer
Pl	Platelet
PO	Pectoral organ
P-Pl	Photocytes-Platelet angle
P-RS	Photocytes- inner reflector surface angle
PVO	Subpectoral organ
R	Inner reflector
Rep	Replicate
R.IA	Illuminated central area of the inner reflector (spectra analyses on Chapter 5 and epi-illumination experiment on Chapter 6)

R.ISA) Sampling area illuminated on the inner reflector (spectra analyses in different areas of middle transversal plane of the organ on experiment at 50º light source on Chapter 6)

RLUs Relative light units

RS Inner reflector surface angle

RS-Pl Inner reflector surface-platelet angle

S Septum

S.D. Standard deviation

SA Sampling area (inner structure analyses on Chapters 2 and 6)

SA.P Sample point (analyses of parabolic quadratic function on Chapter 4)

SAO Supranal organ

Se Spectrometer sensor

Sk skin

SL Standard length

SLe Scale lens

SLe.N.BP Scale lens area not covering the photophore

SO Stereo microscope objective

SP F Spectrometry tests flat photophore angle

SP M Spectrometry tests maximum photophore angle

Sp Inter-platelet artifact space

Sub Subsample

T Tapetum lucidum

TEM Transmission Electron Microscopy

UV Ultraviolet

V Ventral

VL Ventral-lateral

VLO	Supraventral organ
Vn	Ventronasal organ
VO	Ventral organ
W	West
Wl	Wavelength
XRD	X-ray diffraction

CHAPTER 1

General introduction

1. Mesopelagic zone

a. General characteristics

The ocean is the largest habitat on earth, with an average depth of 3700 m and representing more than 90 % of the volume of biosphere [1]. Deep –sea, considered from 200 m depth down, occupies almost 95 % of the ocean's volume [1, 2]. According to physical and biological features [1, 2], water column of the ocean can be classified into several depth zones [3]. Epipelagic extends from the water surface down to 200 m depth in which sunlight intensity is adequate for photosynthesis (photic zone) [1, 2] (Fig. 1). Below, lays the mesopelagic from 200 to 1000 m, where light reaches with enough intensity for the fauna be able to distinguish diurnal and nocturnal cycles but insufficient to support photosynthesis (dysphotic or twilight zone) [2, 4]. From 1000 m down to 4000 m is the bathypelagic zone, the largest and most deserted habitat on earth, where food and mates are scarce and no sunlight penetrates and the only light source is bioluminescence (aphotic zone) [1, 3].

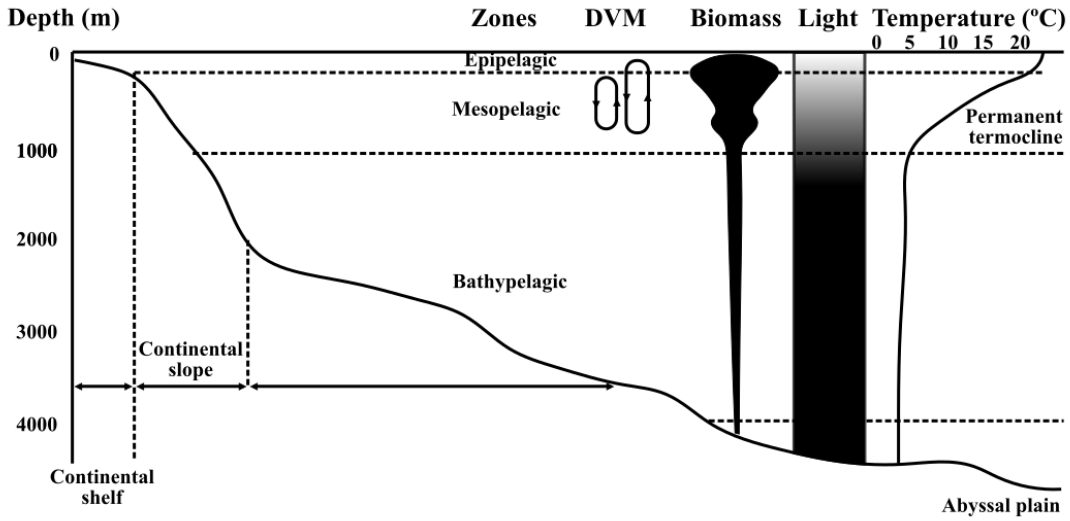

Figure 1 - Schematic illustration of ocean zones and respective biological, biochemical and physical parameters. Adapted from [1]. DVM= Diel vertical migrations

Mesopelagic zone is characterized by very particular environmental conditions, due to gradients in physical and biochemical parameters [4]. Dim light, cold waters with oxygen minimum levels, reduced turbulence, increased hydrostatic pressure, high inorganic nutrient concentration and irregular food supply are the main environmental features the mesopelagic [5, 6]. Such specific environment influences the fauna distribution inhabiting at these depths, holding the greatest biodiversity and biomass in the ocean, mainly in the upper mesopelagic, down to 600 – 700 m depths [3]. It is here where the majority of diel migrant species inhabit, with reflective sides for camouflage, where animals are dark with lower body reflectivity in the

lower mesopelagic, adapted camouflage to the lower light intensity [1–3]. DVMs are a major part of the mesopelagic dynamics [1, 7] and performed by a community mainly composed by crustaceans, cephalopods, siphonophores and fishes [7–11]. Migrants are triggered by sensitivity to sunlight following isolumes [12], ascend to surface waters at dusk where they feed at night and returning back to mesopelagic depths at night, avoiding visual predators [2, 4, 13]. Due to the exchanges of organic and inorganic matter during DVMs, mesopelagic zone to contribute to the biogeochemical fluxes of energy, nutrients, carbon, nitrogen, phosphorous and oxygen in the [4, 7, 14, 15].

b. Light parameters and deep-sea vision

On the water surface at the epipelagic zone, sunlight with longer wavelengths than 580 nm is absorbed and scattered by water molecules to less than 1% on the first 10 m, and shorter wavelengths than 500 nm scattered by phytoplankton and particulates and absorbed Bywater and chlorophyll [16]. Downwelling sunlight reaching the mesopelagic zone is limited to a narrow wavelengths of blue-green 430 – 530 nm [17, 18] with λmax= 472 – 486 nm [17], and highly directional on a vertical angle [3, 16, 19] (Fig. 2). Upper mesopelagic is essentially illuminated by downwelling light and its incidence on objects creates extended light scenes while the major light source on the dimmer lower mesopelagic is bioluminescence, representing a light scene with point source [3, 20, 21]. Adaptations of fish vision for one or both light scenes depends on ecological drivers, environment (change nature of visual scenes) and species-specific ecological traits (natural histories) [3]. Deep-sea fishes can perceive dim downwelling sunlight down to 1150 m depth [22] and detect bioluminescence signals at long distances [3, 23] (Fig. 3). These fishes have eyes with high visual sensitivity by developed numerous adaptations: large eyes and pupils with aphakic gaps [3]; tapetum lucidum [24]; pure-rod retina [25, 26]; high density of large photoreceptor cells [22, 25]; high photoreceptor – ganglion cell convergence ratio [27]; large sized retinal photoreceptor outer segments [25, 28]; and high concentration of rhodopsin [26, 28].

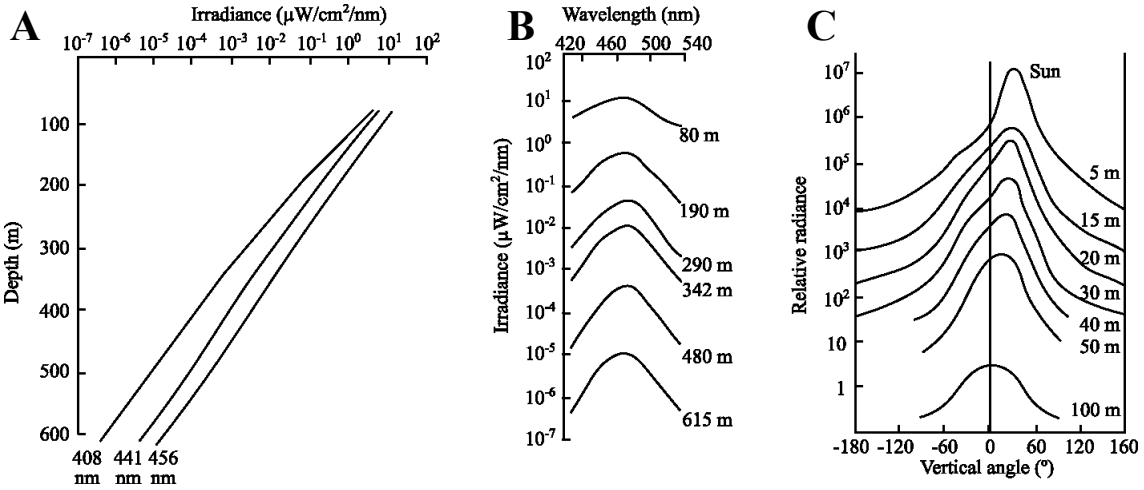

Figure 2 – Sunlight variation with depth on sea water. A) Irradiance at 408, 441 and 456 nm down to 600 m depth at deep-waters of Southeast Tenerife in the Canaries Archipelago. B) Wavelength per irradiance up to 615 m depth at deep-waters of Southeast Tenerife in the Canaries Archipelago. C) Radiance in vertical plane of the sun up to 100 m in the Baltic Sea. (A-B) adapted from [17] and (C) from [19].

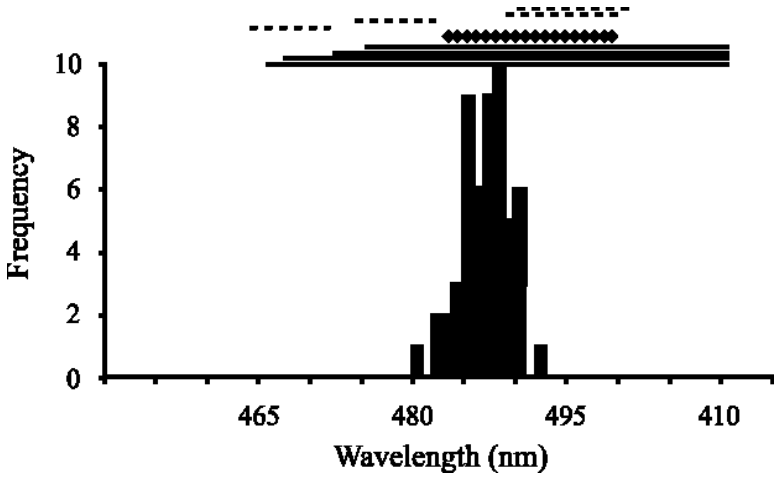

Figure 3 – Visualization of downwelling sunlight and bioluminescence on lanternfishes. Histogram represents the distribution of λmax of rhodopsin. Solid horizontal bars represent the range of the most sensitive visual pigments to bioluminescence, λmax= 450 – 510 nm at a threshold of 10 photons s^{-1}, for four water types, bottom to top: Sargasso, Mediterranean, Antarctic and Celtic Sea. Dashed lines represent the range of most sensitive visual pigments for visualization of downwelling sunlight on depths between 200 – 1000 m., for four water types, from left to right: Sargasso, Mediterranean, Antarctic and Celtic Sea. Lozenge represents the range of most sensitive visual pigments for the visualisation of lanternfish bioluminescence. Adapted from [29].

2. Bioluminescence in deep-sea fishes

Diurnal animals display colourful patterns for visual communication, but in deep-sea where sunlight is almost absent, organisms found another way to produce such displays by emitting their own light. Bioluminescence is the production of light by living organisms *via* an oxidative chemical reaction which consists, generally, in substrate – luciferin -, an enzyme – luciferase –

and a cofactor – oxygen [30]. Luciferins vary among the tree of marine life [31], coelenterazine seems to have widespread use among deep-sea fishes [32] (Fig. 4A). Coelenterazine was reported in Stomiiformes, Myctophiformes and Platytroctidae [33, 34] and it is not used by luminous sharks for whom luciferin remains unknown [35]. In luminous fishes, *Cypridina* luciferin is reported to be obtained from maternal transference in midshipman fish *Porichthys* [36] similar case suggested for coelenterazine in deep-sea fishes [32, 37]. Additionally to its widespread occurrence in mid-water fishes, there are no records of luminous fishes to be able to synthesize coelenterazine, which together with this being the most abundant substance in tissues of the digestive tract of these fishes suggests dietary acquisition [32, 34] as reported in midshipman *Porichthys* from ostracods *Cypridina* luciferin [36, 38].

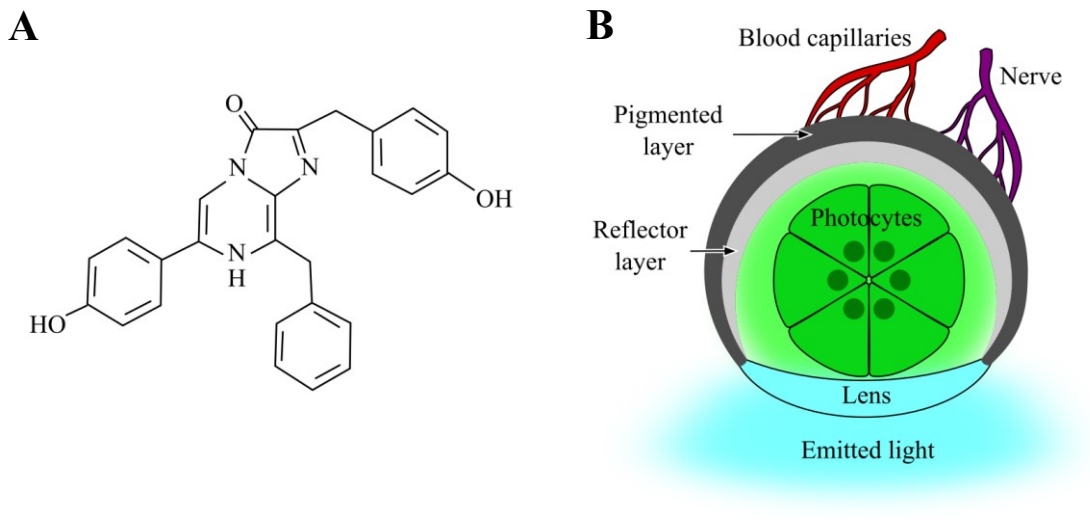

Figure 4 – Intrinsic bioluminescence of marine animals. A) Molecular structure of coelenterazine. B) Schematic illustration of the general structure of photophores on bioluminescent animals. (A) adapted from [30, 31].

Except symbiotic luminous fishes with light organs containing cultures of bioluminescent bacteria, the majority of deep-sea luminous fishes generate their own light (intrinsic bioluminescence) from bioluminescent cells – photocytes - in specific light organs – photophores [39]. Despite photophores exhibit high level of shapes, sizes and complexity between deep-sea fishes, basic structure is shared for all luminous organs [40] (Fig. 4B). Photocytes are grouped in the central photogenic tissue with an external pigmented filter and lens, inner covered by a reflector enclosed in a pigment layer of melanophores [39, 41–43]. Blood capillaries and nerves commonly penetrate the photophore [39, 40] allowing precise modulation of light signals by neural control, reported in sharks, lanternfishes, stomiiformes, alepocephalids and scopelarchids [44–48].

Bioluminescence in the deep-sea realm evolved into a high variety of luminous signals for specific ecological roles, turning out to be even multifunctional for some animals emitting

different light signals [49] and/or different photophores [50]. Bioluminescent signal is characterized by intensity spectral peaks, temporal and spatial light output [51]. Ecological purposes of bioluminescence in mesopelagic fishes can be classified into three main basic roles: interspecific, to attract prey and as a protection from predators; and intraspecific, for reproduction or recognition; and 3. illumination of the surroundings [49, 50, 52]. More than 90% of the organisms in the mesopelagic are bioluminescent [2, 50, 53], greatest majority sharing the most widespread and characteristic ecological role of bioluminescence in the mesopelagic: counterillumination [3, 40, 50, 53]. Moreover, the mesopelagic zone has been suggested as the major realm of bioluminescence in the planet, not just in terms of species diversity and abundance but even the remarkable complexity of photophores [50]. This unusual high level of luminous biodiversity is primarily related to the specific light parameters at these depths [50, 54]. Here, no visual obstacles can be found and only reached by dim sunlight, which allows bioluminescent signals to be seen at long distance [50, 54]. Uniformity of downwelling light penetrating on limited vertical angle and narrow wavelength range [3, 16, 54], explains why so many species inhabit here developed bioluminescent camouflage [16, 54].

3. Lanternfishes

c. Taxonomy and general ecology

Myctophids, or lanternfishes, are deep-sea fishes from the family Myctophidae, which includes 252 species in 33 genera [55], distributed by 10 monophyletic tribes in the two sub-families Myctophinae and Lampanyctinae [56] (Fig. 5). Lanternfishes have highly abundant populations and are distributed in all oceans [6], being the most widespread family of mid-water fishes in the world [57]. They represent more than 20% of the oceanic ichthyofaunal [6] and 50% of all larvae collected in plankton tows [57]. Moreover, 75% of total global catch of small mesopelagic fishes and are used for seasoning, aquaculture food, surimi or cosmetic oils [58]. These fishes inhabit both the upper and lower mesopelagic [2, 6] but development occurs essentially in the epipelagic zone, as reproduction, metamorphosis and feeding [57, 59, 60]. Lanternfishes are dioecious pelagic spanners and females are oviparous with low fecundity rate [61, 62]. Eggs are planktonic and so are daytime feeders pre-metamorphic larvae [6, 63]. During metamorphosis, larvae start performing ontogenic vertical migrations and migrate from epipelagic to mesopelagic depths where they inhabit as adults [64, 65]. Lanternfishes have rapid growth and high mortality rates, with early sexual maturity early and reaching 4 to 35 cm as adults on a life span of 1 to 5 years, measuring [66–68].

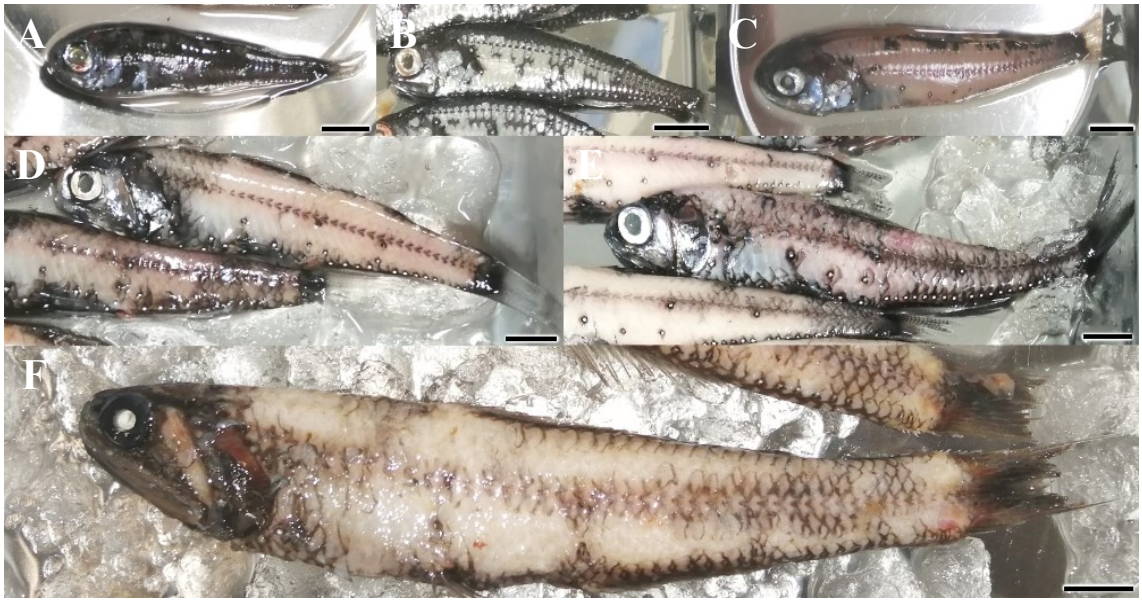

Figure 5 – Photographies of examples of lanternfish species, collected on a vessel of the National Research Institute of Fisheries Science of Japan (中央水産研究所) in North-eastern Japan waters: A) *Hygophum reinhardtii*; B) *Myctophum asperum*; C) *Symbolophorus evermanni*; D) *Diaphus gigas*; E) *S. japonicus*; F) *Notoscopelaus japonicus.* Scale bars: 1 cm.

Myctophids are opportunistic feeders [69], eating mainly zooplanktivorous, namely copepods, euphausiids, amphipods, ostracods, molluscs, chaetognaths, polychaetes, larvaceans and larvae of bivalve and fishes [70–72]. *D. watasei* is a particular cases such as *C. warmingii*, feeding on squids and fish larvae, including lanternfishes due to its the larger body and, consequentially jaw size, comparing to other lanternfishes [69]. These fishes are visually oriented predators and the maximum prey size is determined by the size of the jaw, swallowing whole preys [69, 73, 74]. Generally, lanternfishes are cyclic feeders, performing diel vertical migrations (DVMs) and feeding in shallow waters at night [69]. As part of the mesopelagic community of vertical migrants, ascend to shallow waters at dusk and returning to mesopelagic at dawn [13, 75–77]. Patterns and distances of vary per species which can be divided into: 1. Surface migrants, reaching ocean surface at night; 2. Midwater migrants, ascending to shallower depths at night but not reaching the surface; C. Semi-migrants, only part of the population migrates; D. Passive-migrants, upper limit of distribution expands for shallower waters at night; and E. Non-migrants [75] (Fig. 6). Contrary to other DVM patterns, surface and midwater migrant lanternfish species have a clear day-night habitat separation. Myctophids have a key-role in energetic cycles of marine food web, linking the zooplanktonic primary producers and higher predators, such as marine mammals, seabirds and cephalopods [78, 79] and by performing DVMs, represent a huge energy transfer from shallow waters to deeper oceanic levels [6, 80].

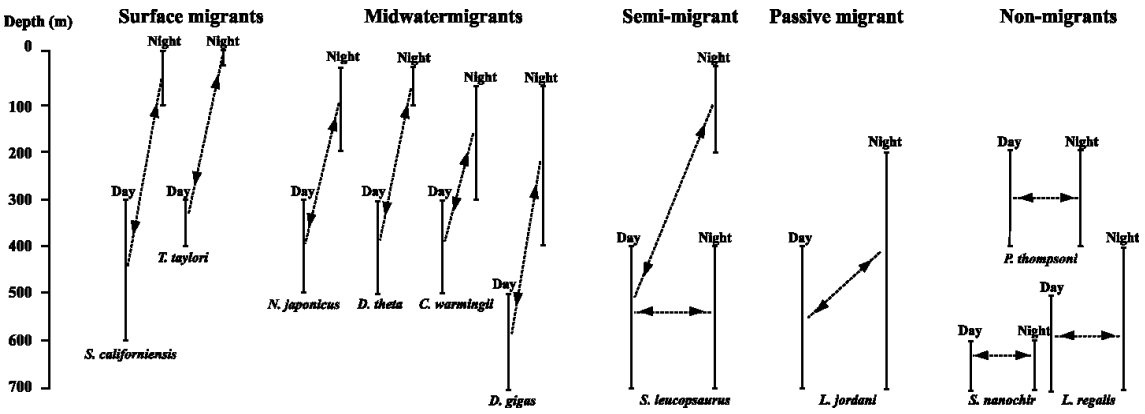

Figure 6 – Illustrative diagram of diel vertical migration patterns between lanternfish species *Symboplophorus californiensis, Tarletonbeania taylori, Notoscopelus japonicus, Diaphus theta, D. gigas, Ceratoscopelaus warmingii, Stenobrachius leucopsaurus, S. nannochir, Protomyctophum thompsoni* and *Lampanyctus regalis*, in North-western Pacific waters. Solid lines represent the range of depths inhabited at day or night. Dashed lines represent the migration distances. Adapted from [75].

a. Visual ecology and bioluminescence

As typical in mesopelagic fishes that live in an environment with extended scene of dim light of downwelling light with light point-sources of bioluminescence [3, 20], lanternfishes have high sensitive eyes adapted for scotopic vision of both light sources [29, 74]. During larval metamorphosis, eyes of deep-sea fishes change shape, size structure and location [81–84], namely substituting pure-cones retinas into pure-rod ones, as reported in lanternfishes [81], to acquire higher visual sensitivity adapted to the mesopelagic light ambient [3, 17, 19]. Simultaneously, photophores develop and becoming functional during metamorphosis as well [39, 40, 84], for counterillumination while migrate to deeper waters [39, 85] during ontogenic migrations [85, 86]. Development of photophores during ontogenic migration from epipelagic larvae to the mesopelagic adult form highlight the importance of counterillumination at mesopelagic depths.

Myctophidae family is 119 million years old and its species-specific bioluminescence arose at 89 million as suggested as a driver to the high species diversity in comparison to other bioluminescent fishes [55]. This is also indicated by the taxonomical value of the position of photophores and photophores groups [63, 87] (Fig. 7).

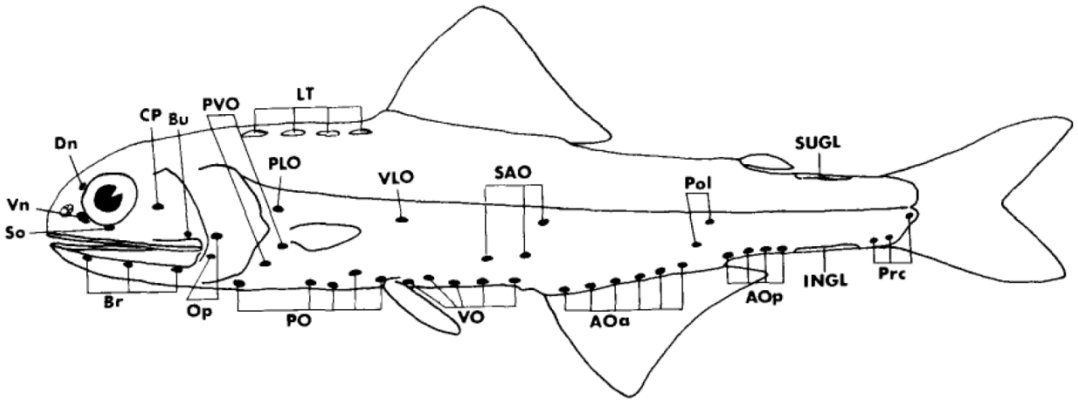

Figure 7 – Illustration showing generic location of photophores in lanternfishes and respective group acronyms. Organs in each group are numbered towards the tail. Adapted from [88].

Coelenterazine is reported as substrate used on bioluminescent reaction of lanternfishes [34, 37, 89, 90]. Photophores of myctophids are under neural control [91–95] allowing a precise regulation and fast regulation of light signals [96] for multifunctional purposes (Fig. 8).

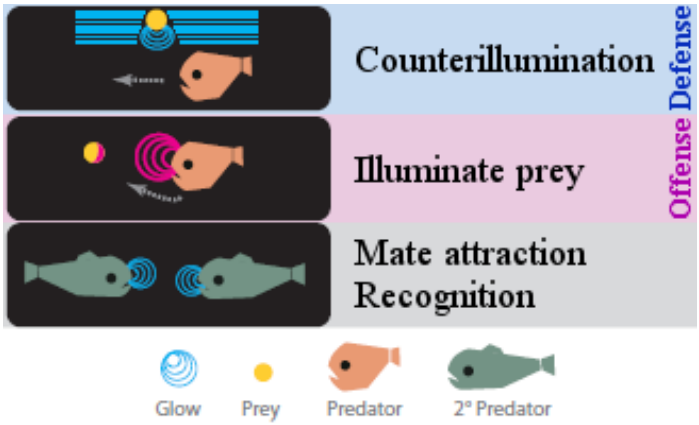

Figure 8 – Illustration of ecological roles of bioluminescence in lanternfishes, except illumination of surroundings. Adapted from [49].

Head photophores of lanternfishes emit bright and rapid flashes [96, 97] have been suggested to roles for illumination [49] and sexual communication for the sexual dimorphic Vn [39, 96], as for caudal organs present in some genera [96, 98]. Ventral photophores have lower number of photocytes and emit steady, constant and lower intensity of light [96] in ventral direction [99, 100] with wavelength λmax= 469 – 476 [101, 102], matching the vertical angle [19] and spectra λmax= 472 – 486 nm [17] of downwelling light in the mesopelagic zone for an adequate counterillumination [16, 18, 40, 103]. Inner structure of head and body photophores was reported in various species of lanternfishes (Fig. 9). General structure is similar to other deep-sea fishes with intrinsic bioluminescence [39, 42, 43, 104, 105], photocytes surrounded by connective tissue covered by an exterior lens, inner reflector and pigment layer [87, 91, 96, 97, 106–109]. Ventral photophores have an additional accessory lens between the photocytes and

the lens which is a modified scale [63, 87, 91, 97]. Scale-lens is proposed to modulate the spectra of light emitted by photocytes and direct light ventrally by dioptric features for counterillumination [106, 108]. Ventral photophores have an uncommon blue-green inner reflector which is suggested to have a spectral modulation function as well [18, 90]. Additionally, species-specific pattern of lateral photophores are proposed to emit light for species recognition [55, 63, 87, 110].

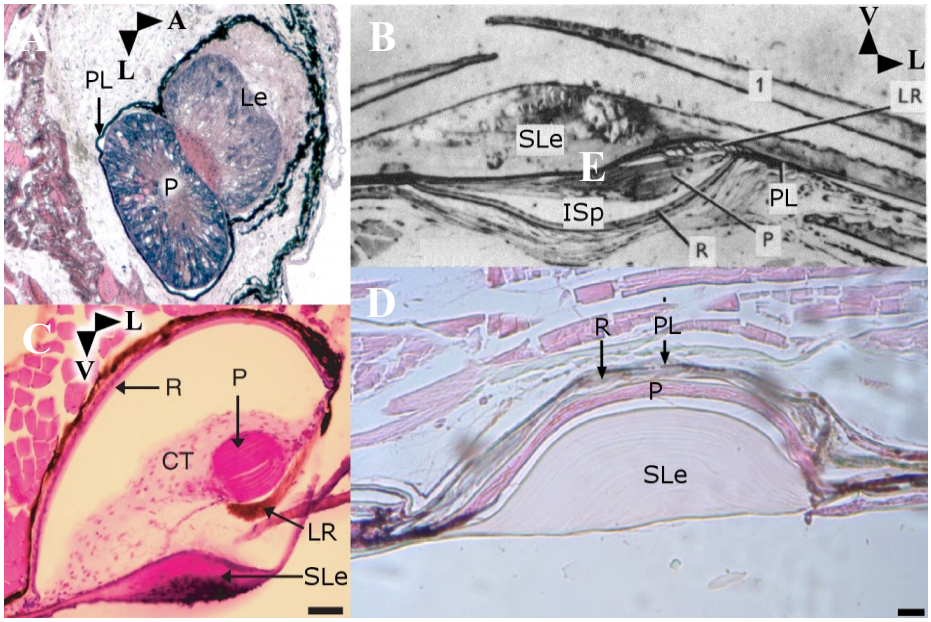

Figure 9 – Photographies of cross sections under light microscopy of lanternfishes photophores inner structure. A) Sagittal section of head photophore on *D. holti*. Transversal sections of ventral photophores on B) *Tarletonbeania crenularis*, C) *Electrona risso*, and D) *Ceratoscopelus maderensis*. PL= Pigment layer; P= Photocytes; Le= Lens; SLe= Scale lens; ISp= Inter-tissue space between photocytes and inner reflector; R= Inner reflector; LR= Lens reflector; CT= Connective tissue; A= Anterior; L= Lateral; V= Ventral. Scale bars= 50 µm. Scale for (A-B) is not presented on the publications. Orientation for (D) same as (C). Adapted from: A) [107]; B) [108]; C) [91]; and D) [106].

4. Aims of the thesis

Main aim of this study is to examine the functional structure of the inner reflector on ventral photophores of lanternfishes and its role on the achievement of adequate counterillumination in the mesopelagic zone, where these fishes inhabit. Additionally, other accessory tissues and its optic functions for light emission on ventral and lateral organs, comparing with head photophores to better understand how structural specifications of photophores are adapted to multifunctional bioluminescent ecological roles in myctophids. Using *Diaphus watasei* as a model, multidisciplinary approach of spectrometry, morphology and ultrastructure is used in this thesis to allow a biophysical approach of the reflector functional structure on modulation of spectra and angle of light emission of lanternfish photophores.

CHAPTER 2

Photophores structure and ecological roles of bioluminescence

1. Introduction

Myctophidae have characteristic head and body photophores, pattern of which are species-specific and has been one of the main basis for taxonomic diagnoses of the family [88]. All photophores occur in pairs, symmetrical to the sagittal body plane of the fish, excluding caudal photophores [87], which lack in some genera such as *Diaphus*[111]. Body photophores are distributed mainly on the ventral surface of the fish body but a few lateral photophores are observed [87].

General structure of photophores does not vary on the same fish or between genera, photogenic tissue covered by an external lens and inner reflector enclosed in a pigmented layer of melanophores [91, 96, 97, 106, 107, 112]. Nevertheless, a few disparities are reported between ventral and head photophores. Head organs have higher number of photocytes [96, 107], while ventral photophores have modified scales as lenses [63, 87, 106, 108], accessory lateral lens reflectors [97] and a blue-green inner reflector [18, 90]. Dioptric and spectral modulation of the emitted light are suggested for scale lenses [106, 108], as suggested for lenses on light organs of other luminous fishes [113]. Lateral lens reflector is proposed to act as a "light-shield", avoiding it to be emitted on the lateral side of the photophore [87]. Coloured inner was suggested to alter the light spectra from photocytes to closer wavelengths of the mesopelagic ambient light for counterillumination [18]. While this coloured reflector is uniquely reported in lanternfishes among luminous fishes, similar structures are present in the photophores of euphausiids [42, 114] and squids [115, 116]. Reflectors on photophores of lanternfishes are assumed to be composed of iridophores with guanine crystals[117], such reported in other mesopelagic fishes, hatchetfish *Agryropelecus* [118] and pearleye fish *Maurolicus* [119].

Head and ventral photophores are suggested to have very different bioluminescent purposes. Both types of photophores are reported to be under neural control [91–95] which allow accurate regulation of light signals for specific bioluminescent purposes [96, 99]. Bright and rapid flashes were reported in Dn head photophores of *Diaphus* [97], similarly to caudal organs of other lanternfish genera [94, 96, 98, 112]. Sexually dimorphic Vn head photophores on *Diaphus* [39] are suggested to have sexual communication role such as on caudal photophores in other myctophids [96, 98]. Similar inner structure of photogenic tissue between caudal and head photophores supports this hypothesis [96, 97]. High intensity light emissions of head photophores on *Diaphus* are proposed to be used as torches to illuminate the surroundings and prey [49]. Lower photocytes number on ventral photophores is related with the lower intensity, continuous and steady of its bioluminescence, compared to head photophores [96]. Together with observed ventral light emissions [99, 100], ventral photophores emit light to

adequately match the dim and vertical downwelling light on mesopelagic depths [3, 103, 120, 121] for successful counterillumination [40].

The aim of this chapter is to relate the inner structural variation of head and body photophores to the hypothesized ecological roles of bioluminescence. Using histology to examine the inner structure of photophores, morphometry for the main tissues that have potential to modulate the light emissions (scale lens and inner reflector of body photophores) and spectrometry of light transmission by the lenses (head and body photophores), it will be analysed the inner structure of organs and tissues to modulate light emissions for specific bioluminescent purposes.

2. Materials and methods

a. Sampling and tissues treatment

Fishes were collected by pelagic trawling in commercial vessels, kept on ice while returning to land. Samples were collected in Kōchi Prefecture (高知県) at Kōchi city, Mimase fishery port (高知市御畳瀬支所); Muroto city, Shiina (室戸市椎名支所) and Takaoka (室戸市高岡支所) fishery ports, Japan (Fig. 10). Two species of *Diaphus* myctophids were collected (Fig. 11), *D. watasei* in 高知市御畳瀬支所 and *D. chrysorhynchus* in 室戸市高岡支所 and 室戸市椎名支所 (see Chapters 5 and 7, respectively). Fishes were kept in closed cooler boxes with laminated ice until reaching the Marine Biology Laboratory of Kōchi University (高知大学海洋生物学研究室). Specimens of *D. watasei* for histology were collected on 21.11.2017 and for lens spectrometry on 20.04.2018. At the laboratory, scale lenses from ventral body photophores of three specimens of *D. watasei* were detached from the body with the aid of forceps and kept in 1M Phosphate buffer (PB, pH 7.4) with 1 g/L of sodium azide at 4ºC. Full body of three specimens for head photophores spectrometry were deep frozen in acetone with dry ice, kept in dry ice until reaching the Luminous Organisms Laboratory of Chubu University (中部大学研究室) where were kept frozen at -80ºC. Full body of 3 specimens for histology were submersed in Bouin's fixative for 3 days at room temperature until reaching the Luminous Organisms Laboratory of Chubu University, where were washed 3 times in 1M PB and kept at 4ºC in the same buffer, with 1 g/L of sodium azide to avoid fungus growth in long-term stocked samples.

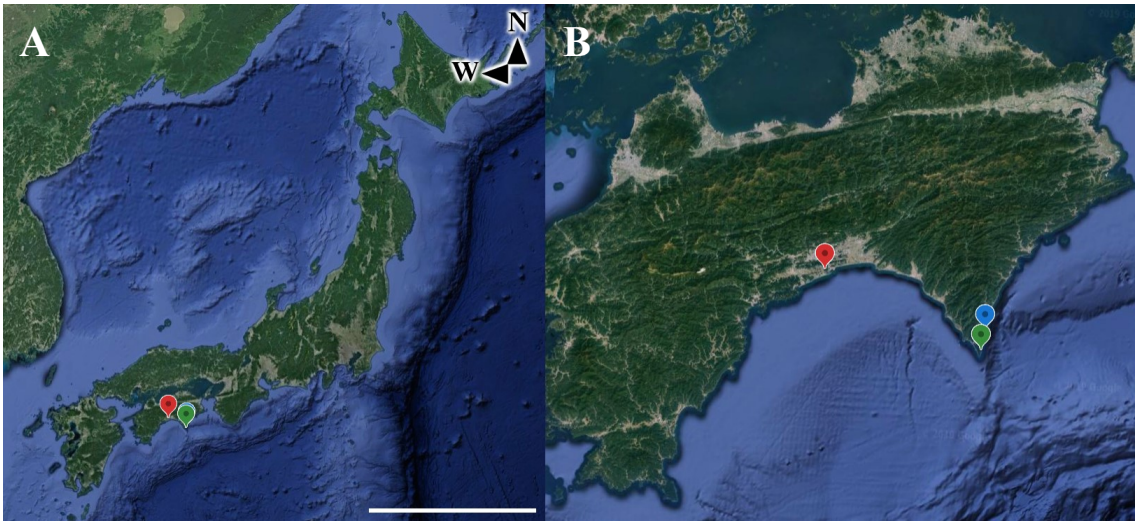

Figure 10 - Maps showing the geographic location of sampling sites. A) Mainland Japan 内地 (北海道, 本種, 球種 and 四国), except Okinawa (沖縄). B) Island of Shikoku (四国).高知市御畳瀬支所 in red (Lat: 33º30'16"N, Long: 133º33'25"E); 室戸市椎名支所 in blue (Lat: 33º19'39"N: Long:134º11'49"E); and 高岡支所 in green (Lat: 33º15'42"N, Long:134º11'03"E). Geographic coordinates between parentheses: Lat= Latitude; Long= Longitude; N=North; W= West. Scale bar= 500 km. Adapted from Google© 2019 (data by TerraMetrics).

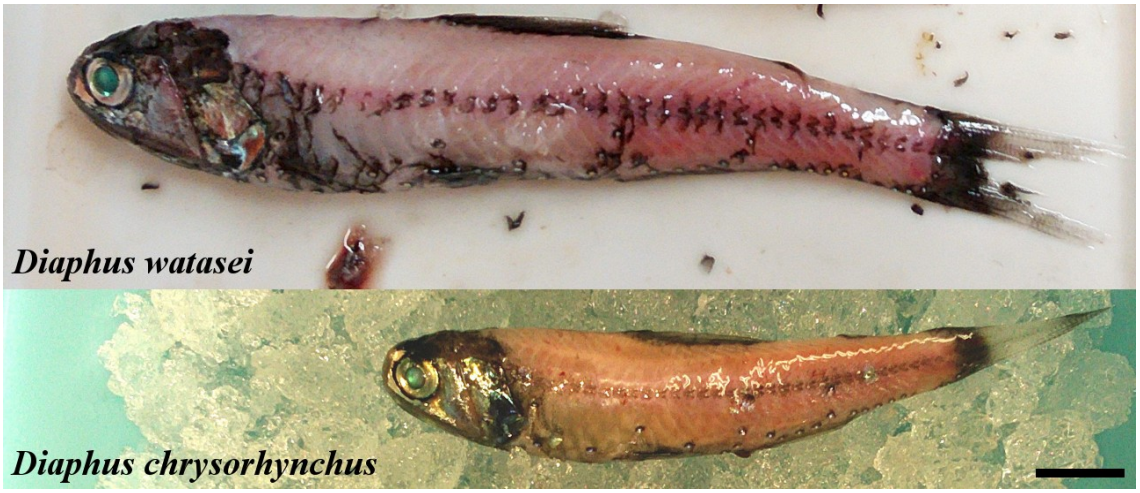

Figure 11 - Photographies on lateral view of sampled *Diaphus* species sampled in Kōchi Prefecture. Scale bar= 1 cm.

b. Histological sections

Being the first approach to relate morphology of photophores and the respective ecological role of bioluminescence in lanternfishes using *D. watasei* as model, methodology is described using detail level adequate to be reproduced in future studies. For terminology purposes on grouping photophores by bioluminescence purpose, "head photophores" is used to include the cranial non-counterillumination photophores (Ant, Dn, Vn) and "body photophores" for branchiostegal and photophores actually located on the organ of the body, although the branchiostegal

photophores are positioned on the head. All samples were collected from one specimen, additional two samples of branchiostegal photophores from the other two specimens. Specimens of *D. watasei* pre-fixed in Bouin's fixative were washed 3 times in 1 M PB and submersed under the same buffer, to avoid tissue dehydration during dissection. Head photophores of one side of the were all included in the same sample by making a sagittal cut along the median plane of the cranium with a regular dissection scissor, and then making a transversal cut posteriorly to the light organs. With the aid of mini-scissors and fine forceps, body photophores were dissected by groups (branchiostegal and VO1 ventral photophores) or individually (lateral and VO2 ventral photophores). For posterior orientation purposes, the anterior side of body photophores samples were cut in triangular shape and a straight cut on the posterior side. Each sample was labelled and placed in a nylon biopsy bag, stapled to avoid being washed away during dehydration procedure.

Samples were dehydrated in ethanol series: 1. 70% (2 days); 2-5. 80-90-99.5I-99.5%II (2 h each) 6. 100% I (overnight); and 7. 100% II (2h). Next, samples were cleared in series of 3 xylene steps (30 min each). Before paraffin embedding, xylene was washed from the samples in 3 steps of paraffin (30 min each), in an oven (IC2405, Yamato Scientific Co. Ltd., Japan) at 60ºC to avoid paraffin solidification. Samples were collected form the biopsy bags with the aid of scissors and fine forceps and, in a metal tray, embedded in 60ºC paraffin, body surface side of samples facing upwards and anterior side of the samples facing right side, for posterior orientation purposes. Paraffin was let to cool down at room temperature for around 10 minutes and submerged in a tray of low flow running tap water (20-25ºC) for around 1 h. Next, metal tray with samples in solidified paraffin was left at -20ºC for around 10 minutes to ease detachment of paraffin from the tray. Finally, with the aid of a razorblade, paraffin blocks for each sample were prepared, anterior side of the samples facing upwards, and glued with hot paraffin to wood base.

Using a microtome (Spencer 820, American Optical Corporation, USA), sections of 6 µm were performed, from the anterior to the posterior side of the samples. Paraffin blocks were cut until all the organ was sectioned. Paraffin sections were picked with the aid of a paintbrush and floated for around 10 minutes in a metal tray with tap water on a heating plate (SP 45D, Hirasawa Co. Ltd., Japan) at 40ºC, to flatten the sections and avoid the wrinkles. With the aid a spatula, 1:1 egg white:glycerol additional coating was applied on the surface side of coated glass slides (FRC-01, Matsunami, Japan). With the aid of paintbrush, sections were gently collected on coated side of the glass slides and let dry on heating plate, and overnight at room temperature covered with aluminium foil to avoid dust to settle on the sections.

Sections were stained with standard procedure of haematoxylin and eosin. Shortly, rehydration was first performed in the following solutions series: 1-2. Xylene I and II (4 min each); 3-8. 99.5I-99.5II-90-80-70% ethanol and tap water (1 min each). Next, glass slides were submersed in haematoxylin stain for 15 minutes followed by 30 minutes in low flow running tap water, as the calcium ions in the water aid in haematoxylin staining. Next, sections were submersed in eosin stain for 30 min , followed by dehydration series of ethanol: 1. 70% (5 sec); 2. 80% (10 sec); 3. 90% (30 sec); 4-5. 99.5% I-II (1 min each). Sections were cleared in series of xylene (I-II, 4 min each), and mounted in Entellan (Merck Millipore, USA) covered with coverslip (NEO No.1, Matsunami, Japan) and let to overnight dry at room temperature.

Histological sections were observed under light microscope (Eclipse E600, Nikon, Japan) at 4 to 60x magnifications (CFI Plan Fluor Series, Nikon, Japan) in the Luminous Organisms Laboratory of Chubu University (中部大学研究室), sections of photophore lenses 10 to 100x (BX43 microscope with DP22 camera and UPlanFL N Series objectives Olympus, Japan) in the Fish Biology Laboratory (魚類生物学研究室). Photocytes and iridophores were identified in the sections by cellular morphology and location in the organ according to [96, 97, 106, 108]. Photocytes were recognized as one group of lamellar cells with elongated nucleus, surrounded by connective tissue and overlayed by the reflector of the pigmented septum (Fig. 12A). Iridophores were identified as iridescent reflective cells, located between the cup and the pigment layer (Fig. 12B). One section was selected for each head photophore (Ant, Dn, Vn), for each of 3 body photophores located on the branchiostegal rays (Br1), and on the ventral (PVO3, VO1, VO2) and lateral (PVO2, SAO2, VLO) surface of the fish body. Sections for analyses were selected by the lowest level of tissue deformation and most central position of photophore, identified by the largest area of photocytes.

Photocytes and accessory tissues with potential optical function (scale lenses and reflectors) were examined using morphometric parameters related to the tissue functional role on light output: 1. Photocytes area (μm^2); 2. Scale lens thickness (µm); 3) Lens reflector length (µm); and 4) Inner reflector thickness (µm). Besides these parameters, organ diameter was also analysed to estimate the morphological parameters relatively to the organ size, in order to avoid bias due to the different organ size between photophores. All morphological measurements were performed using 3 replicates. Lenses of head photophores were not analysed due to its lack of potential dioptric or spectral function. Presumably due to friction of the fishing net to the body of the animal during the fishing process, scale lenses are easily detached from body photophores and commonly missing the photophores of *Diaphus* samples. Although the scale lens was detached on VO2, the lens reflector was found to remain intact, reflector length measured from dorsal-lateral to ventral side of the organ, for lateral (PVO2) and ventral (VO1 and VO2) body

photophores. Scale lenses were only found in sections of 1 lateral (PVO2) and 1 ventral (VO1) body photophores, lens thickness measured along 5 sample areas (SAs) from dorsal-lateral to ventral side of the organ (Fig. 12 C). Inner reflector thickness was measured on 10 SAs for all head and body photophores, from dorsal-lateral to ventral side of the organ or from the inner part of the body to the lateral direction in the case of Vn. Scale lenses, lens reflector and inner reflectors determined to analyse the variation of measured morphological parameter for each tissue, according the location of photophores in the surface of the fish body. Variation of thickness along the scale lenses and reflector allow to estimate the shape of the tissue as well. Scale lenses were previously suggested to have dioptric [106, 108] and spectral [108] roles on modulation of light emitted on ventral photophores of lanternfishes which is related to the shape and thickness of the lens according to dioptric modification of light angles in geometric optics [122, 123]. Scale lens reflector is reported to function as shutter to avoid light to be emitted outside on the lateral side of the organ [87], which length per organ size should may vary from ventral to lateral body photophores. Inner reflector thickness was found to be related to the inclination of iridophores (see Chapter 6) which can modulate the reflection spectra of light interference [124, 125] and angle of light, according to similar structure on tapeta lucida of marine invertebrates and sharks [126–129]. Morphometric measurements were performed using the software ImageJ 1.50i (National Institutes of Health, USA) and exported to Microsoft Office 2000 Excel (Microsoft Corporation, USA) for basic statistical analyses, tables and graphs.

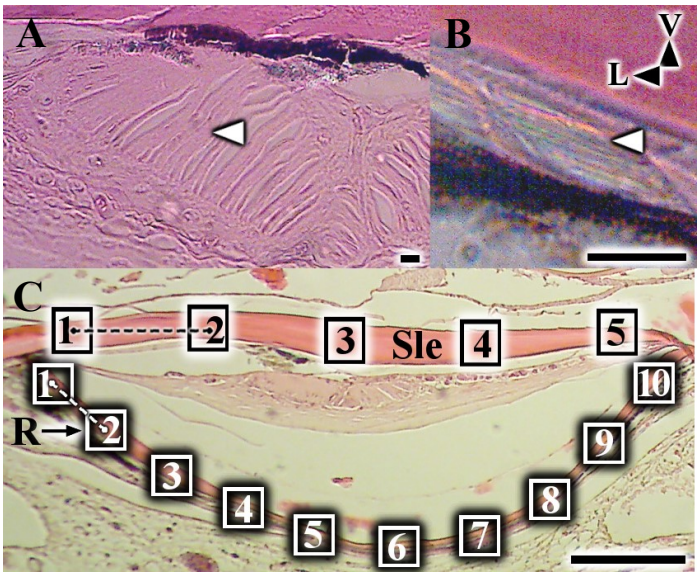

Figure 12 – Light microscope photographies from anterior view showing tissues of *D. watasei* identified by cellular morphology and position exemplified in ventral body photophore: A) Photocytes; and B) Iridophores. C) Generic position of sample areas for thickness measurements of scale lens (black outlined squares, SAs 1 to 5) and inner reflector (white outlined squares, SAs 1 to 10) of photophores. R= Reflector; SA= Sample area; Sle= Scale lens; V= Ventral; L= Lateral. White arrows indicate the respective tissues. Dashed white and black lines represent the uniform distance between SAs along the lens and reflector, respectively Scale bars= A-B) 10 µm; C) 100 µm.

c. Lens spectrometry

Using *D. watasei* as model, this chapter includes the first analysis on optical characteristics of lenses in photophores of lanternfishes. Methodological procedures and spectrometry system is adequately described so it can be reproduced in future studies. For head photophores dissection, heads of 3 specimens in -80ºC were cut with a knife and defrosted in distilled water for around 10 minutes. With the aid of forceps, a small piece (around 5 mm^2) of the head photophores lens from the area in front of Dn dorsally to the nostril, was dissected with mini-scissors (Fig. 13A). With the aid of fine forceps, scale lenses of VO2 ventral body photophores were collected from PB buffer where were stored at 4ºC) (Fig. 13B). Lenses of head and body photophores were washed 3 times in Petri dish (standard size) filled with distilled water, water substituted for each wash. With the aid of fine forceps, surface on both sides of lenses were cleaned with paintbrush, to wipe any debris that can contaminate the measurement of light transmission spectra. Lenses were kept in distilled water until spectrometry analyses.

To measure the spectra transmission of photophore lenses it was used a spectrometer (Kymera 1931-A, Oxford Instruments, UK) with CCD spectrometry detector (Newton DU920P-BVF, Oxford Instruments, UK) and camera lens (Micro-Nikkor 105mm f/2.8, Nikon, Japan). Camera lens was facing a diagonal mirror the open side of a black box with a hole on the top side, from where was ventrally focused as light source, one adjustable arm of dual gooseneck fibre optic illuminator with halogen lamp (Olympus LG-PS 2, Japan) (Fig. 13C). Black cardboard with a central pinhole of around 500 µm of diameter was attached to a Petri dish with double sided tape. Note that diameter of the pinhole is smaller than scale lens area that covers the photophore emission side, the area of the lens that is not covered by the lens reflector and from there the light of the photophore is limited to be emitted outside. This size of the pinhole ensures the light transmission is only measured on the scale lens area where the light is actually emitted outside of the photophore. Petri dish was placed on the hole of the top surface of the black box containing a piece of paper with small letters covering the pinhole. Spectrometer camera window was set on 0.2 mm and spectrometer set to live video mode. Mirror position adjusted until the cardboard pinhole was visible on camera and the position the light source above the pinhole, at a distance of around 1 cm. to the Petri dish. Focus of the camera lens was adjusted to the letters on the paper, to ensure the correct focus on the photophore lens samples.

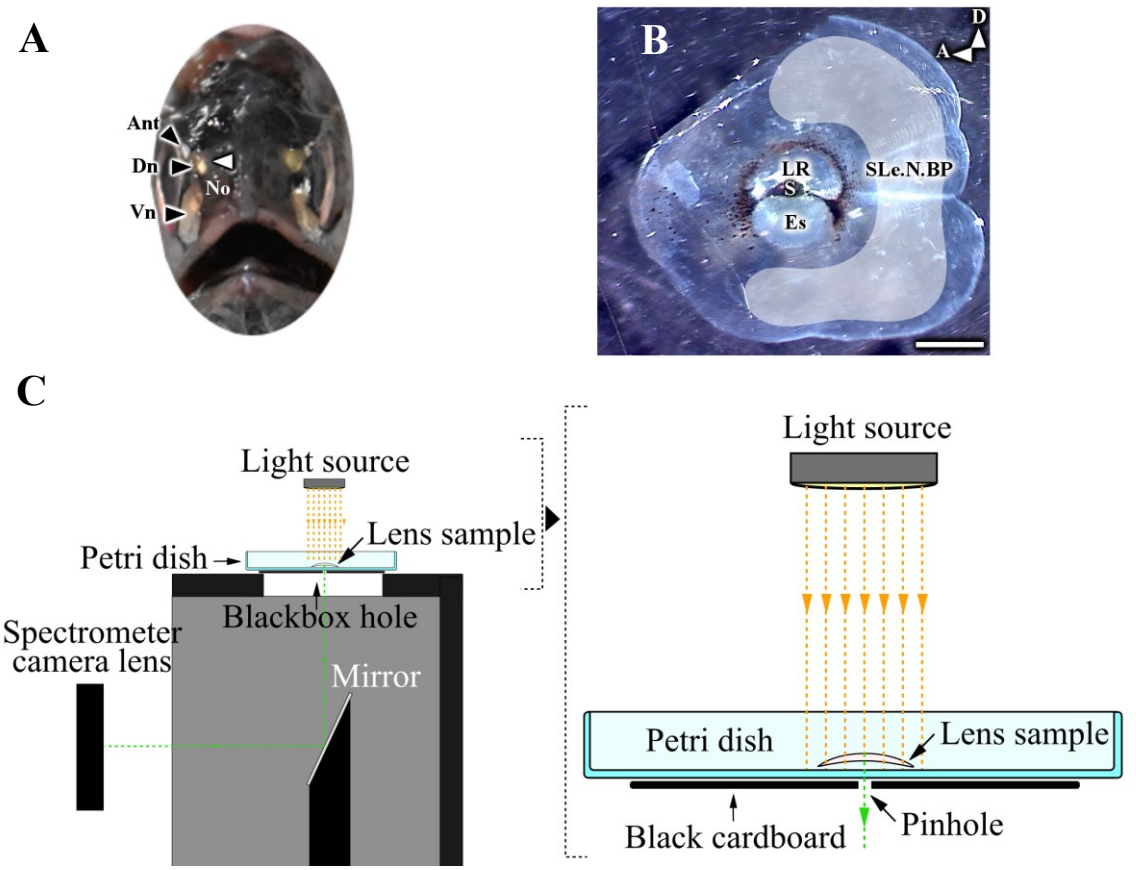

Figure 13 – Spectrometry of light transmission of head and body photophores' lenses of *D. watasei* A) Photograph from frontal view of head showing area of tissue sampled (white arrowhead) from lens of head photophores. B) Stereo microscope photograph from upper view of scale covering VO2 ventral body photophore showing the remaining pigmentation under the scale. C) Schematic illustration representing the spectrometry system used to measure the spectra of light transmittance on lenses of *D. watasei* photophores. Ant= Antorbital organ; Dn= Dorsonasal organ; Vn= Ventronasal organ; NO= Nostril; LR= Lens reflector; S= Septum; Es= Emission side; SLe.N.BP= Scale lens area not covering the photophore; D= Dorsal; A= Anterior. Orange dashed lines represents the emitted from the light source, orange arrow head indicates the direction of light. Green dashed line represents the transmitted light from lens sample, green arrow head indicates the direction of light White transparent represents area measured for the scale lens are that is not covering photophore. Scale bar= 1 mm.

Spectrometer was set to transmittance mode and a drop of distilled water poured on the Petri dish, covering the pinhole. Transmittance spectra of distilled water on Petri dish was measured and used as reference. Samples of head photophores lenses were measured by simply placing the tissue sample on the pinhole and transmittance spectra recorder. For scale lenses, transmittance spectra was recorded from the lens area covering the emission side of the photophore and for a random area other than the part of the lens that covers the body photophore and does not contain melanophores or any other kind of pigmentation. Before measurement, the excess of distilled water removed from the tissue sample with paintbrush to avoid it floating and moving position of the area of the tissue during transmittance spectra measurements while keeping the tissue hydrated. Room lights were turn off before each measurement (including reference of distilled water) and every measurement was done using 3 replicates. Spectrometry measurements were performed using the software Andor SOLIS

4.29.30012 (Oxford Instruments, USA) and exported to Microsoft Office 2000 Excel (Microsoft Corporation, USA) for basic statistical analyses and graphs on light transmittance intensity.

3. Results

a. Inner structure of photophores

General outer morphology varies for different types of photophores observed, namely between head and body photophores (Fig. 14), the only common feature between these groups is possessing a shining inner reflector. Head photophores have silver reflecting colour and are located on the snout, between the nostril and the upper (Ant), central (Dn), and lower (Vn) areas of the eye (Fig. 14B). All head photophores can be observed from frontal view of the head but, from a lateral view, Dn is not visible. Relatively to head photophores, morphology of body ones seems more complex, with two types of reflectors and pigmentation.

Branchiostegal photophores are "bean shaped", elongated on sagittal body plane (Fig. 14C). These photophores are composed by an outer and lateral septum, consisting in silver reflector covered by black pigmented layer of melanophores. Internal reflector seems to be structural coloured as the blue-green colour depends on the angle of observation from ventral view, becoming silver when observed from the side (Fig. 14D). Although not photographed, the same phenomena was observed for the inner reflector on body photophores. These photophores have a similar structure to branchiostegal ones, differing by possessing a rounder shape, septum in median position and more pigmented and an additional lens reflector (Fig. 14E). Lens reflector covers the lateral half of the photophore, separated by the ventral half of the organ where it is possible to observe the coloured inner reflector. Lens silver reflector can be observed from lateral view of the organ (Fig. 14F). After lens reflector removal, inner reflector can be observed covering all the organ in ventral body photophores (Fig. 14G). Lateral body photophores are morphologically identical to ventral ones, except that in the lateral organs the inner reflector is brightest on the median dorsal side and appears faint and degenerated on the ventral side of the organ (Fig. 14H). Curiously, branchiostegal photophore viewed from the side, seem like the lower half of the ventral photophores below septum, from a ventral view.

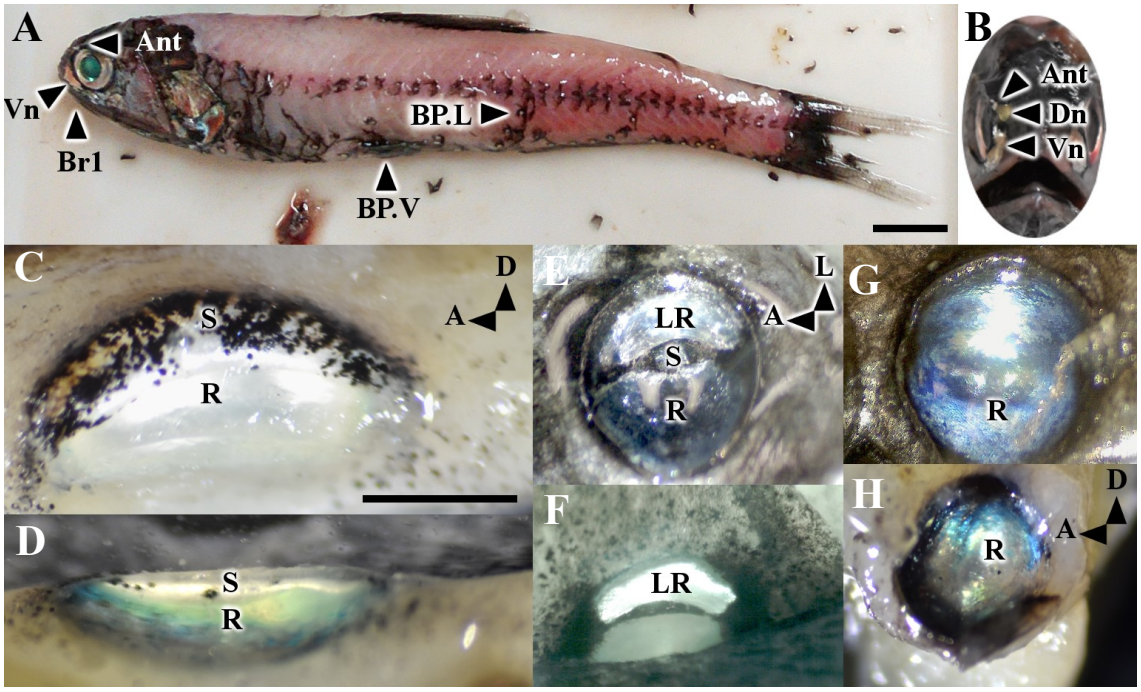

Figure 14 – Outer morphology of photophores of *D. watasei*. A) Lateral view of the fish body showing the location of examples of different types of photophores. B) Frontal view of head photophores. C) Lateral view of branchiostegal photophore, and D) ventral view. E) Ventral view of ventral body photophores, and F) Lateral view. G) Ventral view of ventral body photophore with removed lens reflector. H) Lateral view of lateral body photophore with removed lens scale. Ant= Antorbital organ; Vn= Ventronasal organ; Br= Branchiostegal organ; BP.L= Lateral body photophore; BP.V= Ventral body photophore; S= Septum; R= Inner reflector; LR= Lens reflector; D= Dorsal; A=Anterior. Scale bar: A-B) 1 cm; C-H= 1 mm. A,B,E and G on -80oC defrosted individual; C, D and H on TEM fixative tissue samples (see Chapter 6); F from Bouin's fixed individual.

Inner structure is consistent with the outer morphology features observed on all types of photophores. General structure is similar for different types of photophores. All photophores possess an outer lens exteriorly to the area of photogenic tissue, consisting in photocytes groups enfolded by connective tissue. Internally, the photogenic tissue is covered by the inner reflector. Final internal tissue is the melanophores filled pigmented layer.

General structure is common to all head photophores (Fig.15). Thick lens of what seems to be connective tissue covers all the photophores anteriorly (Fig. 16A-C), as well laterally on And and Vn (Fig. 15A, C). Photogenic tissue covers a large part of the total area of the organ. Thick inner reflector extends lateral-posteriorly on Ant and Vn, and dorsal-posteriorly on Dn (Fig. 16D-F). Extension of lens and reflector spatially more limited in Vn is consistent with the observed outer morphology where this is the only head photophore that is limited to observation from frontal view.

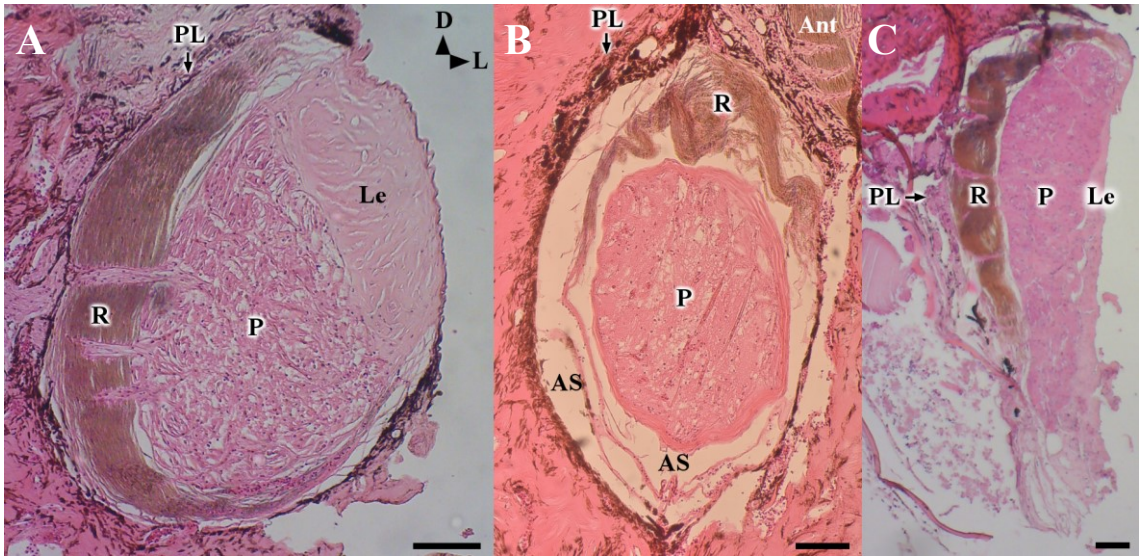

Figure 15 - Light microscopy photographs from anterior view showing the general morphological structure of head photophores of *D. watasei*: A) Antorbital organ; B) Dorsonala organ, with visible lower internal area of Antorbital organ, and C) Ventronasal organ. PL= Pigmented layer; R= Reflector; P= Photocytes; Le= Lens; AS= Internal space; D= Dorsal, L= Lateral. Scale bars= 100 µm.

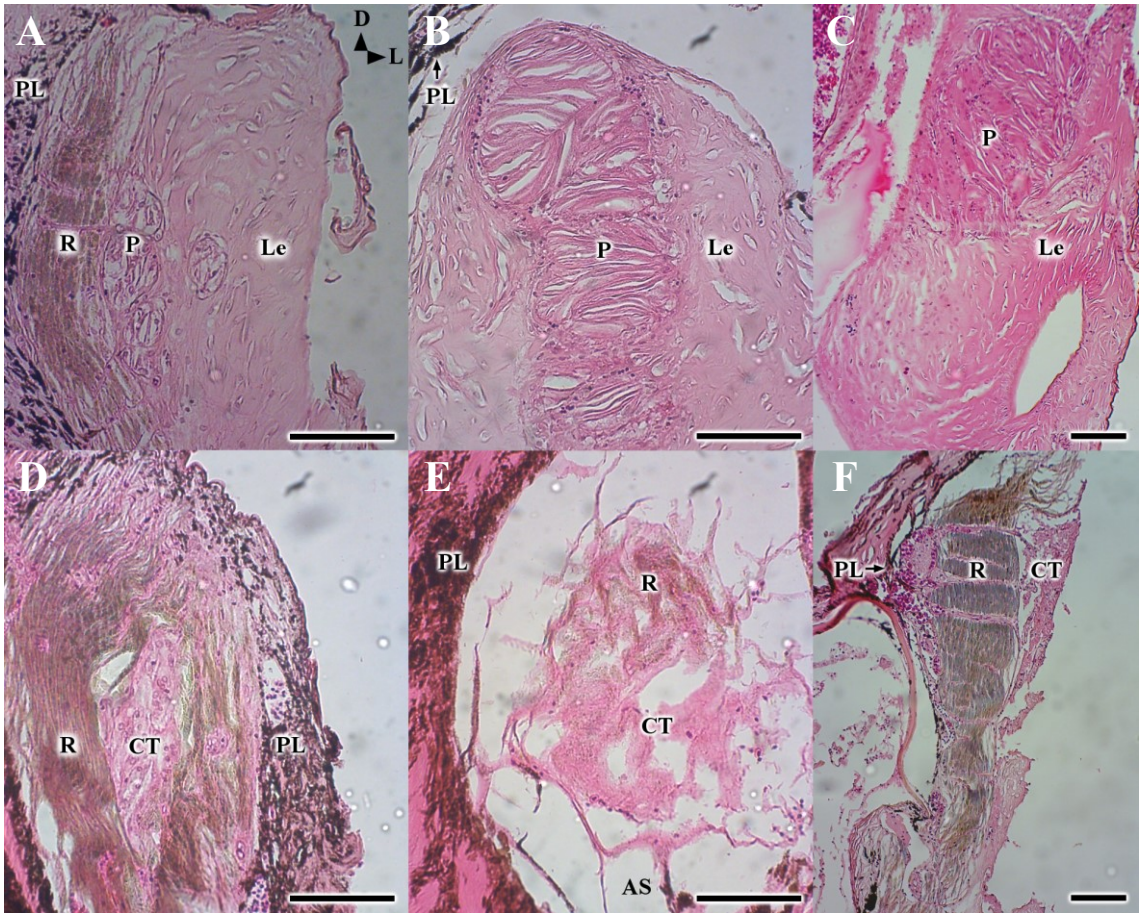

Figure 16 - Light microscopy photographs from anterior view showing anterior area of lenses in head photophores of *D. watasei* for A) Antorbital organ, B) Dorsonasal organ, and C) Ventronasal organ, and posterior reflector area of D) Antorbital organ, E) Dorsonasal organ, and F) Ventronasal organ. PL= Pigmented layer; R= Reflector; P=

Photocytes; Le= Lens; CT= Connective tissue; AS= Artifact space from detachment of photophore from supportive connective tissue; D= Dorsal, L= Lateral;. Scale bars= 100 µm.

Body photophores have a clearly different inner structure from the head photophores, though the main constitutive tissues are the same. Relatively to head organs, thin lens covers a small area of photogenic tissue and a thin inner reflector (Fig. 17). The septum, visible on outer morphology of body photophores and composed by reflective layer covered by melanophores, is also observed on histological sections, covering the photogenic tissue. Photocytes enclosed in a singular group lays on a connective tissue membrane that extends throughout all the median area of the organ. The main difference between branchiostegal and body photophores are: 1. Position of photogenic area and septum; 2. Presence of lens reflector on body photophores; 3. Presence of cup on body photophores; and 4. Organ shape. In accordance of the outer morphological observations, the septum is located in dorsal area on branchiostegal photophores and in the middle area on body photophores. On sections, one can observe that the photogenic tissue under the septum follows the position of this tissue on photophores. On the ventral area of the body photophore from the septum, there is no obstacles to light between the inner reflector and the lens, occupied only by connective tissue. On body photophores, lateral lens reflector extends on between the lens and the photogenic tissue and supportive connective tissue. Another particular feature for body photophores is the presence of the cup extending above all the reflector. It is curious that besides its semi-hard appearance on histological sections, this tissue is so transparent that was not possible to observe on the outer morphology of the organs. While body photophores in sections are shaped as an hemisphere, branchiostegal ones seem a compressed version of it. As previously observed on outer morphology, inner structure of branchiostegal photophores seem like the half ventral part of the body ones.

Internal spaces are observed in sections on head and body photophores. Dn head photophore, between photogenic area, reflector and pigmented layer (Fig. 15B). Body photophores between the connective tissue and the cup, while in the same area on branchiostegal photophores, the connective tissue seems smoother but no space is observed here (Fig. 17). On branchiostegal photophores, spaces are observed between the reflector and the pigmented layer and between lens and connective tissue supporting. Due to the visible detachment of some areas of the reflector and pigmented layer on the left side are assumed to represent artefact space caused by fixation and/or histological sectioning procedure.

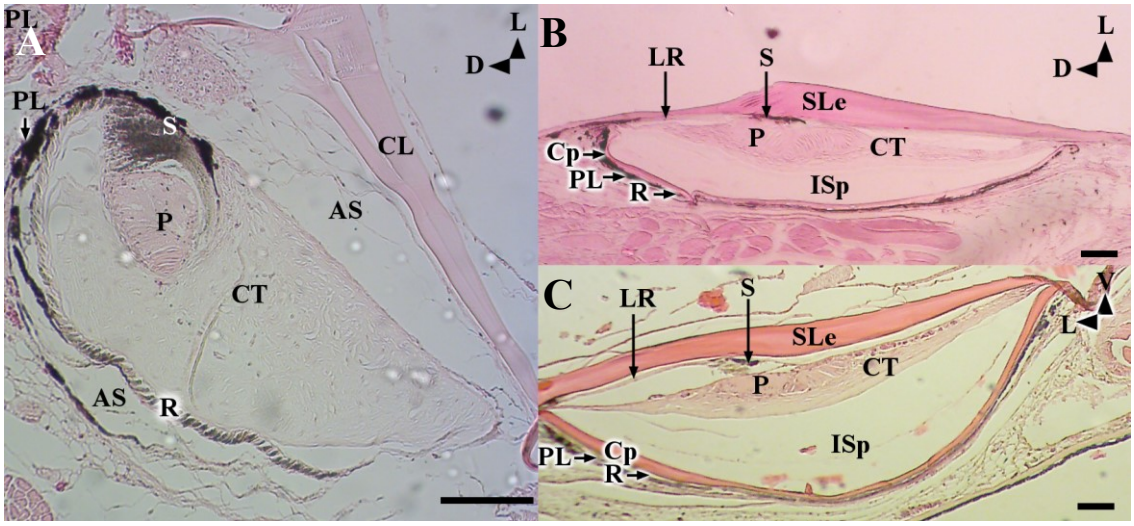

Figure 17 – Light microscopy photographs from anterior view showing the general morphological structure of *D. watasei*'s body photophores: A) Branchiostegal (Br1); B) Lateral (PVO2); and C) Ventral (VO1) body photophores. Br= Branchiostegal organ; PVO= Subpectoral organ; VO= Ventral organ; PL= Pigmented layer; S= Septum; P= Photocytes; R= Reflector; CT= Connective tissue; CL= Cartilage lens; Cp= Cup; LR= Lens reflector; SLe= Scale lens; AS= Artifact space from detachment of photophore from supportive connective tissue; ISp= Inter-tissue space between photocytes and inner reflector; L= Lateral; D= Dorsal, V= Ventral. Scale bars= 100 µm.

Lenses of head and body photophores have clear differences on histological sections. Besides the thickness, the appearance diverges as well between these groups of photophores which is commonly related to different types of tissues (Fig. 18A-C). Within body photophores, branchiostegal and other body photophores have lenses originated from different tissues, branchiostegal cartilage and modified body scales, respectively. Despite the different origin of the lenses on body photophores they share a very similar appearance of non-cellular semi-hard tissue, which seems to be constituted by highly packed collagen layers, parallel to the surface of the organ (Fig. 18D-F). Contrary to ventral, in lateral and branchiostegal photophores this arrangement of collagen layers is limited to the internal and thinner portion of the lenses. Exterior layer is composed by collagen fibres more spaced between them, parallel or oblique to the surface of the organ in branchiostegal and lateral body photophores, respectively. As the area of packed collagen layers is present in all lenses it is denominated as "primary" and the external layer only present in lateral and branchiostegal organs as "secondary". Head photophores have lenses with soft cellular tissue appearance (Fig. 18G). These lenses have very similar features on histological sections to the connective tissue found on body photophores surrounding the photogenic tissue (Fig. 18H).

Reflectors outer morphology is clearly different between the coloured inner reflectors of body photophores and the silver reflective tissues of inner reflector on head photophores, septum on body photophores and lens reflector of body photophores. Not surprisingly, the organization of the reflective material – guanine crystals (see Chapter 3) - in these tissues is different as well. Silver reflective tissues have guanine crystals unorganized in iridophores and

with high variation of spacing between them (Fig. 19A-D). On the contrary, coloured reflectors have layered guanine crystals arranged inside of iridophores along the tissue with low variation of spacing between the platelets (Fig. 19E-F). Even though the crystals seem to be damaged in the photographs (Fig. 19A,B, D, E) or even absent due to dissolution in Bouin's fixative (Fig. 19C), the stated features are observable for all the photographies.

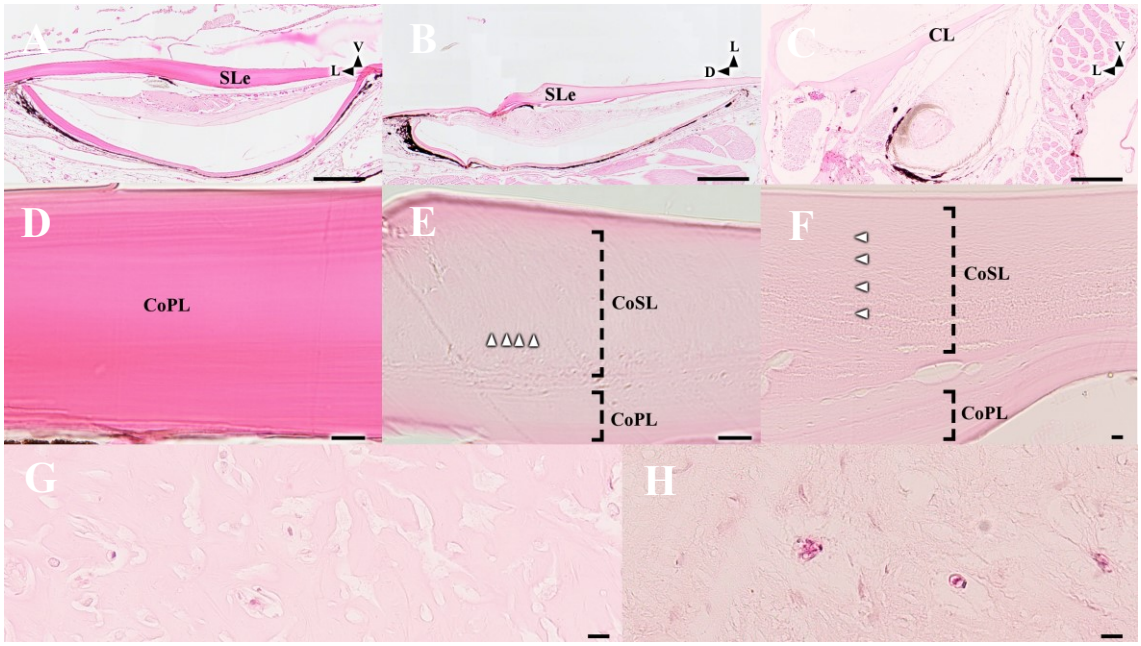

Figure 18 – Light microscope photographies from anterior view showing examples of the histological features of lenses in *D. watasei*'s photophores. A) VO1 ventral; B) PVO2 lateral; and C) Br1 branchiostegal photophores. D) Scale lens of VO1 ventral; E) PVO2 lateral; and F) Cartilage lens of Br1 branchiostegal photophores. G) Connective tissue lens of Dn head; and F) Connective tissue supporting photocytes on Br1 branchiostegal photophores. SLe= Scale lens; CL= Cartilage lens; CoPL= Primary collagen layer; CoSL= Secondary collagen layer; V= Ventral; L= Lateral; D= Dorsal. White arrowheads indicate collagen layers of secondary collagen layer area. Dashed square parentheses limit the areas of primary and secondary collagen layers. Scale bars: A-C= 200 µm; D-F= 10 µm.

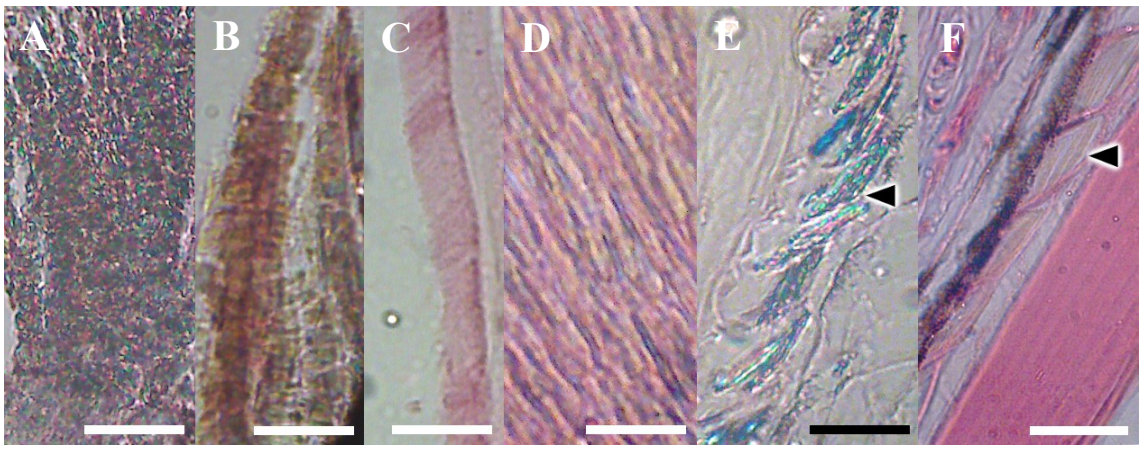

Figure 19 – Light microscope photographs from anterior view showing arrangement of guanine platelets in reflective tissues on photophores of *D. watasei*. A) Septum of Br1 branchiostegal photophore. B) Septum; and C) Lens reflector of VO1 ventral body photophores. D) Inner reflector of Ant head photophore. E) Inner reflector of Br1

branchiostegal; and F) VO1 ventral body photophores. Br= Branchiostegal organ; VO= Ventral organ; Black arrows indicate iridophore cells. Scale bars= 20 µm.

a. Morphometric analyses

Morphometric measurements are in accordance to observations descripted for histological sections, degree of values variation in one SA or sample is assumed to be related to organ or area minor deformations from fixation or histological sectioning procedure (for discriminated averages and standard deviations, see Supplement 1). Organ size varies from 505 µm on VLO lateral body photophore to 2579 µm on Vn head photophore (Fig. 20). Br1 branchiostegal photophores represented less variation around 720 µm, which is not surprised as these are all the same photophores group and position on the contrary of other types of examined organs. Lateral body photophores vary from 505 µm on VLO to 1261 µm on PVO 2 and ventral body photophores from 876 µm on VO2 to 14335 µm on VO1. On head photophores, organ diameter rises from Ant 737 µm followed closely by 894 µm on Dn, to the larger Vn with 2570 µm. It is noticeable that wither for head or body photophores the size diminishes according to position on fish body, from ventral to lateral. Nevertheless, the size gap is higher between Vn to other head photophores when compared to body photophores.

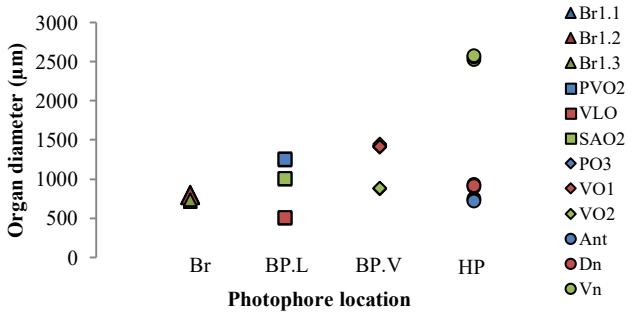

Figure 20 – Distribution plot of organ diameter by location of photophores on *D. watasei* body. Br/▲= Branchiostegal; BP.L/■= Lateral body; BP.V/♦= Ventral body; and HP/●= Head photophore; Br= Branchiostegal organ; PVO= Subpectoral organ; VLO= Supraventral organ; SAO= Supranal organ; PO= Pectoral organ; VO= Ventral organ; Ant= Antorbital organ; Dn= Dorsonasal organ; Vn= Ventronasal organ.

Photocytes area is up to more than ten times higher in head than in body photophores, varying from 2098 µm on VLO lateral body photophore to 219174 µm Vn head photophore (Fig. 21A). Branchiostegal photophores vary from photocytes area of 11024 µm to 1718µm. Lateral body photophores vary from 2098 µm on VLO to 9672 µm on PVO2 and ventral photophores from 2840 µm on VO2 to 9514 µm on PO3. On head photophores, photocytes area varies from 125746 µm on Dn to 219174 µm on Vn. Organ size correction by estimation of ratio photocytes area per organ diameter did not altered the tendencies observed for the raw data of photocytes area measurements for body photophores (Fig. 21B). On the contrary, for head

photophores, after organ size correction Vn exhibits photocytes area per organ dimeter two times than Dn and Ant, with the highest value (Fig. 21C). The same variation tendencies observed for organ diameter are present as well for the photocytes area, with exception to PO3 which is not as ventral as VO1 but has a larger photocyte area. Branchiostegal photophores that have a low organ size comparing to other body photophores, possess the higher photocytes area. This is not surprising if one keep in mind that even that these photophores are smaller on cross sections, are longer on a sagittal plane as previously observed on outer morphology.

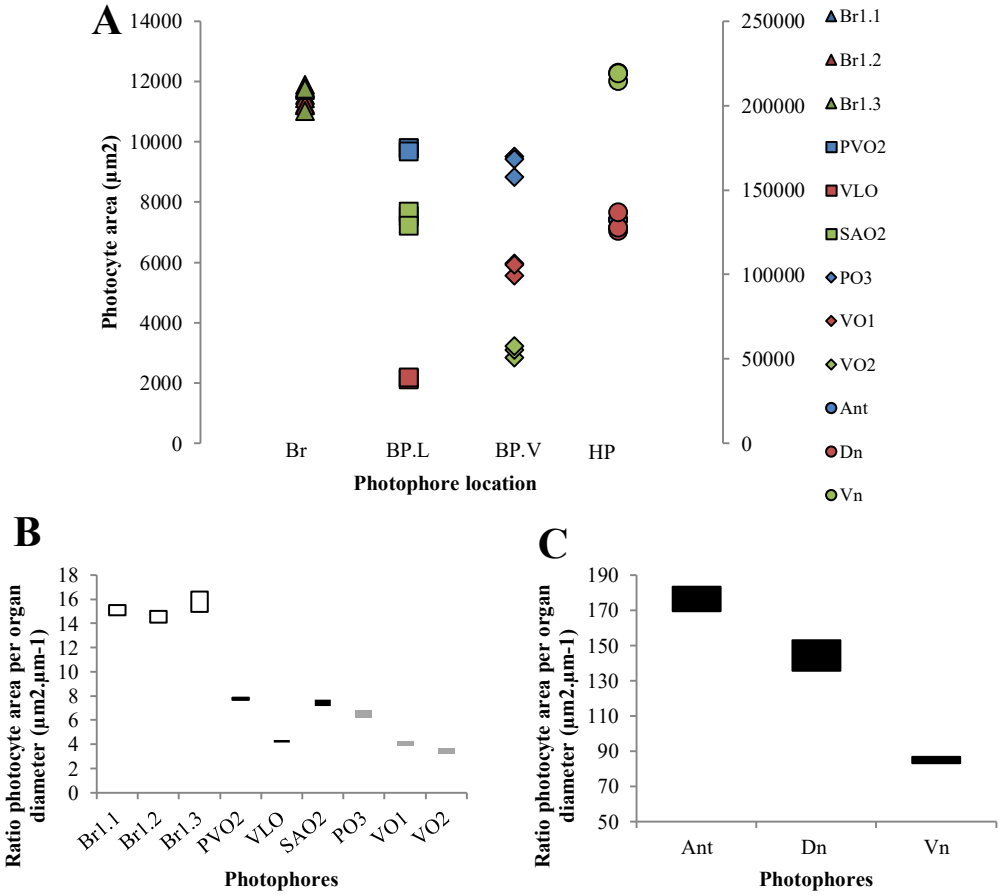

Figure 21 – Photocytes area by location of photophores on *D. watasei* body. A) Distribution plot of photocytes area, secondary vertical axis for head photophores (right) and main vertical axis for other photophores (left). Br/▲= Branchiostegal; BP.L/■= Lateral body; BP.V/♦= Ventral body; and HP/●= Head photophore. B) Histogram of the range of photocyte area per organ diameter on branchiostegal (white bars), lateral (black bars) and ventral (silver bars) body photophores. B) Histogram of the range of photocyte area per organ diameter on head photophores. Br= Branchiostegal organ; PVO= Subpectoral organ; VLO= Supraventral organ; SAO= Supranal organ; PO= Pectoral organ; VO= Ventral organ; Ant= Antorbital organ; Dn= Dorsonasal organ; Vn= Ventronasal organ;

Lens reflector is longer on ventral photophores VO2 (520 – 533 µm) closely followed by VO1 (521 - 526 µm), than in lateral PVO2 photophore (357 – 366 µm) (Fig. 22A). Organ size correction by estimation of lens reflector length per organ diameter did not altered the tendencies observed for the raw data of lens reflector length measurements but show that VO1 values are closer to PVO2 than VO2 (Fig. 22B). As VO1 is the most ventral and PVO2 the most

lateral, there is no observable tendency for lens reflector length in relation to the location of photophores in the fish body.

Inner reflector is up to 20x thicker on head than body photophores (Fig. 23). On head photophores, reflector thickness enhances from the periphery (minimum values, 9 µm on Ant, 14 µm on Dn, 20 µm on Vn) to the middle area of the organ (maximum values, 127 µm on Ant, 154 µm on Dn, 135 µm on Vn). Note that the thickest area of the reflector is located precisely in the middle area of the organ on the middle photophore Dn, while is middle-dorsal on the more dorsal photophore Ant and middle-ventral on the most ventral photophore Vn. Branchiostegal photophores have similar thickness distribution along the organ to head photophores but with lower thickness of reflector, enhancing from the ventral (6 – 10 µm) and dorsal peripheral areas (9 – 14 µm) to the middle area of the organ (16 – 21 µm). Note the reflector reaches lower thickness in the ventral than in dorsal area of the organ. Relatively to branchiostegal, body photophores present lower minimum thickness values and opposite distribution of reflector thickness, becoming thinner from the peripheral to middle areas of the organ. Ventral body photophores vary from 7 – 15 µm on periphery to 2 – 6 µm on ventral photophores, PO3 representing highest values overall regarding VO1 and VO2. Lateral photophores vary from 5 – 21 µm on dorsal periphery becoming thinner until the ventral periphery 1 – 3 µm. Overall maximum values of 21 µm reflector thickness of lateral body photophores and branchiostegal ones are higher than the maximum 15 µm observed on ventral body photophores. These lower values of reflector thickness on the ventral area of lateral photophores are in accordance with the outer morphology observations, reflector seem to be fainted on this are of the photophore. Organ size correction by estimation of inner reflector thickness per organ diameter did not altered the tendencies observed for the raw data of inner reflector thickness measurements for body and head photophores (Fig. 24). Nevertheless, it shows clearly the thickness of peripheral reflector enhances from the ventral to the most dorsal photophores, the only exception being PO3.

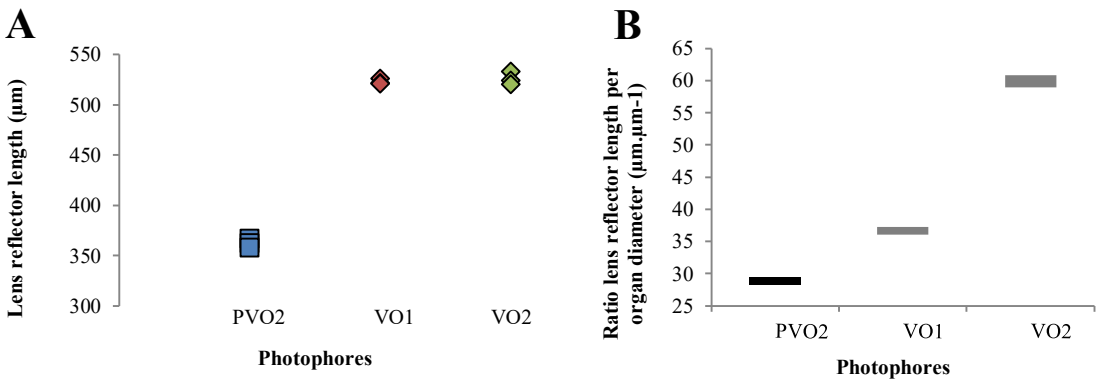

Figure 22 – Lens reflector length on *D. watasei* body photophores. A) Distribution plot for lens reflector length in lateral (PVO2) and ventral (VO1-2) photophores. B) Histogram of the range of lens reflector length per organ diameter lateral (black bars) and ventral (silver bars) body photophores. PVO= Subpectoral organ; VO= Ventral organ.

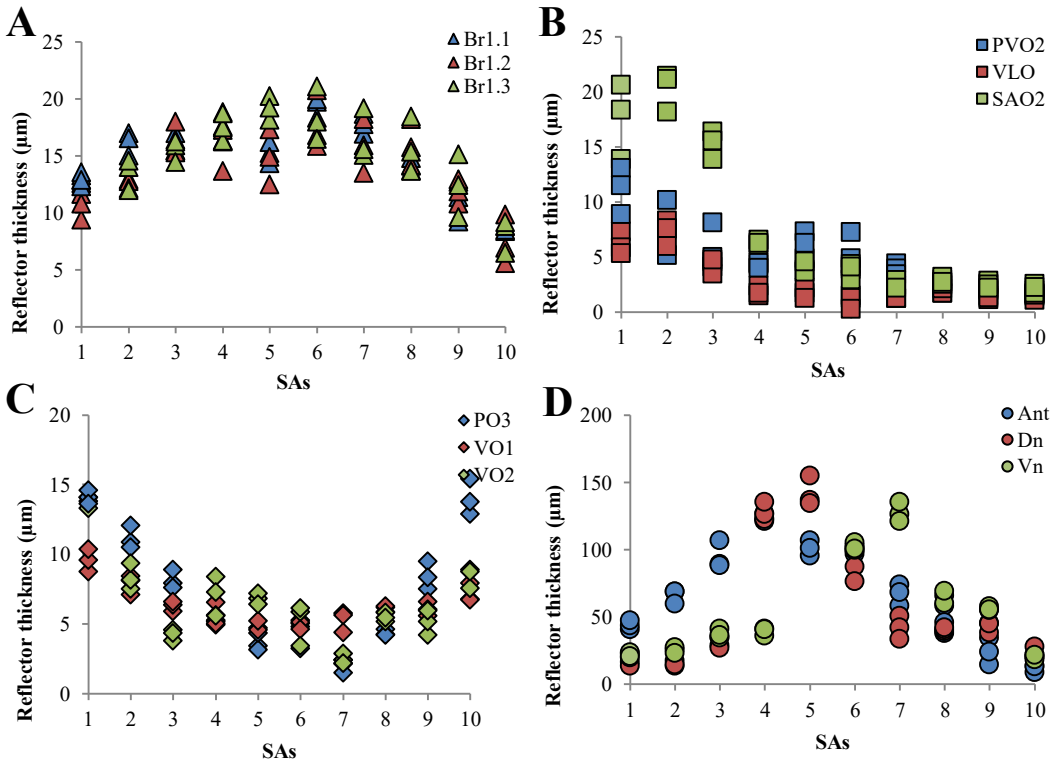

Figure 23 - Distribution plots of inner reflector thickness by location of photophores on *D. watasei* body. ▲= Branchiostegal; ■= Lateral; ♦= Ventral; and ●= Head photophores. Br= Branchiostegal organ; PVO= Subpectoral organ; VLO= Supraventral organ; SAO= Supranal organ; PO= Pectoral organ; VO= Ventral organ; Ant= Antorbital organ; Dn= Dorsonasal organ; Vn= Ventronasal organ;

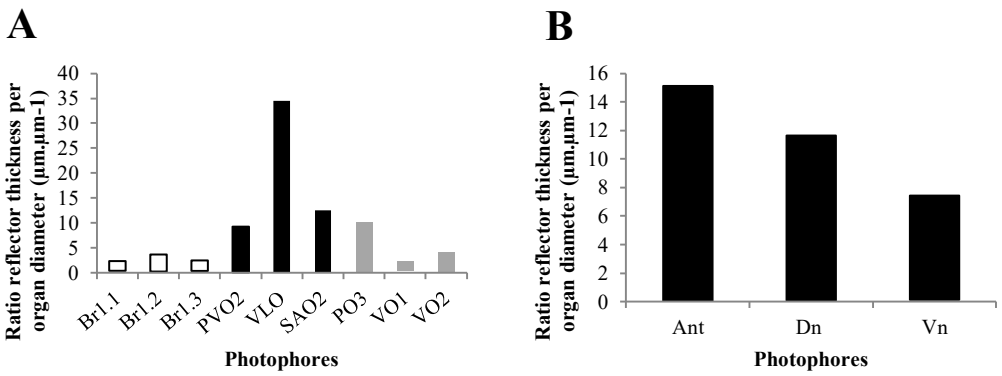

Figure 24 - Histograms of the range of inner reflector thickness per organ diameter of *D. watasei* for: A) Branchiostegal (white bars), lateral (black bars) and ventral (silver bars) body photophores; and B) Head photophores. Br= Branchiostegal organ; PVO= Subpectoral organ; VLO= Supraventral organ; SAO= Supranal organ; PO= Pectoral organ; VO= Ventral organ; Ant= Antorbital organ; Dn= Dorsonasal organ; Vn= Ventronasal organ;

Lens thickness values vary from 15 µm on PVO lateral body photophores to 108 µm on BR1 branchiostegal photophore, both on dorsal peripheral area of the organ (Fig. 25A). Not only the values but the thickness distribution along the SAs is also clearly different between body photophores, indicating shape difference between lenses. Branchiostegal photophores have lenses thicker on the dorsal periphery of the organ (79 - 108 µm), gradually becoming thinner to the ventral area (10 - 32 µm). Body photophores have thicker lens on the middle area, becoming thinner to peripheral areas. Lateral photophores have higher variation of thickness (15 – 93 µm), high maximum values on the middle area (82 – 93 µm) gradually becoming thinner to the periphery on the ventral area of the organ (maximum values per SA, 93 > 77 > 25 µm) and abruptly on the thinnest dorsal area (maximum values per SA, 93 > 35 > 16 µm). Ventral photophores have lower variation of lens thickness than lateral ones, from the thicker the middle area (56 - 62 µm) becoming gradually thinner to the peripheral areas of the organ (32 - 38 µm). From the thickness variation, one can observe that body photophores have plano-convex shaped lenses while branchiostegal photophores have hemi-plano-convex ones, curiously similar shaped and thickness to the ventral half of lateral body photophores lenses. Ventral body photophores have a thinner and uniform lens while lateral ones possess a thicker lens (up to 2 x) on the middle-ventral area of the organ but thinner on the dorsal area, comparable to lens thickness on ventral photophores. Higher variation is observed on lenses of branchiostegal photophores related to body photophores which is expected as, due to sample limitation (see Materials and methods), Br 1 was measured from 3 samples and PVO and VO only one sample per photophore. Organ size correction by estimation of ratio lens thickness per organ diameter did not altered the tendencies observed for the raw data of lens thickness measurements but it is clearly observable the uniform lens on ventral body photophores compared to lateral and branchiostegal ones (Fig. 25B).

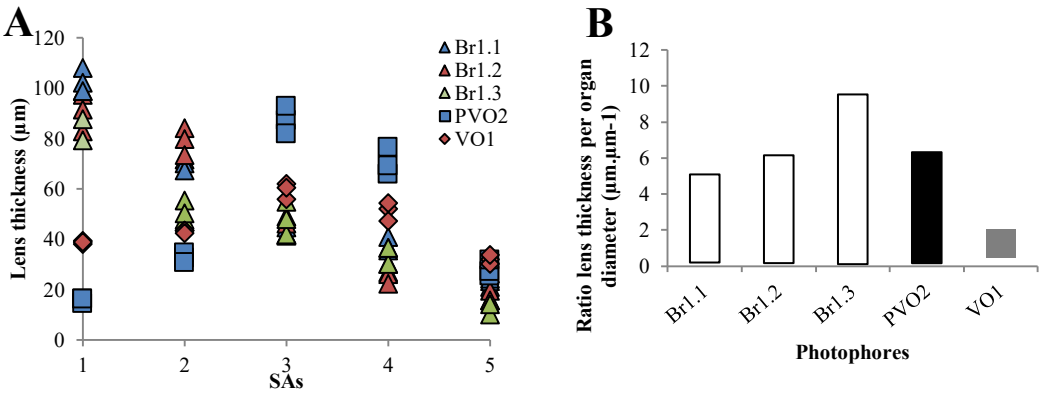

Figure 25 – Scale-lens thickness on body photophores of *D. watasei.* A) Distribution plots by location of photophores on the body of lens thickness. ▲= Branchiostegal; ■= Lateral; ♦= Ventral; and ●= Head photophores. B)) Histogram of the range of lens thickness per organ diameter on branchiostegal (white bars), lateral (black bars) and ventral (silver bars) body photophores. Br= Branchiostegal organ; PVO= Subpectoral organ; SAO= Supranal organ; VO= Ventral organ.

b. Lens spectrometry

Light transmission of head photophore lenses show intensity variation independently of the sample (Fig. 26A). Same degree of values variation is observed within different areas of the same sample (λmax transmittance= 366.89 – 505.36 ± S.D. 99.30 – 162.86 RLUs ,*n*= 9) and between tissues (λmax transmittance= 429.56 ± S.D. 124.24 RLUs ,*n*= 9). Spectral variation is much in a lesser degree either within (λmax= 506 - 514 ± S.D. 32.91 – 50.52 nm ,*n*= 9) or between samples (λmax= 512 ± S.D. 37.14 nm ,*n*= 9). On normalized data, spectral curves are clearly broad with higher transmission area roughly between 550 to 590 nm for all the samples (Fig. 26B).

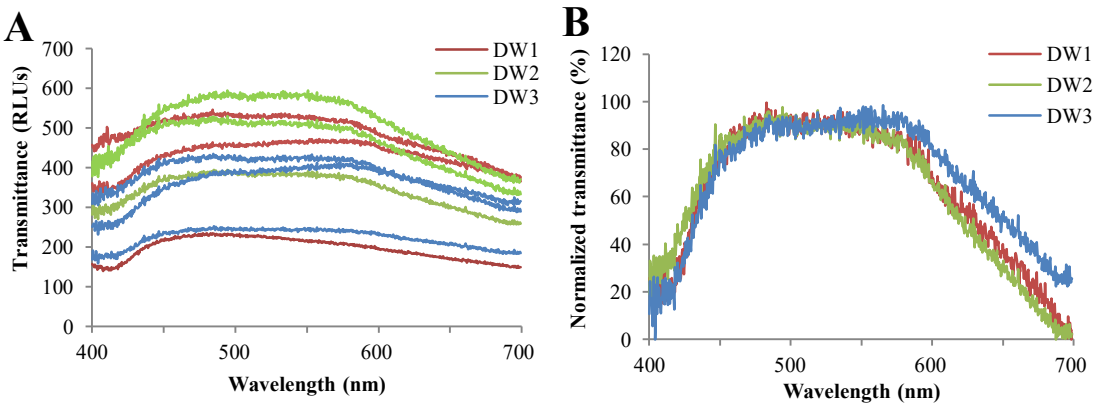

Figure 26 – Transmittance spectra of *D. watasei*'s head photophores lenses: A) Raw, and B) Normalized. DW= *Diaphus watasei*; RLUs= Relative light unit.

Lenses of body photophores have flat light transmission curves over all the visible spectra, either for photophore covering area of the scale lens or the non-photophore covering (outer) area (Fig. 27-28). Variation of cumulative light transmittance for the photophore

covering area is on the same range within ($7.05x10^4$– $1.98x10^5$ ± S.D. $6.22x10^3$ – $5.89x10^4$ RLUs ,*n*= 9) and between samples ($1.18x10^5$ ± S.D. $6.86x10^4$ RLUs ,*n*= 9). Same scenario is observed for light transmittance values on the non-photophore covering area within ($1.71x10^4$ – $7.40x10^4$ ± S.D. $7.70x10^3$ – $2.79x10^4$ RLUs ,*n*= 9) and between samples ($5.38x10^4$ ± S.D. $3.11x10^4$ RLUs ,*n*= 9). Comparatively to the non-photophore covering area, light transmittance is up to 4 times higher on photophores covering area on the same sample and 2 times between samples. Looking at the normalized data, while photophore-covering area have higher transmittance for shorter wavelengths of visible spectrum, non-photophore covering areas present a flatter curve, same transmission for all the wavelengths of visible spectra.

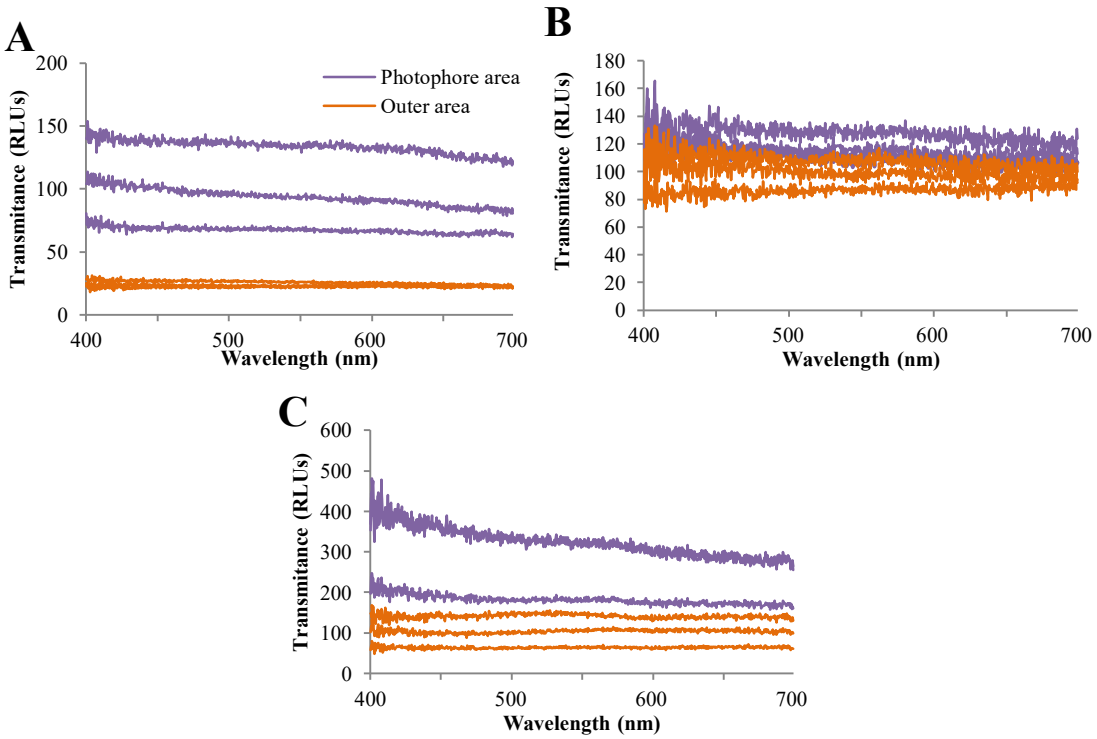

Figure 27 – Raw transmittance spectra of areas covering and non- covering photophore of scale lenses of *D. watasei*'s ventral body photophores for 3 individuals, A-C) DW1-3. DW= *Diaphus watasei*; RLUs= Relative light unit.

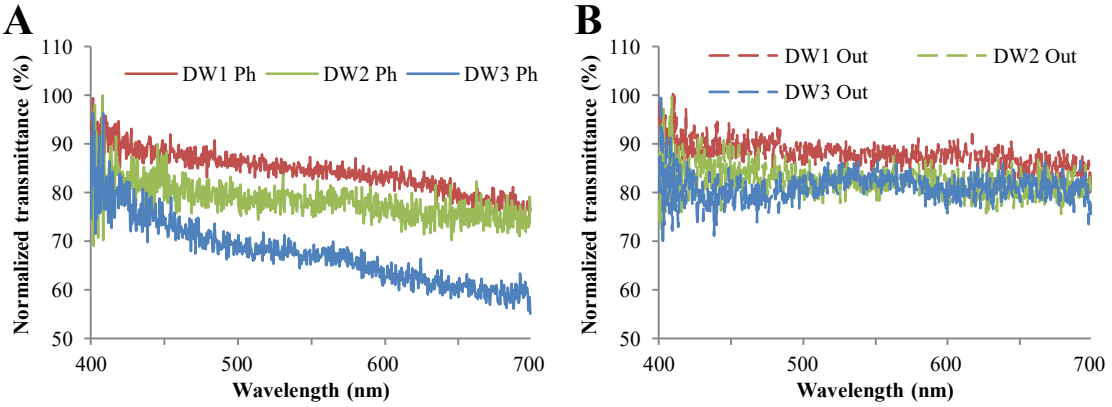

Figure 28 – Normalized transmittance spectra from scale lenses of *D. watasei* body photophores on: A) Covering, and) Non-covering area of photophore. DW= *Diaphus watasei*; RLUs= Relative light unit.

4. Discussion

c. General inner structure

Observed general outer morphology and inner structure of photophores in *D. watasei* are in accordance to the previously described on other myctophid species [87, 91, 96, 97, 106–108]. Although, general structure of different body photophores observed in this study is recorded by previous authors generically as " ventral photophores", not specifying the photophore groups. Based on the inner structures observed, it seems that in the photophores analysed in [97, 108] are actually ventral body photophores while in [91] are actually branchiostegal photophores. Another photophore structure in [106] was not observed in this study, which suggest that particular morphology may differ, at least, between lanternfish genera, or tribe as suggested by [96].

Previous studies did not focus much on specific morphology between different types of photophores, assuming similar inner structure regardless the photophores location on the fish body or its hypothetical bioluminescent ecological role. Aiming higher accuracy on the description of the structural features an effort was made to, additionally to detailed descriptions, include morphometric data for the main constitutive tissues that are described with potential role on the spectra and/or angle of light emission. Moreover, it was avoided to limit the analyses of the inner structure to solely description, as previous authors. Additionally to the inner structure descriptions, morphometric data allows higher precision to compare the main tissues between different types of photophores and its functions on light emission, ensuring a more realistic final estimative of the ecological roles of the light organs.

a. Head photophores

Photophore diameter as well as photocytes area per organ size, are higher on head than body photophores, generally enhancing from ventral to dorsal location on the fish body. Assuming that all photocytes produce the same light intensity per cell, higher area of photophores relates to higher intensity of light emission, as suggested for caudal photophores in lanternfishes with similar inner structure of photogenic tissue [96]. Lenses allow higher transmittance of spectra roughly between 450 and 600 nm which is perfectly adequate to transmit the raw light spectra produced from the photocytes of 454 nm (see Chapter 5). Frontal lenses in all photophores and additional lateral on Vn and Dn allow light emission in these directions for the respective

photophores. As the lenses do not seem to have any spectral neither dioptric role in head photophores it will be discussed deeply only for body photophores in the next section. Reflectors are thicker on the middle area on Dn, middle- dorsal on Ant and middle ventral on Vn. Additionally, all these photophores reflectors extend to the posterior area of the organ for light emission on frontal direction, allowing frontal-ventral light emissions in Dn, frontal-lateral-dorsal in Ant and frontal-lateral-ventral on Vn. In these reflectors, guanine crystals present some degree of disorientation and spacing variably, typical characteristic of broad wavelength reflection commonly observed in iridophores of silver skin of fishes [118, 130, 131]. Inner reflector on head photophores of *Diaphus* species is reported to function as a silver mirror to reflect light produced from the photocytes to outside of the organ [107], similarly to the silver reflectors in caudal photophores present on other lanternfish genera [39, 112]. Silver reflectors are widely reported in light organs of fishes, acting as light guides of light produced by photocytes to outside of the organ [113, 128, 132–134]. Inner reflectors on *D. watasei* head photophores have a similar function in light guidance, for which fit perfectly the broadband spectral characteristics of lenses transmittance and silver reflectors.

Besides individual high intensity emissions due to large photocytes area, all photophores emit frontally in simultaneous. The result is brightest light emission in this direction, adequate to illuminate surroundings and prey [49] and as well fit for the preying strategies in lanternfishes and other zooplanktivorous/ piscivorous mesopelagic fishes [6, 135, 136]. Specific variation of photocytes area and reflector thickness in Ant and Vn might be related to the multifunctional roles of these photophores that emit laterally besides in front (Fig. 29). Vn has the lowest and Ant the highest individual areas of photocytes for head photophores. Moreover, thicker reflectors dorsal-laterally on Ant and ventral laterally on Vn result in light to be emitted principally on lateral direction, avoiding leaking much light in dorsal and ventral, respectively. These characteristics of light intensity and direction are fit for mating, as proposed sexually dimorphic on *Diaphus* species [39] as for caudal organs in other lanternfishes [96, 98], although no clear sexual dimorphism was observed on *D. watasei* specimens so far. As far as I am aware, there is no reported information on the inner structure or ecological role for Ant. Taking into account the lateral head light emissions of Vn, one might extrapolate intraspecific communication for lateral bioluminescence of Ant as well. Contrary to Vn, Ant is the brightest head photophore individually and emissions are directed dorsally instead of ventrally so the interspecific signals may have a different meaning such as recognition or schooling observed on the blinking patterns of flashlight fishes bright sub-ocular light organs [137].

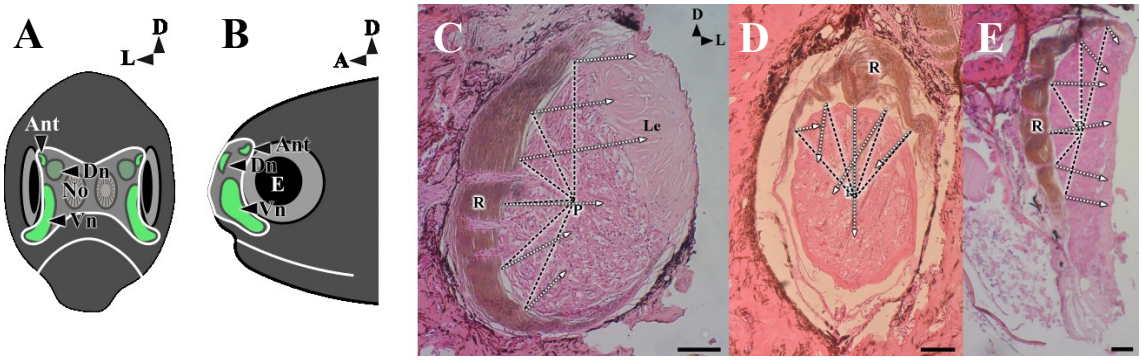

Figure 29 – Schematic illustration of intensity and direction of light emissions of head photophores in *D. watasei* on A) frontal and B) lateral views. Light microscope photograph from anterior view showing light angle and relative intensity produced from the centre of photogenic area and projected outside by the inner reflected through the lens, on C) Ant, D) Dn) and E) Vn head photophores. Ant= Antorbital organ; Dn= Dorsonasal organ; Vn= Ventronasal organ; E= Eye; No= Nostril; R= Inner reflector; P= Photocytes; Le= Lens; D= Dorsal; A= Anterior; L= Lateral. Black dashed lines represent the light emitted from the photocytes and white dashed lines the light projected outside the organ by the inner reflector.

a. Body photophores

Lower photogenic tissue area per organ size on body photophores correlates with the proposed function for counterillumination [40, 99]. Steady and continuous light emission of ventral photophores contrarily to the bright rapid flashes on head photophores, are suggested to be due to the high variation in photocytes number between photophores [96]. Counterillumination theory is based upon the need for the prey to camouflage the body surface from the visual perspective of a predator located below [40, 103]. One can clearly perceives that from a ventral view of the fish body, ventral surface occupies the majority of the visible area, relatively to ventral-lateral and lateral surface (Fig. 30). From this point, the general tendency for higher photocytes area on ventral organs fulfils the light camouflage function, body silhouette being concealed primarily by the light emitted by ventral photophores. Indeed, generally previous studies state ventral photophores to have the major role in counterillumination [55, 87]. As the location on the body surface by the photophores becomes more lateral, lesser area of the silhouette to be occluded. Lower photogenic area per organ size of the lateral body photophores and, consequently, lower light output are adequate for camouflage the flanks, playing a secondary role on the overall counterillumination. Ventral-lateral branchiostegal photophores have the highest photocytes area per organ size, relatively to body photophores. Although, as observed by outer morphology, these photophores are not cylindrical shaped as body photophores but longer on sagittal axis and covering a larger area on this plane which may explain the exceptionally higher photocytes area on transversal sections, relatively to body photophores.

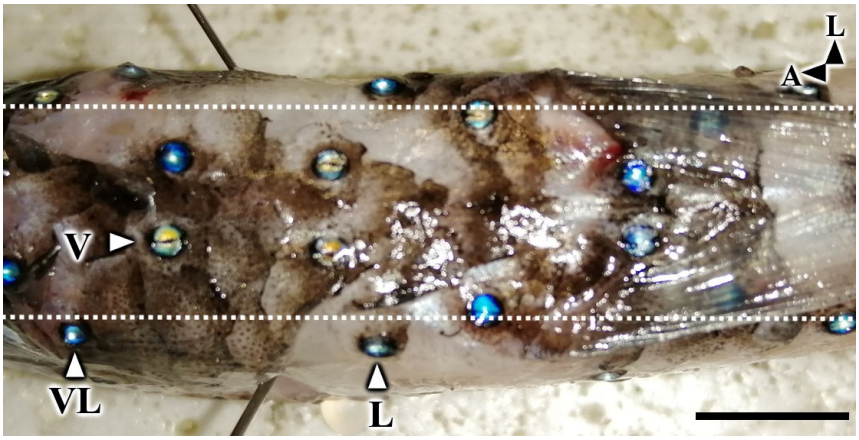

Figure 30 – Ventral view of *D. watasei* body surface showing ventral, ventral-lateral and lateral body photophores. Dotted white line delimitates body surface area covered by ventral photophores (between the lines). V= Ventral; VL= Ventral-lateral; L= Lateral, A= Anterior. Scale bar= 1 cm.

Previous records of body photophores on *Diaphus* and other myctophid species [87, 91, 97, 106–108], all state that photocytes located in a singular group located under the septum, so, in addition to the cell features, we assume this description to located photocytes. Nevertheless, it was observed exclusively on the body photophores, another group of morphologically identical cells located ventrally, side-by-side to the photocytes in the same supported connective tissue (Fig. 31). As these cells are not covered by septum pigment were not accounted as photocytes. Future efforts will be done to confirm whether these cells are not photocytes or if we are facing a novel photogenic tissue in lanternfishes and its role in counterillumination.

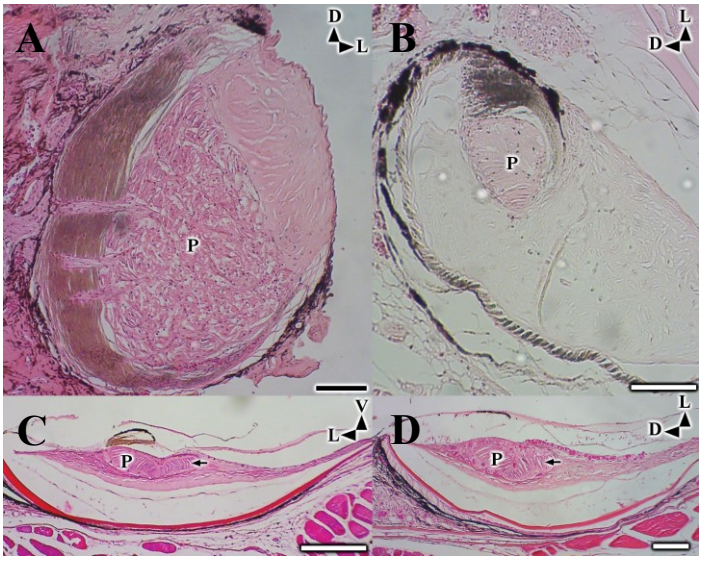

Figure 31 – Light microscope photographies from anterior view of single photocytes areas on photophores and "photocytes-like" cellular group on body photophores of *D. watasei*. A) Photocytes area on Antorbital head photophore. B)Photocytes area on branchiostegal photophore. C) Photocytes area and "photocytes-like" cell group (black arrow) on ventral body photophore. D) Photocytes area and "photocytes-like" cell group (black arrow) on lateral body photophore. P= Photocytes; D= Dorsal; L= Lateral; V= Ventral. Scale bars= 100 µm.

Variety of inner structure and outer morphology of reflectors observed on body photophores seem to be related with the reflective purpose. Similarly to silver the inner reflector of head photophores, silver reflectors of body photophores also share the arrangement of guanine platelets with highly variable spacing between. Septum reflector layer and lens reflector in body photophores act as shields, avoiding bioluminescent emissions to leak outside the organ and redirecting it to the inner reflector, either light produced from the photocyte or from lateral-dorsal area of the photophore, respectively [18, 87]. When guanine crystals are precisely stacked in alternated layers of uniform cytoplasm spacing achieves light interference on selective wavelengths, producing structural colour [124, 125]. Coloured inner reflectors on body photophores seem to be a case of structural colour, arranged in monolayer iridophores with stacked guanine crystals in a similar way to reported colourful fishes skin [138–140]. Wavelength of light interferences on inner reflectors of body photophores is reported to match the downwelling light spectra on mesopelagic depths for an adequate counterillumination [18](see also Chapter 5). Curiously, inner reflectors of body photophores reflect 6 times the light intensity than the silver lens reflectors and 3 times more than the 10 times thicker inner reflector of head photophores (see Chapter 5). Relatively to non-arranged in iridophores with high variably spacing guanine crystals, precisely arranged platelet stacked in iridophores seem to enhance the reflective performance of the reflectors, which is in accordance to fact that the peak of efficiency is found on guanine reflectors precisely spacing in stacks [141].

On ventral photophores, the observed higher thickness of the inner reflector for the peripheral areas of the organ, also observed for peripheral area of lateral organs while branchiostegal ones have always higher thickness. Reflector thickness is related to the inclination of iridophores, thicker areas where the guanine platelets are inclined in lower angles to surface of the reflector instead of positioned parallel to the tissue (see Chapter 6 for more details on ventral body photophores). Higher thickness of the reflectors is observed in photophores positioned more dorsally on the fish body, ventral-lateral branchiostegal and lateral body photophores. Assuming the reflectors of branchiostegal and lateral photophores function in a similar way to the parabolic-like on ventral organs (see Chapter 4), inclined platelets may reflect light from the photocytes in oblique angles, directing the light ventrally, allowing bioluminescence emissions in ventral direction for counterillumination, on light organs not positioned on ventral surface (Fig. 32). Inclined iridophores of guanine crystals on tapeta lucida in crustaceans, bivalves and sharks are reported for similar light purposes on altering reflection angle of light in the eye [126–129]. Ventral area of the inner reflector on lateral body photophores appears fainted on outer morphology observations and its thickness reaches the minimum on body photophores, with almost null values. Contrarily, on the peripheral dorsal side, reflector reaches its maximum thickness. Reflection only from dorsal area from inclined

A **B** **C**

iridophores on these light organs are probably another structural adaptation to direct light ventrally on the most lateral photophores involved in counterillumination.

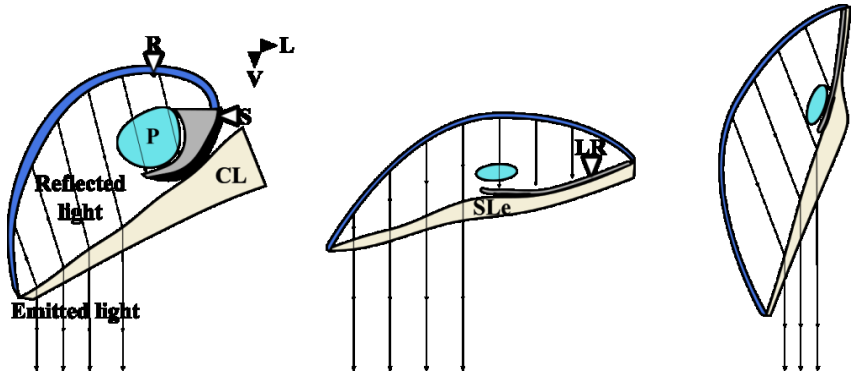

Figure 32 – Schematic illustration showing the ventral role of iridophores inclination and scale lens thickness on reflected and emitted light on body photophores of *D. watasei*: A) Branchiostegal (Br1); B) Ventral (VO1); and C) Lateral (PVO2). Photophores and respective tissues are adjusted to the same size for illustrative purposes. R= Reflector; P= Photocytes; S= Septum; CL= Cartilage lens; LR= Lens reflector; SLe= Scale lens; L= Lateral; V= Ventral.

Flat spectral transmission of body photophores scale lenses are well fit for transmission of any visible wavelengths, as well from the λmax 460 – 470 nm light emissions on *D. watasei* body photophores (See Chapter 5). The variation in spectral curves from head and body photophore lenses seem to be due to the composition of the tissues, as supported by different histological appearance in addition to same flat transmission spectra on covering and non-covering photophore areas of scale lenses. Nevertheless, photophore covering areas seem to be adapted for bioluminescence signals as light transmission is 2-4 times higher than in non-covering photophore areas of the scale. Spectral modulation properties were previously suggested [108] for the scale lens on *Terletonbeania* lanternfish, which does not seem to be applicable according to the first spectral records of lanternfish lenses, in this study. Nevertheless, one cannot discard that spectral properties of lenses may vary between lanternfish genera. Branchiostegal cartilage lenses were not measured, but from its histological similar appearance to scale lenses and both ventral body and head photophores lenses have broad spectral transmission, one can assume a similar case for cartilage lenses. While body photophores have lenses derived from different collagenous tissues, head photophores lenses seem to be composed by connective tissue by its histological similarity to connective tissue supporting photocytes in body photophores, described in [91, 97], which is assumed to be perfectly transparent to allow the maximum photon output of bioluminescent emissions. As both types of lenses have no spectral influence on bioluminescent emissions on *D. watasei*, it seems that the optical role of lenses in photophores is not related to spectra modulation. Previous authors proposed dioptric function for scale lenses in other lanternfishes [106, 108]. Comparing to branchiostegal and head photophores that are surrounded by cartilaginous tissues outside, body photophores which

have cup, are organs that lay only on skin and muscle. Taking this into account, it seems that the function of the cup is solely for support and shaping body photophores.

As observed on outer morphology and inner structure, body photophores can only emit light on the area ventral to the septum – emission area – as the dorsal area is covered by the septum or septum and lens reflector on branchiostegal or other body photophores, respectively. So, as only the ventral half of plano-convex lenses of body photophores, the functional lens is actually an hemi-plano-convex lens, as in branchiostegal photophores (Fig. 32). Ventral photophores have lens scales with tightly packed collagen layers parallel to the organ's surface, which do not seem to have optical properties do alter the direction of light from the reflector. On the other hand, lateral photophores have lenses with an external area where the collagen layers are oblique to the photophore surface. This tissue may have function to alter the light direction, such as for the similar structure of collagen layers in lens pad of scopelarchid fishes [142–144]. Branchiostegal photophores' lenses structure are between ventral and lateral photophores scale lenses, exhibiting also an external area with collagen layers as the lateral organs but layers in both zones all parallel to the surface of the photophores, as the orientation of collagen in the lens of the ventral photophores. In this way, the cartilage lenses of branchiostegal photophores may have an optical function between the ventral and lateral organs scale lenses, altering the light direction but in a much less degree than the lateral photophores, directing it ventrally. Moreover, relatively to ventral body photophores, lenses are thicker on lateral and branchiostegal photophores and receive light on oblique dorsal direction from the inclined iridophores of inner reflectors. According to geometric optics of lenses refractions, thicker lenses have higher refraction index and light is refracted ventrally when the light focus point position is changed dorsally [122, 123]. Extrapolating to the photophore scenario, oblique dorsal light from inner reflector together with high refraction of thicker lenses may direct the light more ventrally. On lateral body photophores, as the inner reflector is only functional on the dorsal area, focus point becomes even more dorsal which results on light to be refracted on a more ventral angle, relatively to branchiostegal photophores. Regarding the ventral body photophores, as light is all reflected in the same ventral angle (See Chapter 4) and lens is thinner, the dioptric effect will be much less than in other body photophores, which will results avoiding light to be diffused in other angles than vertical.

Branchiostegal photophores and PO3 are exceptions from the tendencies on morphometric parameters observed on other body photophores. Branchiostegal and PO3 are located on maxilla and pectoral area of the fish body while other analysed ventral photophores are pelvic. In transversal plane, ventral body surface is larger, flatter and thicker on the pectoral area than pelvic, and the opposite for the maxilla. Camouflage by reflection of silver surfaces in pelagic fishes varies with the body shape on a transversal axis shape [118]. In a similar way, the

shape of the body area may also be related to the observed exceptions on branchiostegal and PO3 photophores, although the reasons are not clear yet. More detailed analyses on the inner structure of different groups of branchiostegal and pectoral photophores would be required to understand this scenario.

a. Conclusions

In this chapter was observed that *D. watasei* developed photophores for diverse ecological functions of bioluminescence through adaptation of structural and optical characteristics of the main tissues involved in light emission, photocytes, lenses and reflectors. Head photophores have simple structure with numerous photocytes capable of frontal high intensity flashes [96] simultaneously from all photophores that seem to be used for illumination of prey and surroundings [49]. Additionally, Ant and Vn emit lateral light signals as well, which gives them, additionally to illumination, multifunctional purposes of bioluminescence for intraspecific communication [39, 49]. Body photophores exhibit a much higher level of complexity, with dioptric lenses, coloured and accessory reflectors to achieve an adequate spectral and angular for successful counterillumination [18, 40, 87, 97, 108], downward emissions being observed on body photophores of lanternfishes *Myctpohum* [99] and *Tarletonbeania* [100]. This subject will be examined with in more detail in further chapters of this thesis. Observed structural and optical features indicate that the functional role of lateral body photophores is counterillumination and not intraspecific communication, such as species recognition [55, 63, 110]. For the first time, it is reported in photophores of lanternfishes, different structure and tissues origin for the same ecological purpose, namely, branchiostegal, ventral and body photophores for counterillumination. Additionally, was determined that these divergences are correlated to the position of light organs on the fish body.

Future studies will be developed to clear out the number of photophore groups, mechanisms of dioptric role of scale lenses, angle reflection of iridophores inclination on thicker areas of the reflector and the “exceptional” structure of branchiostegal and pectoral photophores. Coelenterazine autofluorescence in cryosections of photocytes; histology of different groups of branchiostegal and pectoral body photophores; spectrometry of refraction in scale lenses; TEM microscopy of scale-lenses and reflectors in branchiostegal and body photophores, will allow to understand better the structural and optical characteristics of photophores and its roles on counterillumination. Regarding the structural adaptation of head and body photophores for multifunctional bioluminescent roles, it would be interesting as well to develop molecular studies to comprehend in what degree the general basic structure is related to an ancestral form

of photophore linage that evolved into the observed diversity of light organs for different ecological purposes. In parallel, structural studies on photophores of different genera of lanternfishes would be desirable to examine the functional structure relatively to phylogeny and ecology of Myctophidae family. Besides the reflectors structure, iridophores shape and arrangement are also related to the tissues reflection, which is examined in the following Chapter 3.

CHAPTER 3

Guanine crystals morphology in iridophores of reflective tissues

1. Introduction

Colouration of fishes is remarkably variable and adapted to specific purposes of visual communication, such as silver sides of small pelagic fishes for camouflage [118] and the colourful patterns of coral reef fishes for intraspecific communication [145]. In vertebrates, these amazing colours are produced by pigmented cells called chromatophores, which include colours from brown to black– melanophores -, yellow - xanthophores -, red – erythrophores -, white – leucophores – and metallic or iridescent - iridophores [146]. Latter are responsible for the colouration of reflective tissues of fishes by being composed by stacks of guanine crystals [118, 128, 147].

Guanine is commonly found on reflective tissues of organisms along the Tree of Life due to its high refractive index and the fact that it is readily available in cells as nitrogenous metabolite [141, 148]. Guanine crystals are formed from the degradation metabolism of guanine nucleic acid [141], reported grown and shaped in intracellular vesicles on iridophores on skin of carps [149]. Guanine is characterized by if not the first, one of the highest refractive indexes known in biogenic reflective structures which allows high reflection intensity [141, 148], compared to other substances such as collagen [124].

Despite its chemical nature, arrangement of crystals (platelets) inside the iridophore defines its spectral reflection properties [118]. Silver metallic appearance of fishes skin are obtained by variable spacing and angle of cytoplasm between crystals, leading to non-selective and broadband wavelength of reflected light [131, 141]. Contrary to diffusing reflectors that scatter light according to Lambert's Law as observed in white colours of spiders, specular (mirror-like) reflectors project light on a regular angle of reflection [128, 141]. Multilayered thin films in stacks, parallel to each other, composed by layers with regular thickness uniformly spaced results in coloured reflections [125]. The alternated layers of thin films composed by two materials with different refractive indexes produces the physical phenomenon of light interference, which produces the brilliant structural colours on butterfly wings, cuticle of beetles and skin of cephalopods and fishes [124, 141, 147, 150]. Thin guanine crystals (less than 1µm for thin films) with high reflection index of (1.83) and lower for cytoplasm (1.33) between them [124] allows the observed coloured reflections in iridophores of reflective tissues of fishes [138–140, 151]. Wavelength of reflected light depends on the thickness of platelets and cytoplasm and the angle of light incidence on the platelet surface [125]. Knowing that the thickness of platelets are fairly uniform in iridophores within reflective tissues of fishes skin [147], reflection colour is controlled by angle of light and thickness of cytoplasm, shorter angle of light incidence and thicker spacing of cytoplasm resulting in reflection of longer wavelength [124, 125].

Guanine crystals have various shapes and arrangements on different taxa such as the cubic shaped crystals on white spiders [152], the 3D iridophores on chameleons skin [153] and more common 2D multilayered stacks in fishes and invertebrates such as cephalopods, copepods and bivalves [147, 154]. Guanine crystals on fish reflective tissues have typical hexagonal elongated shape, with different length/width ratio within and between tissues and species wither for silver or structural coloured light reflection [118, 147]. While guanine iridophores on structural coloured tissues of fishes - other animals such as copepods - are only reported to be arranged in monolayers [138, 140], silver tissues are commonly composed by multilayered reflective cells [130, 147, 155], as the broad light reflection of the latter does not require precise arrangement of crystals [141, 147].

Reflectors in photophores of luminous fishes are widely assumed to be composed by guanine crystals [117], despite this has only be confirmed on a few cases, such as for the midshipman fish *Porichthys* [156], flashlight fish *Anomalops* [133] and pearleye fish *Maurolicus* [119]. Similarly to euphausiids [42, 114] and squids [115, 116], two reflectors with different reflective functions are reported in lanternfishes body ventral photophores: 1. Silver lens reflector, functioning as "light shutter" [87, 97]; and 2. Blue-green inner reflector, alter light spectra emitted from photocytes to the outside of the organ, matching the downwelling light at mesopelagic depths for counterillumination purposes [18]. As far as I am aware, there are no descriptions of the silver inner reflectors of head photophores in lanternfishes. Arrangement of guanine iridophores of the silver inner reflector in the ventral photophores of the hatchetfish *Argyropelecus* guide light from the photogenic chamber to outside the organ in a ventral angle for counterillumination [118]. Ventral angle of photophores for counterillumination was examined for the same species and the viperfish *Chaulodius* [103], similarly to the downward light emissions observed in ventral photophores of lanternfishes [99, 100]. However, the functional structure was never analysed in the case of lanternfish light organs, either for the reports on silver lens reflector [87, 91, 97, 108] or the inner coloured one [18, 90]. In the latter tissue, a remarkable unique shape of "hexagonal iridescent elements arranged in honeycomb pattern" was noticed decades ago [157, 158].

Even if the functional role of the hexagonal pattern is unknown on the inner reflector of lanternfishes photophores, similar arrangement is known for smaller guanine iridophores on the cuticle of sapphirinid copepods for camouflage by light interference [141, 159]. Indeed, coloured guanine iridophores are commonly used for spectral camouflage in fishes skins [138, 140, 147, 151]. Additionally, arrangement of guanine iridophores in scales of silvered skin fishes is reported to maximize light reflection [155] the angle inclination of the reflective cells on the body surface to be adapted to the angle sunlight penetrating shallow waters, allowing an adequate camouflage on small pelagic fishes [118].

Lanternfishes are characterized by having head and body photophores for multifunctional bioluminescent signals. While head photophores are reported to emit bright and rapid flashes, ventral organs have steady and constant glow with low intensity, relative to head ones [96, 97]. Different bioluminescent light between these photophores are due to a precise and fast regulation of light by neural control [91–95] and a higher number of photocytes in head photophores, comparatively to ventral ones [96]. High intensity flashes of head photophores on *Diaphus* are proposed to be used as torches to illuminate the surroundings and prey [49] and sexual communication [39]. On the other hand, observed downwards light emissions ventral photophores of myctophids [100] are adequate spectral [101, 102] and angular [99] luminous glow to match the dim and vertical downwelling light on mesopelagic depths [3, 103, 120, 121] for successful counterillumination [40].

This chapter focus mainly on solving the question of the functional structure of the unique hexagonal arrangement on lanternfishes ventral photophores. In comparison to other reflective tissues of fish body, it is also in the aims to analyse the iridophores arrangement and morphology of platelets, and confirmation of guanine nature of crystals in photophores inner reflectors. Using *Diaphus watasei* as model, UV spectrometry (together with FTIR and XRD) on head and body photophores inner reflectors, microscopy observation of platelets arrangement and morphometry analyses on reflective tissues will be performed. Altogether, this approach allow to describe the morphology and arrangement of iridophores on different reflective tissues and relate it to specific reflective functions.

2. Materials and methods

a. UV spectra of guanine

Samples of *D. watasei* were collected on 21.11.2017 at Mimase fishery port in Kōchi city (高知市御畳瀬支所), Japan (see Chapter 2). One fish was defrosted from -80ºC on distilled water for around 10 minutes. With the aid of fine forceps and mini-scissor, five ventral and one head photophore and body photophores were dissected. Head photophore used was Vn, due to its larger size and, consequently, larger reflector area and guanine content, compared to Ant and Dn. Sampled tissue for head photophore was all used while for body photophores the scale lens reflector was removed, if present.

Methodology for UV absorbance spectra of guanine was adapted from previous reports of guanine in tapetum lucidum of teleosts [160–162]. Sampled tissues were mashed with a plastic pestle for around 1 minute in 1 ml of 0.1M NaOH, in 1 ml eppendorf tubes. UV light

absorbance was measure using a UV/Visible spectrophotometer (Ultrospec 2100 pro, Amersham Biosciences/GE Healthcare, UK). Commercial anhydrous guanine powder (Fujifilm Wako Pure Chemicals, Japan) in 1M NaOH was used as positive control and 1M NaOH as negative control. Due to high content of guanine in the tissues, order to avoid spectrophotometer saturation and allowing absorbance values to be measured correctly. Sampled tissues homogenates were diluted 2 times and commercial guanine 10^4 times. UV spectra was analysed between 250 – 300 nm based on the spectral range reported in [160–162]. Absorbance spectra was measured at 1 nm waveband intervals for controls while samples were tested in 2 steps. First, UV spectra was measured at 10 nm waveband intervals between 250 – 300 nm to determine the position of wavelength peaks. Spectral peaks were found to be located between 270 – 275 nm, interval where the spectra was then measured in 1 nm waveband to determine the accurate wavelength λmax. Light intensity was posteriorly corrected respectively to dilution of samples and commercial guanine in and to the spectra of solvent NaOH. Microsoft Office 2000 Excel (Microsoft Corporation, USA) was used for calculations on dilution corrections, basic statistical analyses and graphs.

b. Crystal morphology

Samples of *D. watasei* were collected and frozen at -80ºC on 21.11.2017 at Mimase fishery port in Kōchi city (高知市御畳瀬支所), Japan (see Chapter 2). Smaller individuals of *Diaphus* were collected by pelagic trawling on a vessel of the National Research Institute of Fisheries Science of Japan(中央水産研究所) at the North-eastern Japanese waters of the Pacific Ocean and kept frozen at -20ºC. Taxonomical identification of smaller *Diaphus* was only possible until genus level so it will be stated as *Diaphus* sp. (Fig. 33). Morphometric measurements were made on five individuals of each species on body standard length (SL, mm), and eye and body photophores diameter (mm) using nine and five organs, respectively.

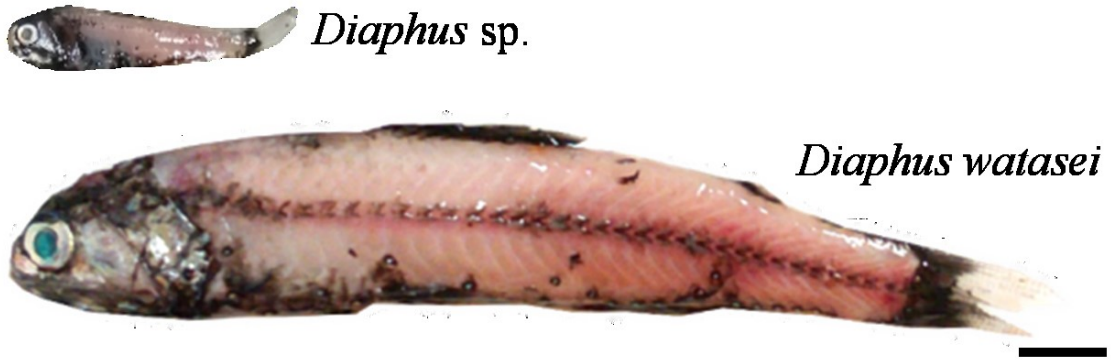

Figure 33 – Photographs from lateral view showing the size difference between the two species of *Diaphus* used in this chapter. Scale bar= 1 cm.

This is the first study on platelets morphology in iridophores of photophores reflectors in bioluminescent fishes, so the methodology is presented in a way that it can be easily reproduced in future studies. Two fishes per species were defrosted in distilled water for around 10 minutes. *D.* sp was used for comparison of platelets length variation per organ size on tapetum lucidum and inner reflector of body photophores. Reflective tissues were sampled with the aid of fine forceps and mini-scissors and placed in 1 ml eppendorfs tubes with 200 µl of distilled water. In *D. watasei* head photophores, Vn from both sides of the head were used, due to larger size and easier dissection than Ant and Vn. All the photophores from the body were used, excluding damaged organs. In the case of head photophores and skin, whole sampled tissue was used. For body photophores, lens reflector, when present, was peeled with forceps and placed in a different tube than the organ for *D. watasei* and discarded for *D.* sp. Eyes were enucleated from the orbits and kept in distilled water during dissection, to ease the process. Cornea was cut out, in *D. watasei* the iris was peeled from its inside surface with fine forceps. With the aid of paintbrush and minis-scissors, vitreous humour and retina were gently removed to the maximum amount possible while avoiding damage to the tapetum lucidum. Tapetum lucidum was collected with the aid of fine forceps and mini-scissors. Tubes with samples were gently stirred to avoid damaging the platelets in the supernatant. With the aid of plastic Pasteur pipette, supernatant was poured on glass slide for microscopy (MAS-GP type A, Matsunami, Japan), and covered with glass coverslip (Neo No.1, Matsunami, Japan). Platelets were observed under a light microscope (Eclipse E600, Nikon, Japan) at 40x magnifications (CFI Plan Fluor Series, Nikon, Japan). Length and width were measured from platelets photographs and length/width ratio calculated.

Observed crystals amount in homogenates varied highly between samples, so the number of platelets analysed per tissue was then established to 50. Length/width ratio of crystals was calculated and used to analyse the variation of morphology between tissues. Data analyses on statistical hypothesis of unequal variances on different samples was performed using

unpaired two-sample Student's t-test (α=0.01). Morphometric measurements were performed using ImageJ 1.50i (National Institutes of Health, USA) and exported to Microsoft Office 2000 Excel (Microsoft Corporation, USA) for statistical analyses, tables and graphs.

3. Results

c. Guanine nature of inner reflectors of photophores

UV absorbance of homogenates from inner reflector of head and body photophores in 0.1M NaOH are compared the positive control of anhydrous commercial guanine in 0.1M NaOH, and the negative control 0.1M NaOH. Absorbance vales are more than 10^4 higher for anhydrous guanine than homogenate samples, which is expected for the positive control, higher content of guanine in the powder higher content than in the samples (Fig. 34). Value of absorbance λmax is higher in head photophores (0.36 RLUs) comparatively to body photophores (0.32 RLUs), which results in the spectral curve of the head photophores being similar to the positive control, while body photophores is more flat. Anhydrous commercial guanine have absorbance λmax on 271 nm. Relatively to NaOH, absorbance values are around 3 times higher in samples and the spectral curves show well defined peak, supporting the absence of guanine in negative control solution. Position of λmax absorbance spectra was primarily determined by 10 nm band tests, located between 270 – 275 nm. On 1 nm band tests, the peaks are more clear and for both head and body photophores, absorbance λmax = 271 nm, same as in anhydrous guanine used as positive control.

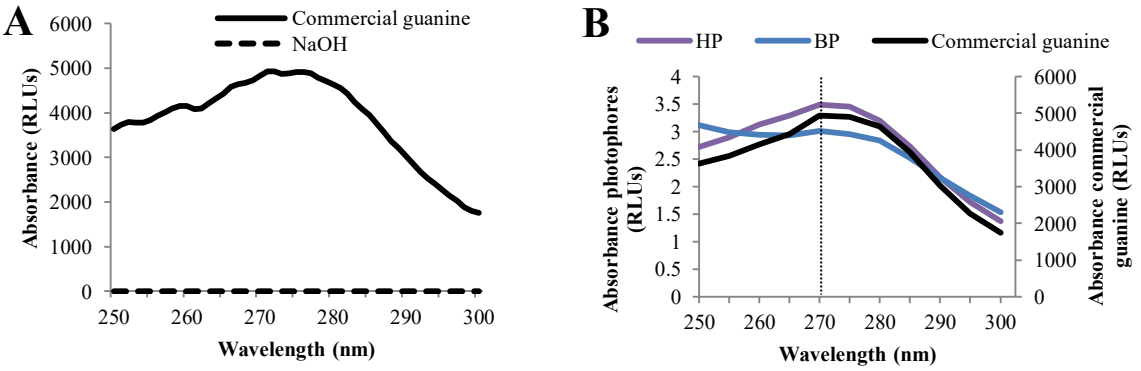

Figure 34 - UV absorbance of guanine from inner reflector of photophores of *D. watasei*, for commercial anhydrous guanine and samples the presented values are corrected for dilutions and NaOH spectra. A) Negative (0.1M NaOH) and positive (anhydrous guanine, NaOH corrected) controls [250 - 270 nm interval, 1 nm band]. B) Head and body photophores, and commercial guanine showing the same peak of absorbance λmax=271 nm (pointed line). HP= Head photophore; BP= Body photophores. RLUs= Relative light units.

a. Arrangement of iridophores and platelets morphology

Body length is higher on *D. watasei* (SL=103.67 ± 3.65 mm, *n*= 5) than *D.* sp (SL=34.59 ± S.D. 0.73 mm , *n*= 5), as for the diameter of body photophores on *D. watasei* (1.07 ± S.D. 0.27 mm, *n*= 9) relatively to *D.* sp (0.42 ± S.D. 0.07 mm, *n*= 9), and eye diameter on *D. watasei* (5.66 ± S.D. 0.31 mm, *n*= 5) and *D.* sp (2.15 ± S.D.0.08 mm, *n*= 5). Morphometric measurements between the two analysed *Diaphus* species show smaller values on *D.* sp for both organs, eye and photophores, adequate to the purpose of variation of iridophores shape in relation to organ size.

Arrangement of iridophores varies between sample reflective tissues (Fig. 35A-C). Silver tissues all have in common multilayers of loosely arranged iridophores, randomly oriented on head photophores inner reflector and skin (Fig. 35E,G) or roughly aligned in lines on iris and body photophore lens reflector (Fig. 35D,F). Note that the aligned iridophores are curved follow according the peripheral curvature of the circular organs and on it seems an oblique angle to the surface of the organ. Coloured reflectors present a higher degree of iridophore organization, tightly packed in hexagonal pattern circumferentially arranged (Fig. 35H,I). In both cases the iridophores are arranged positioned with longer axis perpendicular to the centre of the hemispheric organs.

Reflective tissues analysed shared the characteristic hexagonal elongated shape of guanine platelets, even though some are more elongated than others (Fig. 35J-M). Looking at the width/length distribution, body photophores inner reflector clearly stands out from the other reflective tissues (Fig. 36A). Relatively to other tissues on *D. watasei*, platelets of the inner of body photophores have an unusual low width/length ratio resulting in an almost hexagonal shape (Fig. 36B). Shape is highly conservative for crystals on this tissue, independently of the platelet size, as the variation of width and length is proportional (for more details on averages and standard deviations of platelets shape, see Supplement 2). Relatively to inner reflector of body photophores, other reflective tissues exhibit high width/length ratio, more variation in crystal shape per tissue and some degree of overlap for platelets distribution between tissues. Highest differences in distributions of platelets morphology between inner body photophore reflector and other tissues are confirmed by Student's *t*-test reaching lowest *p* for all run paired tests ($p = 1.83^{-27} – 3.53^{-23} < 0.01$). Guanine crystals "standard" shape is represented by the skin, body photophores lens and head photophores inner reflector, which seem to have very similar shapes even though the platelets are larger in head photophores. This is confirmed by Student's *t*-test, revealing very small differences on distribution of crystals morphology between inner reflector of head photophore and skin ($p = 0.004 < 0.01$), and no differences between head photophores inner reflector and body photophore lens reflector ($p = 0.34 < 0.01$) and between the

latter and skin (p= 0.09<0.01). Reflective tissues in the eye, tapetum lucidum and iris, is also a peculiar case, both composed by the most elongated platelets measured with the highest width/length ratio. Indeed, these two tissues show high differences in distributions of crystal morphology to non-eye tissues, iris (p= 1.60^{-25} – 2.44^{-14} <0.01) and tapetum lucidum (p= 7.71^{-19} –2.60^{-16} <0.01), but not between the two eye tissues (p= 0.28>0.01).

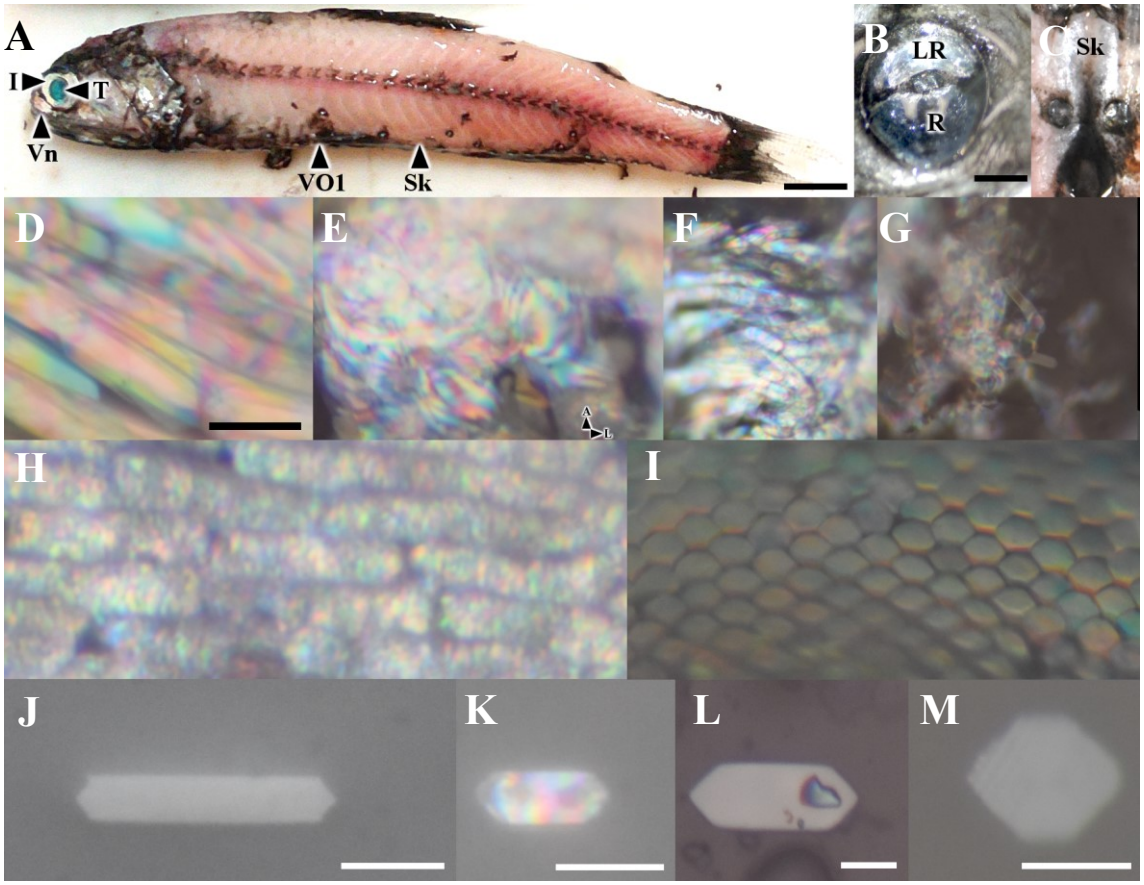

Figure 35 – Reflective tissues in *D. watasei* and respective iridophore arrangement and morphology of guanine platelets. A) Lateral view of fish showing location of sampled reflective tissues. B) Ventral view of VO1 body photophore. C) Ventral view of skin on ventral body surface. Light microscope photographies showing iridophores arrangement on: D) Iris; E) Head photophore; F) Lens reflector of body photophore; G) Skin; H) Tapeta; and I) Inner reflector of body photophore. Light microscope photographies showing examples of guanine platelets morphology on: J) Tapeta; K) Skin; L) Head photophore; and M) Inner reflector of body photophore. I= Iris; T= Tapetum lucidum; Vn= Dorsonasal organ; VO= Ventral organ; LR= Lens reflector; R= Inner reflector of body photophore; Sk= Skin; A= Anterior; L= Lateral. Scale bars= A) 1 cm; B-C) 500 µm; D-I) 50 µm; J-M) 20 µm. Photographs of iridophores arrangement on tissues (D-I) were shot from TEM fixed samples (see Chapter 6).

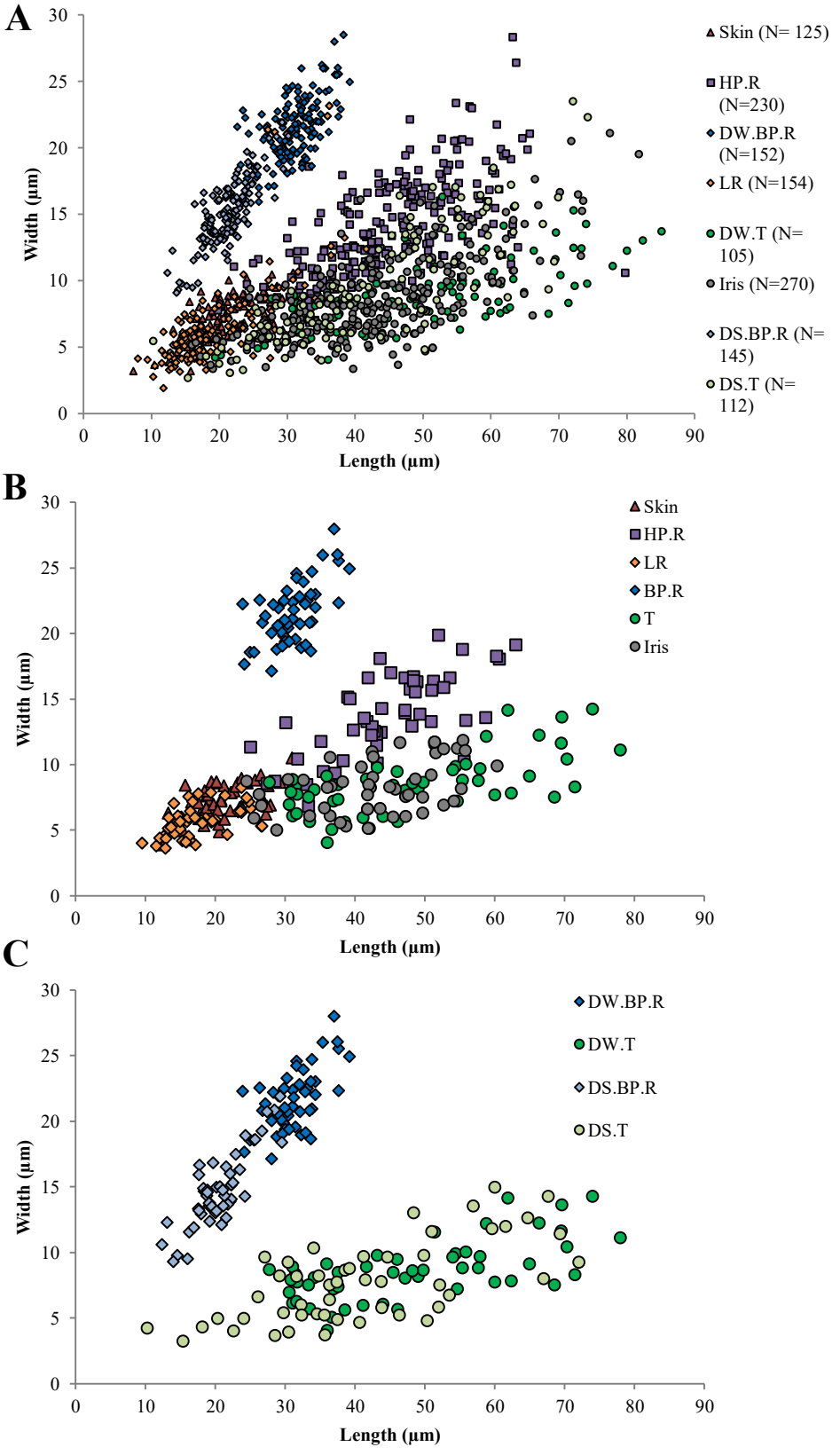

Figure 36 – Distribution plots of platelets morphology from reflective tissues of *Diaphus*: A) Raw data for *D. watasei* and *D.* sp; B) Representative data after removal of outliers and doubles between reflective tissues in *Diaphus watasei* (N= 50); and C) Tapetum lucidum and body photophores between species of *D. watasei* and *D.* sp (N= 50).BP= HP.R= Inner reflector of head photophore; LR= Lens reflector; BP.R= Inner reflector of body photophore; T= Tapetum lucidum; DW= *D. watasei*; DS= *D.* sp.

Similarly to *D. watasei*, platelets shape differs between inner reflector of body photophores and tapetum lucidum (Fig. 36C). On the other side, crystal shape does not vary between *D. watasei* and *D.* sp, neither for inner reflectors of body photophores or tapetum lucidum. This is confirmed by Student's *t*-test results for high differences of platelets morphology distribution between *D. watasei* photophores and *D.* sp tapetum lucidum ($p=4.99^{-21}<0.01$), and no differences on inner reflector body photophores ($p=0.15>0.01$) and tapetum lucidum ($p=0.77>0.01$) between species. Nevertheless, for both tissues, minimum platelet size are lower for the smaller species *D.* sp and the maximum platelet size higher for the larger species *D. watasei*.

4. Discussion

b. Guanine nature of photophores inner reflectors

UV absorbance λmax of inner reflector on head and body photophores matched with anhydrous guanine, confirming the platelets observed to compose the inner reflectors on head and body photophores are guanine crystals. Higher absorbance λmax in head than body photophores indicates higher content of guanine in head photophores. This supports the observed multilayered platelets in head photophores and its thicker inner reflector (see Chapter 2). UV absorbance λmax results are in accordance with previous reports of guanine in tapeta lucida of fishes [160–162] and it is supported by our reports using Fourier-transform infrared spectroscopy (FTIR) and X-ray diffraction (XRD) (see Supplement 3). High refractive index of guanine crystals makes them adequate for structural colour by light interference [124, 125] and high reflection [141] observed on inner reflectors of body and head photophores (See Chapter 5). Reflectors in photophores of luminous fishes are generally assumed to be composed by guanine crystals [117]. Nevertheless, this was only confirmed in midshipman fish *Porichthys* [156], flashlight fish *Anomalops* [133] and the pearleye fish *Maurolicus*[119].

a. Arrangement of iridophores and morphology of platelets

Observed variation of iridophores arrangement seem to be related with the tissues reflection functions. Multilayered iridophores in silver tissues support the observed inner structure of these reflective tissues (See Chapter 2). Head photophores and skin are composed by iridophores with no apparent precise orientation. This type of guanine iridophores arrangement was previously observed in silver skin of fishes, including myctophids [118] and it seems to maximize light

reflection on skin of koi carps [130, 155]. Iris and lens reflector of body photophores have iridophores arranged in lines at an oblique angle from the surface, curving as it follows the peripheral curvature of the organ. This arrangement may be due to similar spatial accommodation as both are thin tissues attached to the inner surface of the exterior lenticular layer of circular organs (cornea in eyes, scale lens in body photophores). Moreover, both tissues have functions of "light shields" to delimit the passage of light, outside to the emission ventral area of photophore for lens reflector [87] and inside to the pupil for the iris [128].

Morphology of guanine crystals in reflective tissues of fishes was previously reported as elongated hexagons, although the size and shape may vary for longer, shorter, thinner or thicker platelets [118]. Unique "perfect" hexagonal iridophores on the inner reflector of body photophores of lanternfishes was previously described [157, 158]. In this study, the shape uniqueness of these iridophores is proven for the first time, by crystal morphometry and statistical analyses, relatively to other reflective tissues on *D. watasei.* Nevertheless, the question still remains: what is the purpose for the exclusive "perfect" hexagonal guanine iridophores on the inner reflector of body photophores? Head photophores are bioluminescent organs with functional inner reflectors, where the iridophores are arranged in disoriented multilayers with large platelets shaped as normal elongated hexagonal in guanine crystals. All these divergences in arrangement and crystal shape between photophores in *D. watasei* indicate that the specificity of "perfect" hexagonal iridophores in body photophores inner reflector, is not related to bioluminescence function of the organ. Moreover, guanine crystals in the photophores of hatchetfish *Argyropelecus* also have elongated hexagonal shape [118]. For iris and tapetum lucidum, both have the same particular longer shape that was only found in these two reflective tissues of the eye, suggesting what might be a case of organ-specific shaped crystals. However, this is not applicable to body photophores, as iridophores in the lens reflector have the common elongated hexagonal shape of guanine crystals.

Tapetum lucidum shares the same hexagonal tight arrangement of iridophores monolayer and structural colour features of inner reflector on body photophores. Moreover, both lay on inner surface of hemispheric shaped organs. As longer iridophores of tapetum lucidum are found in the eye with higher organ diameter, iridophore shape of body photophores could be related to structural colour relatively to the spatial accommodation relatively to the organ size. To test this hypothesis, iridophore shape of both structural coloured tissues in *D. watasei* were compared to the smaller organs of a smaller species of the same genus, *D.* sp. Longer iridophores shape on tapetum lucidum and "perfect" hexagonal ones in body photophores were also found in the smaller species. In this way, the iridophore shape on body photophores is not related to the structural colour function in relation to organ size. Moreover, structural colour was observed in iridophores with typical elongated hexagonal shape of guanine crystals in the skin

of fishes [118, 138, 151]. Vesicles with a precursor crystalline anhydrous found on koi carp skin are responsible for shape manipulation of guanine crystals [149]. Morphologic variety of platelets is organically manipulated for optimization of reflection functions [154], which suggests that the unique hexagonal shape of iridophores on body photophores inner reflector is achieved for a specific additional function besides structural colour.

a. Hexagon iridophores and bioluminescence

The "Honeycomb Theory" is a mathematical model that explains the mechanism behind the natural interlocking geometry of regular hexagonal arrangement, widespread on nature mostly known in the honeycombs of bees [163]. This seems to be the pattern with highest spatial efficiency on covering a surface with tiles of equal shape and size. Hexagonal arrangement maximizes the tiles size while minimizing the spacing of gaps between them. In a curved surface, this interlocking system allows the periphery of the tiles above and below to be meet in the same angle to each other and the six vertices of each tile also oriented in the same angle on each tile. This allows a smoothed curved surface, where all the tiles are oriented in a regular parallel angle to the curved surface

On the scenario of inner photophore reflector, the high spatial efficiency of hexagonal pattern result in the maximum coverage of the reflector surface area with reflecting guanine platelets. Guanine crystals are reported to be formed from the degradation metabolism of guanine nucleic acid [141, 149]. Hexagonal pattern allows the maximization of size iridophores size and taking into account that each is composed by many layered crystals, platelets are reduced to the minimum number possible, representing high energetic conservation in metabolic production of the guanine crystals (Fig. 37A). Hexagonal interlocking allow minimum gaps between iridophores where light from photocytes leaks and is not reflected to outside the photophore. Minimizing the loss of generated energy as photons represents another feature of high energetic performance of the reflector. Tapeta lucida in fishes represent a similar scenario to maximize the light reflection, reflecting the photons back to the photoreceptors which allows doubling the photon catch on visual cells to enhance visual sensitivity [24, 164, 165].

The hexagonal pattern also ensures a regular reflection angle on surface of iridophores positioned in parallel to the curved surface of the reflector (see Chapter 6). From the centre of the reflector to the periphery, when iridophores interlock with the ones positioned above, hexagonal pattern allow the same angle of connected platelets which results in the same angle of reflection between the iridophores (Fig. 37B). Hexagonal arrangement allows positioning of each individual iridophore in which the 6 vertices of the platelets are in the same angle to the

reflector surface. According to the hexagonal crystal geometry [154], this ensures that photons focused from the same direction on the platelet are reflected on the same angle (Fig. 37C). Moreover, as all light reaching the inner reflector is produced from photocytes in the centre of the organ [18, 97, 106, 118, 166], every iridophores receives the same number of photons. Laying with parallel surface to the curved reflector, by reflecting the same light intensity in the same direction, positioning of iridophores, hexagonal arrangement produce the same maximum intensity light output along all the reflector in the same angle (Fig. 37D). Iridophores arrangement in inner reflector of body photophores produces a similar system to reflect light on a regular precise direction as the tapeta lucida in hemispheric shaped eye of sharks [129, 167].

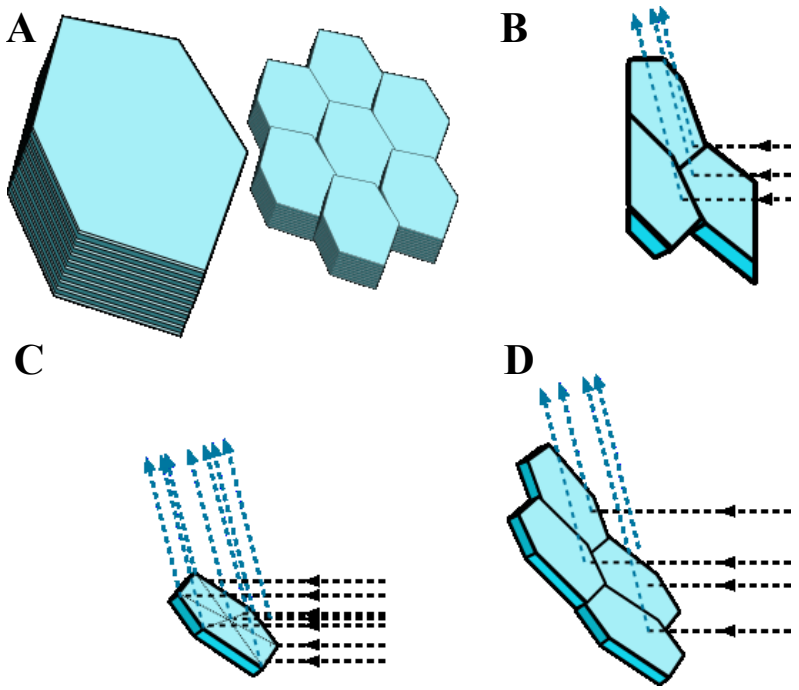

Figure 37 – Schematic illustration of hexagonal arrangement of iridophores in inner reflector of *D. watasei* body photophores. A) Maximized size (left) and half-sized (right) of iridophores occupying the same area showing platelets inside (theoretical number of platelets N=10 for illustrative purposes). B) Regular reflection angle of horizontal light from 3 interlocked iridophores. C) Reflection angle of horizontal light from the edges and centre of one iridophore. D) Overall reflection angle of horizontal light from 4 interlocked iridophores. Dashed black lines represent vertical light angle; dashed blue lines represent angles of reflected light from the iridophores. Black arrow heads indicate the direction of vertical light blue arrowheads indicate the direction of reflected light from the iridophores. Black dotted lines (D) represent the division of iridophore area, crossing at the centre.

Monolayered arrangement in hexagonal pattern results in iridophores oriented to maximize the light reflection output on a regular direction, by allowing all the platelets in the tissue to reflect simultaneously on the same angle. This explains the high intensity of light interference spectra observed on the inner reflector of body photophores (see Chapter 5). In *D. watasei*, inner reflector from hexagonal interlocking of guanine platelets produces a light output characterized by maximized, even and simultaneous light intensity in a precise direction from all iridophores. Additionally, spectra of light emission to outside of the photophore is modulated by the coloured inner reflector [18, 90], on a selected wavelength produced by light interference

from the stacked layers of guanine crystals in the iridophore, reflection spectra being dependent on the cytoplasm thickness between the platelets [117, 118, 124, 125, 141]. Taking into account that counterillumination requires bioluminescence of photophores to match the intensity, angle and spectra of downwelling light surrounding the animal [18, 40, 99, 168], light output from body photophores of *D. watasei* seems to be adequate for a successful camouflage. Counterillumination light is reported to be constantly regulated in *Diaphus* and other lanternfishes to match the environment light intensity [99, 109] by neural pathways [91–95]. Estimated intensity maximization on ventral body photophores from the reflection of hexagonal pattern of iridophores seems perfect to achieve a match to the ambient by the maximum threshold of emitted light intensity. Ventral photophores of mesopelagic fishes are reported to emit light on perfect ventral angle to match downwelling sunlight for counterillumination [18, 103, 117] and downward light emissions were observed on body photophores of lanternfishes *Myctpohum* [99] and *Tarletonbeania* [100]. *D. watasei* photophores are positioned in the body on an angle to ensure that all light from the inner reflector surface is emitted outside the organ on a ventral angle (see Chapter 4). Ventral bioluminescence emissions from the surface of the inner reflector with hexagonal pattern of iridophores that ensures light reflection in the same direction, indicate a good match to the ventral angle of downwelling light. Bioluminescence of lanternfishes [101, 102, 110] and from the inner reflector of *Diaphus* [18] has λmax= 460 - 490 nm, namely λmax= 460-470 nm from ventral body photophores of *D. watasei* (See Chapter 5) which matches with the light peak of the mesopelagic zone (λmax= 472 – 486 nm [17]) for a successful counterillumination [120]. Additionally, sapphirinid copepods have cuticle with hexagonally interlocked iridophores that are spectrally tunable for camouflage purposes [154, 159].

a. Conclusions

Guanine nature of inner reflector of lanternfish head and body photophores is confirmed for the first time in this study. Guanine crystals are adequate for structural colour and high light intensity [124, 125, 141] observed in *D. watasei* photophores. This chapter includes the first morphological and statistical examination of “perfect” hexagonal shaped guanine crystals from inner reflector of lanternfish photophores. In this study it is contained as well the first physical approach of light reflection on hexagonal interlocked guanine iridophores on light organs of bioluminescent animals. It was found that the hexagonal arrangement of iridophores ensures maximum intensity along all the reflector in the same angle to match downwelling light in the deep-sea, for a successful counterillumination in the mesopelagic realm [16, 103]. Moreover,

this pattern of iridophores seems to achieve high energetic efficiency by minimizing metabolic costs of iridophores and the light losses on gaps between them.

Future analyses should be developed for a deeper examination of the biophysical implications of light reflection on the hexagonal arrangement of iridophores in lanternfish photophores and its energetic performance. Spectrometry of individual iridophores under epi-illumination microscope and biophysical modelling of energetic costs for metabolic manufacture of guanine crystals and photon losses on gaps between iridophores, would be valuable to understand better the light reflection and energetic performance of hexagonal interlocking of iridophores. To allow an adequate angle of light emission for counterillumination, reflector shape where the iridophores lay needs to be estimated, which can be found in the next Chapter 4.

CHAPTER 4

Parabolic inner reflector on body photophores

1. Introduction

The ocean surface is bathed by sunlight at daytime, and starlight and/or moonlight at night. Even though the spectral, intensity and angular light parameters are fairly different between these astral illumination on the epipelagic ambient [20, 120, 169], as further the photons penetrate the pelagic depths the downwelling light becomes more and more uniform [3, 17, 19]. Water molecules, phytoplankton and particulate matter in the epipelagic waters rapidly absorb and scatter light of long and shortwave wavelengths of the visual spectra [3, 16]. Comparing to epipelagic, only dim light on vertical angle of a narrow waveband on blue-green reaches the mesopelagic zone [3, 16, 17, 19]. Upper mesopelagic is an extended light scene mainly irradiated by downwelling light, only some of that light reaching the lower mesopelagic below, becoming point source light scene mainly illuminated by bioluminescence [3, 20, 21]. Level of visual adaptation of deep-sea fish species to these two light scenarios are dependent on species natural histories and environment they inhabit [3]. In the case of lanternfishes, highly sensitive eyes can detect sunlight and bioluminescence signals at long distances with extreme efficacy [3, 23].

Mesopelagic fishes have, besides the remarkable eyes, other astonishing traits of adaptation to the particular and complex light scenario of this twilight zone. Possibly the most distinctive characteristic of mesopelagic fishes is the high incidence of bioluminescent species and abundance [50, 170]. This is related to the unique light parameters of this dim environment where no visual obstacles can be found, allowing bioluminescent signals to be seen at long distances [50, 54]. Despite the diversity of multifunctional ecological roles of biological light signalling for intra- and interspecific communication roles, counterillumination is the most widespread on mesopelagic animals and highly incident on these species when compared to the ones inhabiting other depths [3, 40, 50, 53]. Regular vertical angle of dowelling light penetrating these depths with narrow wavelength range [3, 16, 54], makes it simple, relatively to shallower waters, to match by light emissions of ventral photophores [16, 54]. On the other side, sunlight does not reach the aphotic depths from bathypelagic and below which does not make light camouflage such an ecological advantage at those depths [1, 2]. Altogether, this explains why counterillumination is such a particular feature of mesopelagic fishes and general fauna.

Photophores of mesopelagic animals reach the structural zenith of complexity on the planet [50]. Euphausiids and have light organs with specific multi-reflectors, generally an inner coloured tissue and accessory silver structures for counterillumination [42, 114–116]. Structural coloured reflector alters the wavelength of light emitted from the photocytes and the silver reflectors guide it to outside the organ on a ventral direction, ensuring an adequate match of spectra and angle to the downwelling light on the deep waters [117]. Similar system of

reflectors is present in photophores of lanternfishes which bears an inner glue-green reflector and an accessory silver lens reflector [18, 87, 97, 108]. Lens reflector is proposed to be a "light shutter", blocking light to be emitted outside on the area of the photophore covered by this tissue [87]. Inner reflector is a good spectral match to the downwelling light on the deep sea which suggests its role as spectral modulator for counterillumination [18]. In fact, the angle of light emissions from ventral photophores of deep-sea fishes and its relation to counterillumination was only reported for the viperfish *Chauliodus* and the hatchetfish *Argyropelecus* [103]. Additionally, the silver inner reflector on the latter species was examined and found that it acts as multifunctional reflector mechanism to guide light from the photogenic chamber to outside the organ in a ventral angle [118]. Light emissions were observed to be directed in ventral direction from body photophores of lanternfishes [99, 100] but from the point of view of angle of bioluminescence, there are no records of any analyses whatsoever for any of the two reflective tissues.

Parabolic mirrors are characterized to reflect all light on a vertical angle [171] which is why it is widely used in giant telescope segmented mirrors [172]. As far as I am aware, this was never applied on biological reflective tissues, which became one of the aims of my thesis, presented in this chapter, after noticing on histological sections (see Chapter 2) of ventral body photophores of *Diaphus watasei* that the inner reflector shape resembles a parabola. Additionally, potential for light guidance of the accessory silver lens reflector was included on the study. With histology, digital image processing and mathematical calculations, a novel biophysical approach for reflective system of photophores based on parabolic mirror was performed in order to determine the mechanism to match the angle of downwelling light on lanternfishes.

2. Materials and methods

As in this chapter is established the first methodology for inner reflectors parabolic in bioluminescent photophores, methods are adequately described to be reproduced in future studies. Sampling of *D. watasei* and posterior methodological procedures for preparation of histological sections were same as in Chapter 2. Photographies of histological sections under 10x magnification of three ventral body photophores (PO3, VO1 and VO2) were selected for estimation of inner reflector shape.

As described in Chapter 2, angle in which the organ lays on the surface of the fish body varies even between ventral photophores, namely between pectoral (PO3) and pelvic (VO1 and VO2) ones. Small angle variation between ventral body photophores was not significant for the

aims of Chapter 2, but as in this chapter is required a more realistic approach, the horizontal angle of photophore in the body surface was estimated. Photophores were dissected by group, i.e, the pair of photophores located symmetrically on opposite sides of the sagittal axis of the ventral surface of the fish body, which can be observed on sections under stereo microscope (Fig. 38A). More dorsal edge between pair of photophores and tracing a line from this point to the most ventral edge of photophore that suffered less deformation of the pair during the histological sections procedure. Horizontal angle was estimated between these two lines. Finally, photographies of histological sections of the 3 ventral body photophores were tilted according to the estimated horizontal angle (Fig. 38B-C).

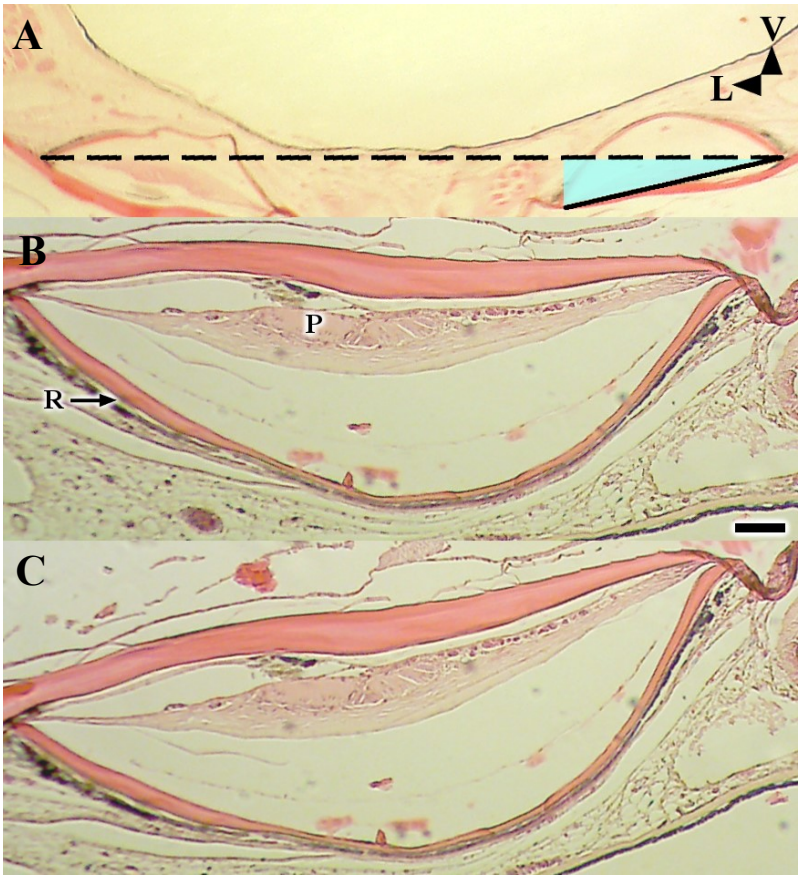

Figure 38 - Photographs from anterior view of histological sections from *D. watasei* 's VO1 ventral photophores exemplifying the procedure to position the organ on correct horizontal angle that is naturally on the fish body surface. A) Stereo microscope photograph representing the line traced between lateral edges of both photophores of the pair (dashed line), traced line between the lateral edge and ventral edge of the organ (solid line) and horizontal angle of photophore (light blue transparent triangular area). Microscope photographies of photophore A) before and C) after horizontal angle correction. P= Photocytes; R= Inner reflector; VO= Ventral organ; V= Ventral; L= Lateral. Scale bar= 100 µm.

Photocytes and iridophores were identified as described on methodology of Chapter 2. To sample the inner reflector shape and the position of the photocytes group, 3 replicates of sample points (SA.P) were traced, in crescent order from the lateral to the ventral periphery of the reflector (N=20) and the periphery of the perimeter tissue (Fig. 39A). This allow to obtain the numeric position of the sampled points by vertical and horizontal coordinates which were

plotted in graph (Fig. 39B). Points along parabolic curve can be calculated from quadratic function that defines the parabolic curve [171]. A quadratic equation was approximated from the distribution of the measured sample points to define the parabolic curve representing the shape of the inner reflector, for each replicate. One replicate for each photophores was chosen for posterior calculations, criteria for the selection being the highest R value, which represents the replicate for which the approximated quadratic curve describe more accurately the distribution of sample points, and consequently, the reflection shape.

On quadratic equations, $ax^2 + bx + c$, the a value describes the parabolic curvature, wider parabolas with lower a values. Focus is described as the point on the vertical axis equidistant from the vertex and the *latus rectum* (Fig. 39C). Any point of the parabolic curve is at the same distance to the *latus rectum* and the focus point, so when these two distances are divided the obtained value is 1. This value defines the eccentricity (e) which distinguishes conical sections, ellipse circle e= 0, ellipse e< 0, parabola e=1, and hyperbola e>1 [173]. According to the mathematical description of the parabola, focus point and eccentricity were estimated from the quadratic function approximated to the sample points of the reflector, to describe the parabolic curve of the reflector shape. From the vertex (0,0) and the a value of the quadratic equation, focus point can be estimated $(0, \frac{1}{4a})$. *Latus rectum* was calculated as the line vertically equidistant of the focus point to the vertex and a random point (any than the vertex) was calculated from the quadratic equation. Distances from this point to the *latus rectum* and the focus point were calculated and divided, estimating the eccentricity of the parabolic shape of the inner reflector of photophore. The eccentricity e=1 confirms that the reflector shape is a parabola and it behaves like a parabolic mirror [171]. According to the theory of reflection on parabolic mirrors, any light from the focus point is projected by the reflector upwards on vertical angle (Fig. 39D). Extrapolating to the inner reflector of body photophores, if the reflector is parabolic and the light source (photocyte cell) is located on the focus point, all the light is emitted on a vertical angle, which allows to explain the modulation of light emission angle from the photocytes to outside the organ, by the reflector, that is assumed to match the vertical angle of downwelling light penetrating mesopelagic waters for an adequate counterillumination [40, 103]. Horizontal angle and sampling points were measured using ImageJ 1.50i (National Institutes of Health, USA) and respective points coordinates exported to Microsoft Office 2000 Excel (Microsoft Corporation, USA) for approximation of quadratic curves, to estimate descriptive parameters of parabola, basic statistical analyses, quadratic tables and graphs.

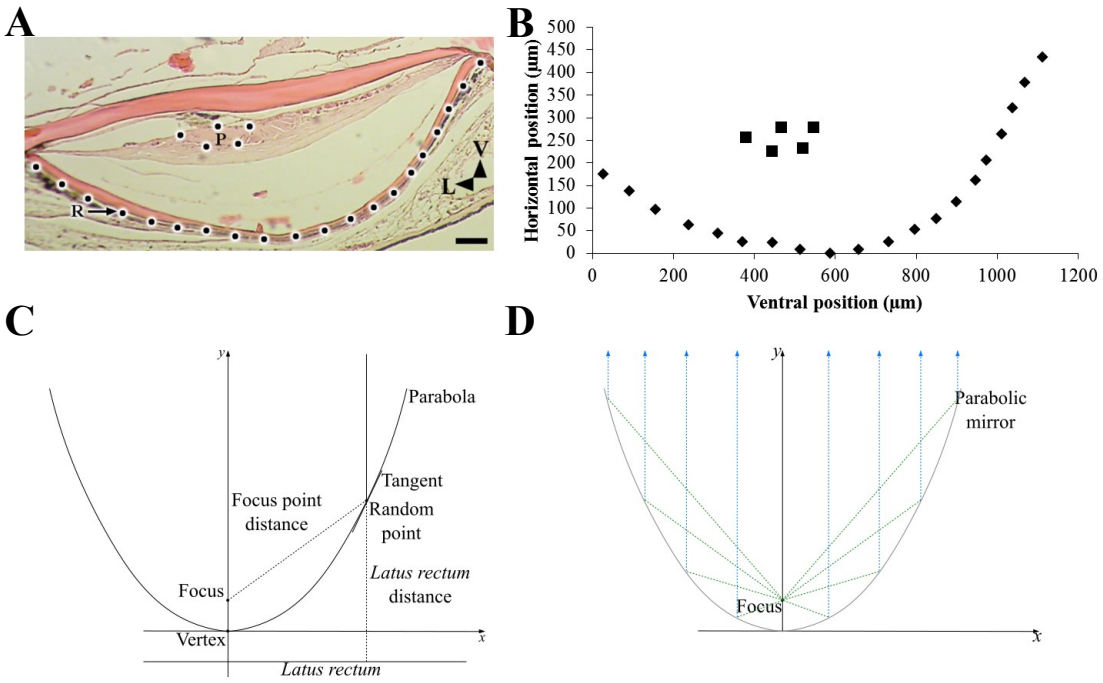

Figure 39 – Schematization of methodological procedures established for estimation of parabolic curve parameters in inner reflector of *D. watasei*'s ventral body photophore. A) Anterior view of histological section example (VO1) showing sample points (SA.P) on reflector (crescent order from left to right) and photocytes group. B) Position of reflector surface traced from sample points in (A). C) Illustration of a generic parabola showing the referent vertex, focus point, *latus rectum*, tangent and eccentricity (adapted from [171, 173]). D) Schematic illustration representing the reflection on parabolic mirror from the focus point [171]. P= Photocytes; R= Inner reflector; VO= Ventral organ; V= Ventral; L= Lateral. Dashed green lines represent the light emited from the focus point and blue dashed lines the reflected light by the parabolic mirror. Scale bar= 100 µm.

3. Results

Horizontal angle varies between photophores examined (PO3= 16 º; VO1= 14 º; VO2= 26 º) from different parts of the fish. Average values only show the position of the points it will not be presented (for more detail on averages and standard deviation per sample point (SA.P), see Supplement 4). Standard deviation of sampled points from histological sections represent variation of points position (Fig. 40). Some variation is observed on the same degree for all the photophores and does not seem to be any tendency for more variation in any specific sample (S.D; PO3: horizontal= 2.7 µm [SA.P 1] – 25.75 µm [SA.P 9], vertical= 1.02 µm [SA.P 20] – 14.79 µm [SA.P 18]/ VO1: horizontal=1.5 µm [SA.P 20] – 44.94 µm [SA.P 12]; vertical=1.35 µm [SA.P 8]– 25.7 µm [SA.P 17]/ VO2: horizontal= 2.31 µm [SA.P 6] – 74.99 µm [SA.P 7]; vertical= 0.38 µm [SA.P 4]– 12.32 µm [SA.P 7]).

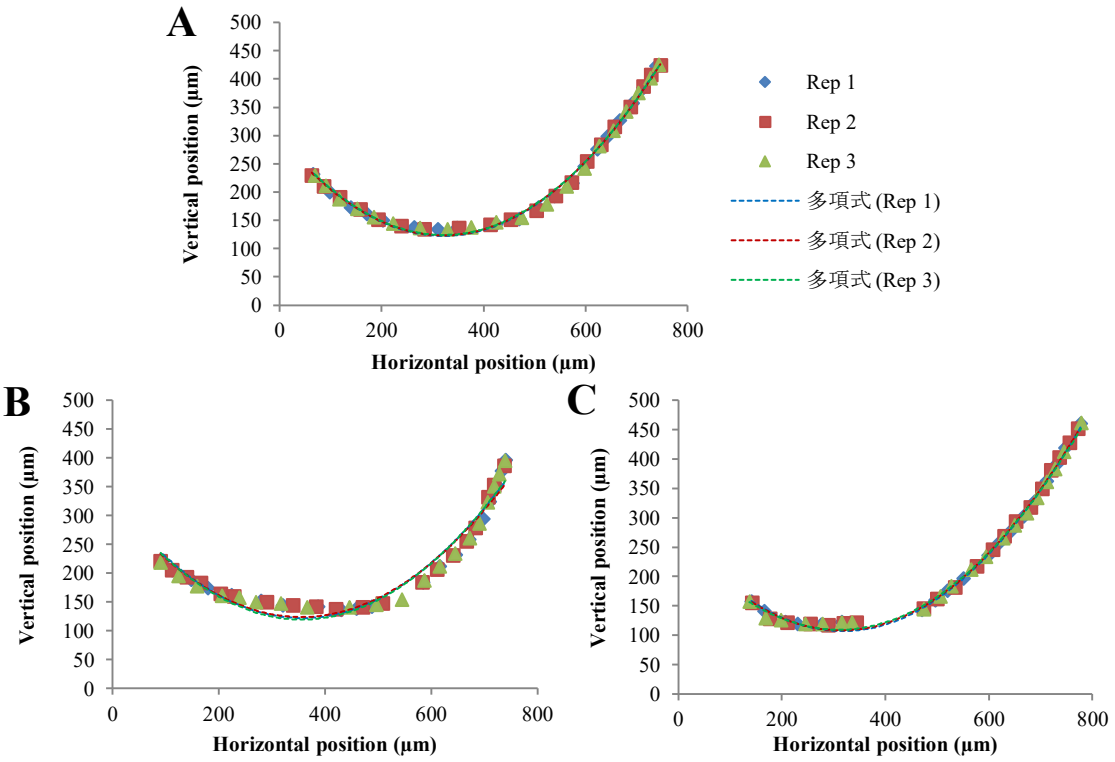

Figure 40 - Raw data of position of sampling points and respective approximation quadratic curves from inner reflectors of *D. watasei*'s ventral body photophores: A) PO3; B) VO1; and C) VO2. PO= Pectoral organ; VO= Ventral organ; Rep= Replicate.

Parabolic curves are similar between photophores as the parameters that describe parabolic curves have close values (Fig. 41). *a* values of quadratic equations are low, representative of parabolas with wide curvature, all replicates for each photophore show the same value (*a* value; PO3= 0.0017; S.D. VO1= 0.0016; VO2= 0.0016). Approximated quadratic equations to the sampled points have values of R^2 close to 1.00, representing a good fit to the reflector shape (R^2; PO3= 0.99-1; VO1= 0.95; VO2=1.00). Eccentricity values are close to 1.00, that describes a parabola, indicating that the reflector are close to a parabola (*e*; PO3= 1.02; VO1= 1, VO2= 0.98). Focus point is located on the top of the photocytes group for all photophores examined.

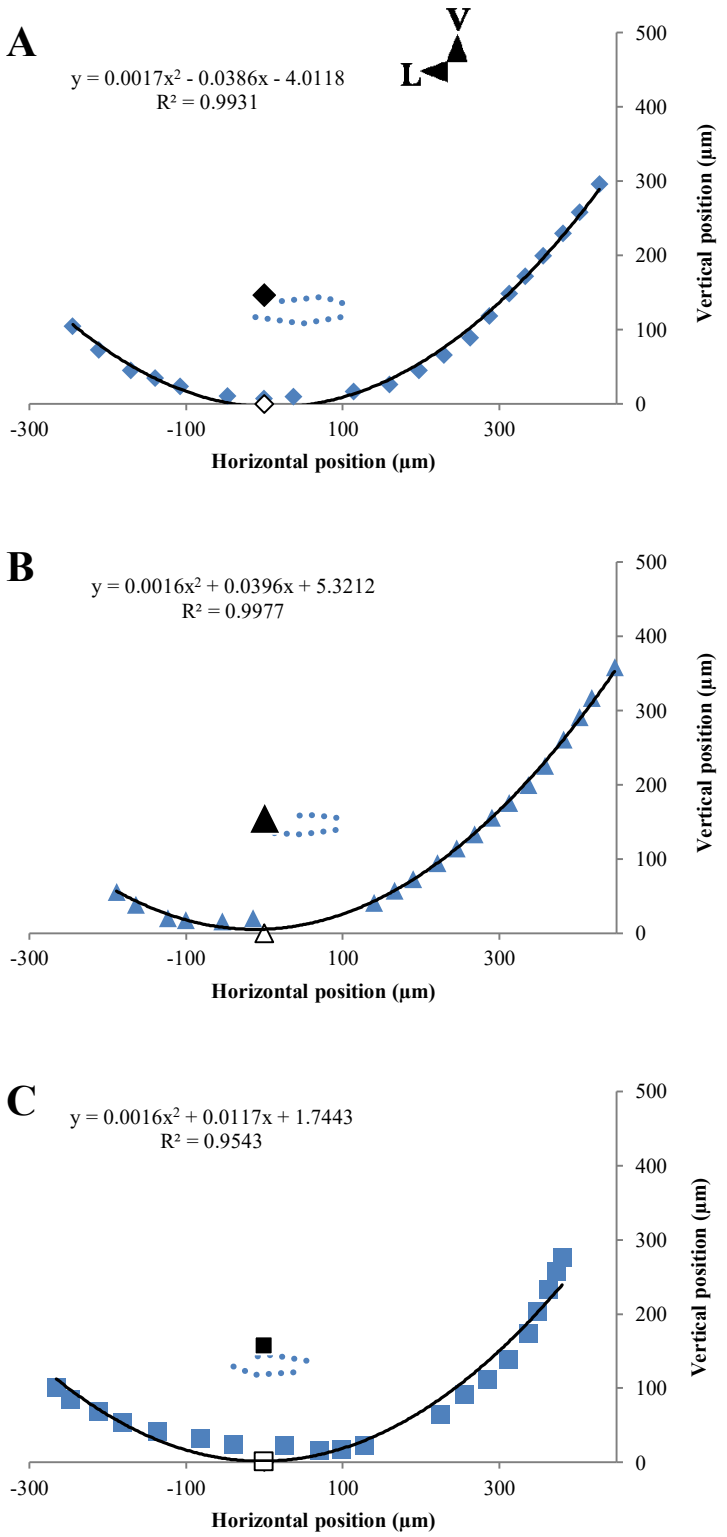

Figure 41 – Position of sampling points traced from inner reflector of *D. watasei*'s ventral body photophores, after normalized vertex position (x=0, y=0), and respective approximated quadratic curves, photocytes area and focus point for photophores: A) PO3; B) VO1, and C) VO2. PO= Pectoral organ; VO= Ventral organ; V= Ventral; L= Lateral. Black symbols represent focus point and white symbols vertex. Black lines represent the curves calculated by approximated quadratic functions from the sampled points. Dashed lines represent photocytes area.

4. Discussion

b. Parabolic shape of the inner reflector

Shape of the inner reflector on ventral body photophores is parabola-like curve, confirmed by the estimated quadratic equations and respective parameters, that are used to mathematically describe a parabola. *a* value does not vary between replicates of each photophore which suggests that the approximated quadratic functions fit well to the sample points tracing the reflector. This is confirmed by the quadratic functions R^2 values (0.95 – 1) close to 1, indicating a significant fitness of the estimated model function to the sample points distribution. Eccentricity characterizes the shape conic sections, measuring its deviation from a circle [173]. Eccentricity value $e=0$ describes a circle, $e<1$ an ellipse, $e=1$ a parabola and $e>1$ an hyperbola. Looking at the eccentricity of the quadratic equations for the examined reflectors, we can see that for VO1 $e=1$ is the closest to parabola, while VO2 $e=0.98$ is mathematically an ellipse with tendency for parabola, and PO3 $e= 1.02$ an hyperbola with tendency for parabola. In this way, the calculated shape of reflectors are not all representative of mathematical parabolas, which is defined in this study as "parabola-like" shape. However, variation found between replicates for position of sampled points tracing the reflector curve is probably the cause of deviation from mathematical parabola, resulting in the calculated parabola-like reflector curves. Variation of measured position of sample points is assumed to be related with minor tissue deformations during fixation and histological sectioning. This assumption is supported by the small variation values and the lack of tendency on these for deviation from mathematical parabola for the estimated quadratic functions, either for ellipse or hyperbola. Then, it is assumed that the estimated parabola-like reflector curves are very similar to each other and thus reflect light in the same way, as described on the theory of reflection in parabolic mirrors [171]. According to this theory, on parabolic shaped mirrors, light emitted from the focus point is reflected on a vertical 0^o angle for all points of the curve. Focus point calculated from the quadratic equations are located on the top of the photocytes for the 3 analysed photophores. Position of focus point on the photogenic tissue ensures that light emitted from these cells is reflected in a vertical angle to outside the photophore. Deviation of focus point from the middle area of top of the photocytes on PO3 and VO1 is assumed to be also a repercussion of the quadratic equations variation from minor tissue deformations.

a. Light emission angle and counterillumination

Iridophores and contained guanine crystals need to accomplish a final structural requirements for the "parabola-like" reflector be functional as a parabolic mirror. Angle of light reflected from the focus point by a point *P* on the parabola curve is defined not only by the coordinates of focus point, coordinates of *P* but also the tangent line of *P* on the parabolic curve [171]. To fulfil the requirement of the tangent of *P* in the mathematical model, guanine platelets in iridophores are oriented parallel to the surface of the reflector in ventral body photophores (see Chapter 6). Moreover, the hexagonal arrangement of the iridophores allow simultaneous reflection with maximum and regular intensity on same direction for all the iridophores (See Chapter 3). This orientation of platelets and reflection output is adequate to ensure the light reflected by the iridophores follow the parabolic shape of the tissue. Curiously, giant telescopes use parabolic mirrors with hexagonal segments for similar purposes, such as Keck Observatory in Hawaii [172].

Position of the photophores in the ventral surface of the fish body results in the vertical light from the parabola-like reflector to be emitted in a ventral direction (Fig. 42A). On the mathematical model of parabolic reflection, light reflected by the parabola curve on vertical angle is emission from the focus point [171]. However, in lanternfish photophores, light is not emitted from a focus point but in reality from one group of many "focus points", i.e. the photocyte cells [18, 97, 106]. As the focus point were estimated on the top of the photocytes group, the point of maximum distance from the focus point is then located on the bottom of the photocytes. Effect of off-axis light emission on parabolic mirrors reflection angle was theoretically demonstrated by [174]. Light emitted from photocytes between the top and the bottom of photogenic tissue and focused on the inner reflector is projected outside the photophore from ventral to slightly lateral angles. Lens reflector located on the lateral side of the body photophores functions as a light shield avoiding light to be emitted outside [87]. Light produced by bottom photocytes and reflected on deviated lateral angles from the ventral are blocked by the lens reflector, which as the role to avoid light to leak in lateral angles (Fig. 42B). Even though the iridophores arrangement could not be observed clearly on histological sections (see Chapter 2), the arrangement of oblique platelets to the organ surface (See Chapter 3) and broad band reflection (See Chapter 5), are adequate for a light guide light to outside in a vertical angle. Similar mechanisms are reported in silver reflectors on photophores of hatchetfish *Argyropelecus* [103, 118], and accessory silver reflectors that guide light from main inner structural coloured reflector on euphausiids [42, 114] and squids [115, 116] for counterillumination purposes [117]. In a similar way, the lens reflector might function guide the light from the inner reflector on the lateral side of the photophore, projecting it to the emission

side of the photophore. Light projected by the lens reflector, passing through the photocytes, is re-emitted outside by the inner reflector on a vertical angle. In this way, the lens reflector might not function as a shutter to avoid lateral light leaking but also as a light guide, to ensure that all the light is reflected on a ventral angle. Below 200 m, downwelling sunlight penetrates ocean water in a constant vertical angle to which the angle of bioluminescence needs to match to ensure an advantageous counterillumination [3, 103]. Ventrally directed light emissions from ventral photophores of *D. watasei* match perfectly the angle of downwelling light on the mesopelagic zone, where this lanternfish inhabits. Bioluminescence emissions from the photocytes is angle modulated by the parabola-like inner reflector and guided by the accessory lens reflector, on *D. watasei* ventral photophores to achieve a successful counterillumination.

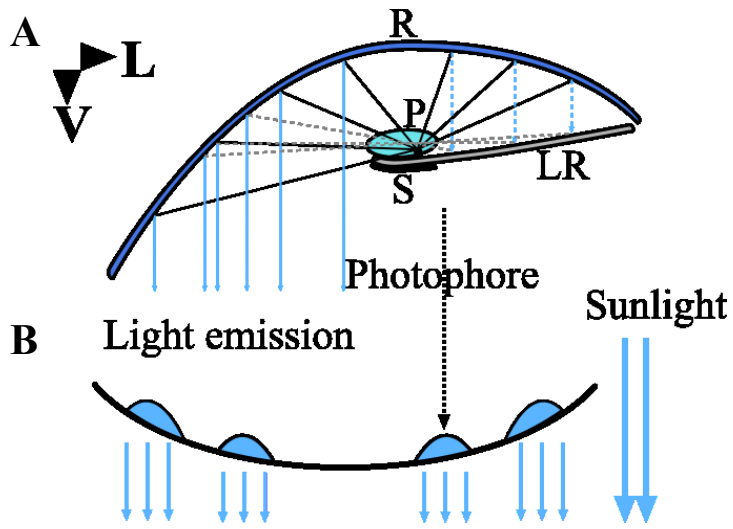

Figure 42 – Schematic illustrations of angle of bioluminescence of *D. watasei*'s ventral body photophores for counterillumination. A) Light emitted from the photocytes is reflected by the inner reflector on a vertical angle in ventral direction (light on the lens reflector side is omitted). B) Position of the of parabola-like shaped photophores on ventral body surface of the fish and their light emission angle related to downwelling sunlight at mesopelagic depths. Blue and silver dashed lines indicate the direction of light from the inner reflector to the lens reflector on and from the latter again to the inner reflector of the emission side of the photophore, passing through the focus point, to emit light outside, respectively. R= Inner reflector; P= Photocytes; S= Septum; LR= Lens reflector; V= Ventral; L= Lateral.

On a transversal plane, angle vertical of body surface in fishes diminishes from ventral to middle lateral just below the lateral line [103, 118] where lateral photophores of lanternfishes reach the maximum dorsal position [63, 87]. Photophores are dermal organs on lanternfishes [109] and other mesopelagic fishes [175] and would tend to follow the surface inclination. Indeed, it was found that the horizontal angle of the examined ventral body photophores enhances (i.e. vertical angle diminishes) as the organ location on body becomes more lateral. On ventral photophores, the surface angle does not seem to vary enough to alter the emission from vertical angle. This is supported by the high similarity in parabolic parameters and focus point positioned on the photocytes group for the 3 photophores tested, differently located on the ventral body surface. On a scenario where the inner structure remains the same, smaller vertical

angles of body surface where lateral photophores lay would alter the emission to significantly lateral angles, comparatively to ventral photophores. However, inner structure seem to vary according the location of the photophores on the fish body (See Chapter 2). As photophores are located more lateral, scale lens gets thicker, on the inner reflector only the dorsal area remains functional and the iridophores inclination enhances. Variation of inner structure on lateral photophores may have the purpose to compensate the lower vertical angle of body surface where these organs lay, comparatively to vertical photophores. Angle compensation by inner structural alterations should allow vertical light emissions on a ventral direction for an adequate counterillumination.

Morphometric analyses for photocytes area, angle of iridophores inclination on inner reflector and scale lens thickness vary in accordance to the location of the organ on the fish body photophores, from ventral to lateral location on the fish body (See Chapter 2). Among ventral photophores, pectoral organ PO3 was a clear exception. In this chapter, *a* value of PO3 on the 3 replicates is slightly higher than the two pelvic photophores and $e > 1.00$. While in the pelvic photophores *a* and *e* do not vary in accordance, it happens for PO3 which results in a wider parabola-like with tendency for a hyperbolic curve [171, 173]. Comparing to other photophores, exceptional variation on parabolic parameters and morphometric values of PO3 might be related and could be a consequence of tissue deformation. On the other side, one cannot exclude the possibility that the divergence in body shape on the transversal plane of pectoral and pelvic areas of the fish body may require slight differences in inner structure of the photophore tissues to achieve an adequate emission angle for counterillumination. To understand this scenario, morphometric measurements and reflector curve analyses should be performed from the inner structure of other pectoral ventral photophores.

a. Conclusions

Angle of light emission for counterillumination was previously reported for non-parabolic silver reflectors of mesopelagic hatchetfish *Argyropelecus* [118], general light emission angle on deep-sea viperfish *Chauliodus* [103] and shallow water ponyfishes *Gazza* and *Leiognathus* [176]. Downward light emissions were observed on body photophores of lanternfishes *Myctpohum* [99] and *Tarletonbeania* [100]. Parabolic In this chapter is established the first biophysical approach of parabolic reflectors in luminous fish photophores for counterillumination, using lanternfish *D. watasei* as model. Parabola-like inner reflector with focus point located on the photocytes and an accessory lens reflector as light shutter and guide,

reflects light emissions on a ventral angle that matches the downwelling sunlight in deep-sea for a successful counterillumination.

Investigation work in this chapter will be continued in the future for a deeper knowledge of the reflection system on lanternfish photophores. X-ray microtomography will be performed on lateral an ventral body photophores of *D. watasei* and posterior 3D modelling of paraboloid inner reflector and accessory inner structures. Besides the angle, spectra of light emission from body photophores of *D. watasei* to downwelling light is required for counterillumination. Analyses on this subject will be presented in the following Chapter 5.

CHAPTER 5

Spectral modulation of light emission in body photophores

1. Introduction

Bioluminescence is the light produced by animals itself from chemical reaction where, generally, in the presence of oxygen as co-factor, luciferin substrate is oxidized by a luciferase enzyme, producing light [30]. Among the classes of luciferins, coelenterazine is widely spread on photophores of marine animals, inclusively present in lanternfishes [34, 37, 89, 90]. Although, fishes are not capable of synthesize coelenterazine which, together with high concentration of this luminous substrate on the digestive tract of these animals, suggests diet to be the source of coelenterazine input [32, 34]. Similar case is reported in midshipman *Porichthys* that obtains *Cypridina* luciferin by ingesting ostracods [36, 38]. Within the diverse fauna of coelenterazine "users", peak of light emission varies between different types of luciferase between wavelength λmax= 452 – 480 nm from decapods *Heterocarpus* [30] and *Oplophorus* [177] to sea pen *Renilla* [178] and copepod *Metridia* [179].

Mesopelagic fishes are commonly bioluminescent and use counterillumination as defence strategy from the visual predators [40], such as the majority of other fauna that inhabits these depths [16, 54]. Extended light scenario of dim downwelling light with no visual obstacles [50, 54], penetrated by narrow blue-green spectra on a regular vertical angle make the mesopelagic zone the most advantageous depths for counterillumination [2, 50, 120]. From the upper to the lower mesopelagic, downwelling light becomes dimmer and bioluminescent signals more visible, resulting in an environment with a complex gradient of two light sources [3, 20, 51]. Such as other mesopelagic luminous fishes, lanternfishes have highly sensitive vision to both downwelling and bioluminescent light sources [29, 74]. These visual adaptations crucial for the survival of these animals as they perform diel vertical migrations to shallower waters from dusk to dawn, encountering changing of light scenarios from the mesopelagic zone where they inhabit at daytime [1–3, 74]. In the particular case of midwater migrators such as *Diaphus*, they do not reach the ocean surface at night [75], namely in *D. watasei* that migrates from 2005 to 258 m depth [180].

For a successful counterillumination, besides intensity and angle, light emissions must match the downwelling light spectra at the depths which the animal inhabits [40], mesopelagic zone in the case of lanternfishes [13, 75–77] which is illuminated by a range of wavelength λmax= 472 – 486 nm [17]. The majority of mesopelagic animals ensure the spectral adequacy by filtering the light emitted by the photophores with outer pigmented filter below the lenses, which "cuts out" the wavelengths that are far from the range of downwelling light [18, 43, 120]. Rare cases are observed in euphausiids [42, 114] and squids [115, 116]. that possess inner coloured reflectors to alter the light spectra projected from the photogenic tissue. Among fishes, this kind of reflectors instead of pigmented filters are only reported in lanternfishes, for the

same purpose of counterillumination [18]. Reflectors of photophores in fishes are widely assumed to be composed by guanine crystals [117] which have the capacity of structural colours [124], such as observed in skin of shallow water fishes for camouflage [138, 140, 145, 151]. Parallel guanine platelets in iridophores with high refractive index, alternated by cytoplasm spacing of lower refractive index are able to produce reflective colours by light interference [118, 141], spectra becoming gradually on long waves as the thickness of cytoplasm enhances or the angle of light incidence on the surface of the platelets diminishes [124, 125]. However, the spectral mechanism behind the coloured inner reflector of lanternfishes is still unreported.

Spectra of light interference is manipulated by osmoregulation in tunable iridophores of fishes skin for camouflage [138, 145, 146, 151] with a very similar inner structure as the observed for the inner reflector of body photophores on Chapter 2. Additionally, even it is not yet confirmed, osmoregulation is proposed to be the system behind the tunable iridophores in sapphirinid copepods [159] which are arranged in an hexagonal interlocking pattern for camouflage [141, 154], similarly to the observed in Chapter 3 for the inner reflector of ventral body photophores of *D. watasei*. Moreover, the spectral manipulation on this coloured reflector of light from photocytes in [18, 90] was based on spectra of bioluminescent reaction between *Diaphus* luciferase and *Cypridina* luciferin by [181], and as it is known by now that is lanternfishes use coelenterazine [34, 37, 89, 90], representing an inaccuracy of spectral estimations for reflection of light from the photocytes. Altogether, it seemed essential to measure the inner reflector spectral modulation of light from the actual *Diaphus* luciferin-luciferase and if it has some level of variation that are adequate for tunable iridophores. Additionally, reflection spectra of other reflective tissues analysed on Chapter 3 was required for comparison purposes and reflective function of the tissues. This chapter is focused on such analyses by using methods of biochemistry to obtain purified *Diaphus* luciferase and spectrometry to measure the spectra of such reaction and inner reflector.

2. Materials and methods

a. Luciferin-luciferase reaction spectra

Deep-frozen fishes of *D. watasei* species were collected on 20.04.2018 at Mimase fishery port in Kōchi city (高知市御畳瀬支所), Japan (see Chapter 2). Two individuals was picked from -80ºC and defrosted on ice, with the aid of a distilled water squirt. Procedures for purification of *Diaphus* luciferase and luciferin-luciferase reaction was adapted from [30, 34]. Thirty body photophores were dissected with mini-scissors and fine forceps, and mashed for 5 minutes with

a plastic pestle in 1 ml eppendorf tubes with 500 µl of extraction buffer (20 mM Tris-HCl, 50 mM EDTA, pH8.2) with 50 mM DDT and protease inhibitor (Nakalai tesque Inc., Japan). Samples were centrifuged (4ºC, 17400 G, 20 min) in a high speed refrigerated micro centrifuge (MX-100, Tomy Digital Biology Co. Ltd., Japan) and the supernatant collected to tubes with 0.45 µm centrifugal filter (Merk Millipore, USA) and posteriorly 10K centrifugal filter (Merk Millipore, USA) ,centrifuged under the same conditions. The first filtration removes tissue remains on supernatant and the second one discards molecules with high molecular weight.

Luminescent active fractions (3 ml) were separated by gel filtration using a 200 pg chromatography column (HiLoad 16/600 Superdex, GE Healthcare, Sweden) and a liquid chromatography system (AKTA prime plus, GE Healthcare, Sweden). Aliquot of purified luciferase (20 µl) was mixed with commercial coelenterazine (JNC corp, Japan) of 0.013 mM final concentration, in 480 µl of extraction buffer. Bioluminescent spectra was measured using a crystal cuvette in a spectrophotometer (FP-777, JASCO, Japan), under adequate setting parameters (high sensitivity 2 nm waveband, 1000nm/min, 400 – 700 nm interval). Spectra measurement was performed using light accumulated from 10 trials for high accuracy of wavelength λmax. Spectrophotometry analyses were performed using Spectra Manager (JASCO, Japan) and exported to Microsoft Office 2000 Excel (Microsoft Corporation, USA) for reflection corrections from luciferin-luciferase reaction spectra, basic statistical analyses and graphs.

b. Spectra of body photophores and tapetum lucidum

Analyses of spectrometry were performed on specimens of *D. watasei* freshly caught on 26.02.2019 at Takaoka (室戸市高岡支) and on 28.02.2019 at Shiina (室戸市椎名支所) fishery ports in Muroto city, Japan (see Chapter 2). Individuals were kept on ice in a closed cooler box until the end of the experimental tests at the Marine Biology Laboratory of Kōchi University (高知大学海洋生物学研究室). Five ventral body photophores were tested on one fish from Takaoka (Fig 43A) and two from Shiina (Fig 43B-C). Tapetum lucidum was analysed on a specimen collected at Shiina fishery port (Fig 43D). Photophores were selected based on the observable colourfulness and brightness of reflection, representing organs with inner reflector in good conditions. Same selection criteria was used for tapetum lucidum. Reflection spectra of coloured tissues was measured using a fibre optic spectrometer (Flame-S, OceanOptics Inc./Ocean Insight, USA) linked to a tungsten halogen light source (HL-2000-LL) Ocean Optics Inc./Ocean Insight, USA) via bifurcated fibre optic cable (R400-7-VIS-NIR, OceanOptics Inc./Ocean Insight, USA) to an ocular of a stereo microscope (Zeiss, Stemi 2000) (Fig. 43 E).

Body photophores were dissected with mini-scissors and the lens reflector peeled with fine forceps, to avoid interfering with the light reflection on the inner reflector. Methodology for reflection spectra measurements were adapted from [18, 150]. Photophore is placed on a Petri dish, lens surface upwards and oriented with lens reflector side facing the stereo microscope and ventral side facing the observer, to ensure all the photophores are analysed in the same position related to the fish body sagittal plane. Reflection spectra of vertical white light was measured under 4x magnification using 400 µm optical fibre that results in a 100 µm illuminated central area of the inner reflector and from where the reflection spectra was measured (R.IA), similar size than the diameter of the photocytes group (see Chapter 2) for a realistic and accurate approach on area of light received on the reflector by the photocytes. Photophore was positioned under the objective on the highest reflective area of the inner reflector, observed using the free ocular of the stereo microscope. As the light is emitted from the light source and received on the spectrometer sensor on a vertical angle, as expected according to the parabolic-like shape of the reflector (see Chapter 4), light reflection can only be measured from a small z on the centre of the photophore, where the reflector lies parallel to the light source and spectrometer sensor. Within this central area, with the aid of the ocular and live recording mode of the spectrometer, the photophore position was gently adjusted so the SA was ensured to be positioned on the place of the reflector that projects the highest intensity of reflected light. This ensures that the reflection spectra is measured from the most parallel iridophores to the vertical angle of light source and spectrometer sensor (see Chapter 6).

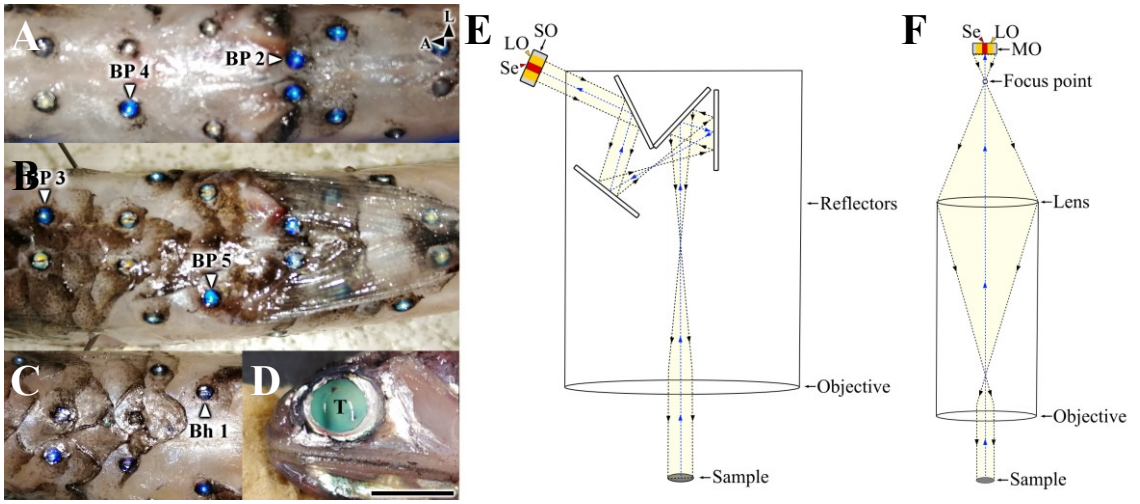

Figure 43 - Ventral view showing the location of tested *D. watasei*'s ventral body photophores in ventral body surface of: A) Specimen 1; B) Specimen 2; C) Specimen 3. D) Lateral view of left eye tapetum lucidum in *D. watasei* (note that the photograph was long after the spectral reflection tests for this tissue). Schematic illustration of the mechanisms used for spectrometry tests on: E) Fresh fishes, body photophores and tapetum lucidum, under stereo microscope; and F) TEM fixed silver tissues, under light microscope. BP= Body photophore; T= Tapetum lucidum; L= Lateral; A= Anterior; Se= Spectrometer sensor; LO= Fibre optic light source on; SO= Stereo microscope objective; MO= Microscope objective. Scale bar= 1 cm.

For measurements of light reflection of the tapetum lucidum, without enucleating the eye from the fish, cornea was cut out using a mini-scissors and fine forceps. With the aid of paintbrush and minis-scissors, vitreous humour and retina were gently removed to the maximum amount possible while avoiding damage to the tapetum lucidum. Fish was placed under the stereo microscope and tapetum positioned under the objective and light reflection spectra measured in the same way as for inner reflector of body photophores.

Lambertian optical diffuser of white polytetrafluoroethylene (WS-1, OceanOptics Inc./Ocean Insight, USA) was used as reflection standard. Each measurement was set for an averaged from 5 scans to allow high accuracy of the reflection wavelength λmax. Nevertheless, preliminary tests were made to confirm the accuracy of this method (see Supplement 5). Measurements of light spectra of the inner reflector on body photophore were performed under white light. Although, in the real scenario, the reflector only receives light produced in photocytes, generated by reaction of coelenterazine and respective luciferase, which has a different light emission spectra [30] than the white light [18]. Actual *in vivo* bioluminescent spectra from the photocytes and reflected by the inner reflector was obtained by multiplying the luminescence spectra of luciferin-luciferase reaction and reflection spectra under white light. Spectrometry analyses were performed using OceanView 1.6.7 (OceanOptics Inc./Ocean Insight, USA) and exported to Microsoft Office 2000 Excel (Microsoft Corporation, USA) for reflection corrections from luciferin-luciferase reaction spectra, basic statistical analyses and graphs.

c. Spectra of silver reflective tissues

Specimens of *D. watasei* were collected on 25.01.2019 at Mimase fishery port in Kōchi city (高知市御畳瀬支所), Japan (see Chapter 2). Fishes were kept in a cooler box, on ice until reaching the Marine Biology Laboratory of Kōchi University (高知大学海洋生物学研究室). Vn head photophore, a sample of silver skin (around 2 cm^2) from the ventral surface of the fish body, VO2 ventral body photophore and one eye were dissected from one specimen. A small incision was made on the cornea with a scalpel to ensure an adequate fixation of inner tissues of the eye. Lens scale was gently removed from the VO2 photophore, ensuring the lens reflector was neither removed or damaged from the surface of the organ. Tissue samples were fixed overnight in 5ml plastic tubes at 4ºC, according to fixation methods for TEM microscopy according to [182], in 2% glutaraldehyde/ 4% PFA fixative solution in (pH 7.4) in 0.05 mol/L sodium cacodylate buffer. On the day after, fixed tissues were washed 3 times and stored in 0.1 mol/L sodium cacodylate buffer at 4ºC, until the experiments at the Luminous Organisms Laboratory of Chubu University (中部大学研究室). Methodology for measuring reflection spectra was

adapted from [138], with the same spectrometry system as in the previous section for structural coloured tissues in fresh fishes, but instead of a stereo microscope, using of light microscope (D5500, Nikon, Japan) (Fig. 43F). This spectrometry system under light microscope also need an additional accurate adjustment for the focus point of the spectrometer sensor, ensuring higher accuracy for reflection wavelength λmax. Tissues were washed in distilled water and placed with reflective side upwards, on a glass slide for microscopy (MAS-GP type A, Matsunami, Japan), under 4x magnification objective (Plan Fluor Series, Nikon, Japan). Using the binoculars and live recording mode of the spectrometer, tissues were position to ensure the SA is located on the highest light intensity place of the reflective surface of the tissue. Reflection spectra was measured on skin, inner reflector of body photophores, lens reflector of VO2 body photophore and iris. Spectrometry procedure and data analyses were performed in the same way in the previous section for body photophores and tapetum lucidum, except luciferin-luciferase reaction spectra correction is not applicable on silver tissues.

3. Results

Bioluminescence reaction spectra was measured from purified extract of *D. watasei* luciferase mixed with commercial coelenterazine. Obtained spectral curve has a well-defined peak and narrow shape with light emission λmax= 454 nm (FWHM= 61 nm) (Fig. 44).

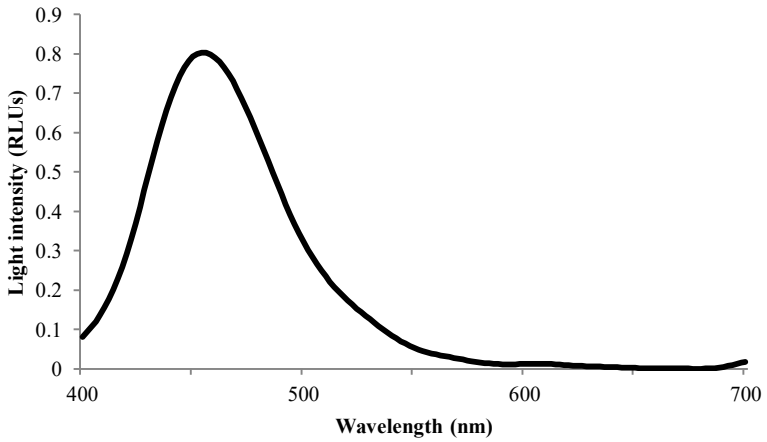

Figure 44 – Spectra of bioluminescent reaction of commercial coelenterazine and purified *Diaphus* luciferase. RLUs= Relative Light Units.

Reflection spectra was measured from silver and coloured reflective tissues. Silver tissues show flat spectral curves with broad wavelength and low intensity, relatively to coloured tissues (Fig.45). In crescent order of average values, light intensity observed in skin (12.91 – 71.53, Average 20.25 RLUs), lens reflector of body photophore (21.52 – 38.83, Average 22.67 RLUs), iris (26.86 – 46.37, Average 29.54 RLUs), and head photophore inner reflector (41.57 –

47.67, Average 42.72 RLUs). Note that curve spectra of skin is slightly convex, relatively to curves of other silver tissues.

Comparing to silver tissues, structural coloured reflectors have higher light intensity up to 5 times higher and well defined broad curves. Tapetum lucidum show reflection spectra on λmax= 494 nm (FWHM= 124 nm) and intensity maxima= 278.187 RLUs. Inner reflector of body photophore have reflection spectra λmax= 486 nm (FWHM= 82 nm) and intensity maxima= 359.88 RLUs.

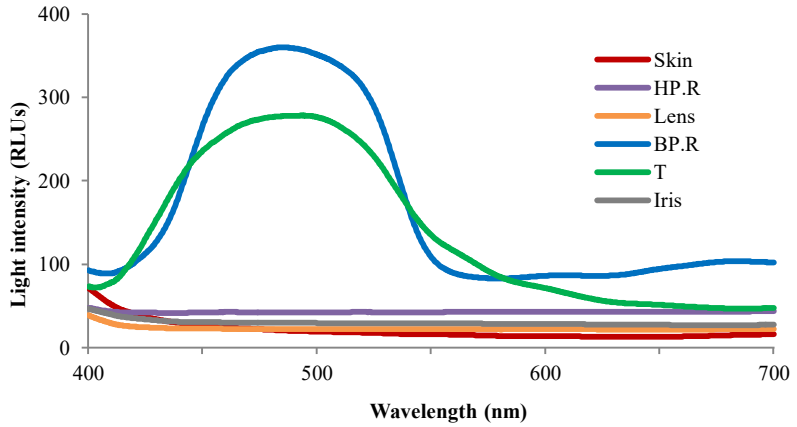

Figure 45 – Reflection spectra of *D. watasei*'s reflective tissues. HP.R= Inner reflector of head photophore; LR= Lens reflector; BP.R= Inner reflector of body photophore; T= Tapetum lucidum; RLUs= Relative light units.

Measured reflection spectra under white light are described by broad curves with well-defined peaks and high variation in light intensity than on spectral peaks (Fig. 46A-B). Reflection spectra λmax= 476 - 526 nm (506 ± S.D. 15.07 nm) and FWHM= 84 – 114 nm (104 ± S.D. 1), intensity maxima= 73 – 364 RLUs (270 ± S.D. 119.48 RLUs). Measured reflection spectral curves were corrected to reflect luciferin-luciferase reaction spectra, altering the spectral curves. After correction, reflection spectra λmax= 460 - 470 nm (464 ± S.D. 3.27 nm) and FWHM= 48 – 59 nm (56 ± 5.19 nm) (Fig. 46C). Variations of λmax up to 2 nm are assumed as noise from readings of spectrometer sensor.

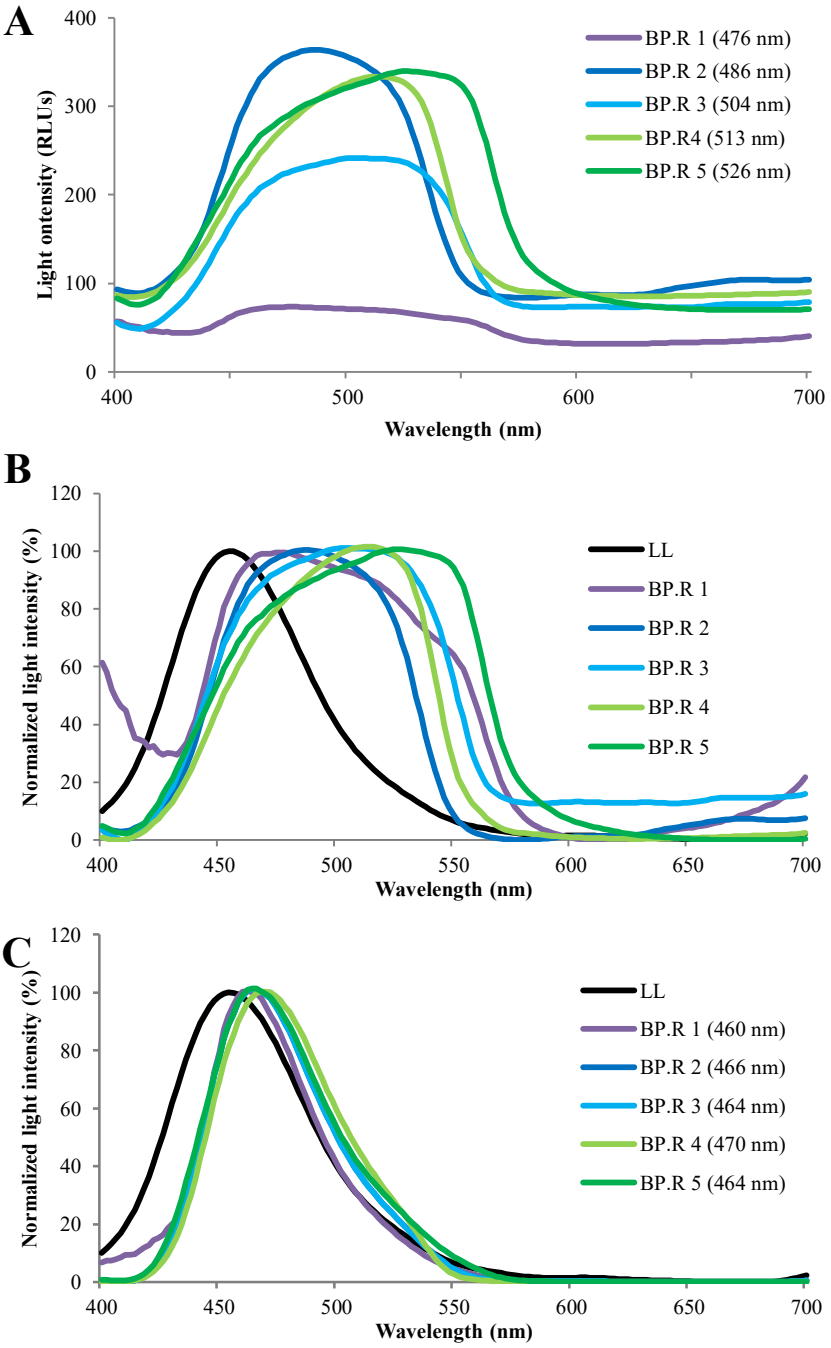

Figure 46 – Reflection spectra of *D. watasei*'s ventral body photophores. A) Raw data. B) Normalized spectra (%) of luciferin- luciferase reaction and reflection of 5 photophores before; and B) After calculation reflection spectra of luciferin-luciferase reaction. BP.R= Inner reflector of body photophore; LL= Luciferin-luciferase reaction.

4. Discussion

d. Reflection of silver tissues

Flat spectral curves with no defined spectral peaks were observed for all analysed silver tissues, producing broadband reflection over the visible wavelengths. Silver reflection is obtained from iridophores with stacked crystals that are not parallel to each other and separated by variable range of cytoplasm spacing, as reported in koi carp skin [130]. This disordered arrangement of platelets result in reflection on most or all wavelengths of visible light are reflected in a wide range of angles [118]. Broadband reflection is adequate for the reflective function of silver reflective tissues as do not seem to have any spectral modulation function, supported by inner structure and iridophores arrangement (Chapters 2 and 3).

While structural coloured spectral measurements were performed on fresh specimens, silver tissues were obtained from TEM fixed samples. Comparatively to coloured tissues, lower intensity of light reflection in silver ones may be a consequence of sample fixation. Facing a high probability of biased observations on data collected from tissues in such different fixed conditions, light intensity reflection will not be discussed between silver and coloured tissues. Nevertheless, as all silver tissues were treated in the same way and time span, reflection intensity between these will be adequate for discussion. Lower intensity and convex shape of reflection curve of skin may be related to iridophores damage when overlaying scales are detached during the fishing process, as for all collected fishes only a few scales remain overlaying pelvic photophores positioned under the pectoral fins. Lens reflector of body photophores and iris have close intensity that could be related to of both reflectors functions as light shields in the respective organs [87, 128], supported by the same linear arrangement of iridophores (Chapter 3). Head photophore inner reflector show high intensity than the remaining silver tissues which may be related to the different purpose of this tissue, to project light outside of a light organ with high intensity light output [49, 96, 97].

a. Structural colour reflection

Colour observed by our eyes matched to the λmax reflection spectra obtained for both analysed coloured tissues, tapetum lucidum and body photophores inner reflector. Obtained broad spectral curves are similar to the characteristic shape reflection spectra on reported structural coloured guanine iridophores in fish skin [124, 138, 159]. In fact, colour of tapeta lucida is reported to be produced by light interference of guanine platelets stacked in iridophores for lanternfishes [26] and other teleosts [24]. Similarly to this ocular reflector, coloured reflection

of the inner reflector on body photophores seems likely to be produced by light interference from the observed guanine crystals. This is also supported by both coloured reflective tissues share the same hexagonal interlocking pattern of iridophores, regardless the different crystal morphology (Chapter 3). Iridophores of photophores inner reflectors could also be observed in histological sections. Unfortunately, long time in Bouin's fixative was needed to allow adequate cross sections of the hard lens on the eyes, resulting in guanine iridophores of tapeta lucida being dissolved by the fixative and could not be observed in cross sections.

Structural colour is obtained from light interference spectra by platelets stacked on parallel layers, interspaced by cytoplasm [124]. As the thickness of platelets cannot be altered, reflection spectra by light interference in guanine iridophores is dependent on the cytoplasm thickness, when enhancing it produces longer wavelength spectra [125]. Greener λmax reflection spectra of tapetum lucidum should be related to thicker spacing between crystal platelets than in body photophores, as observed in guanine iridophores for multi-coloured patterns on iris of the neon tetra fish *Hyphessobrycon* [124] and cuticle of sapphirinid copepods . Nevertheless, λmax spectra is curiously close for both analysed coloured reflective tissues, which indicate that *D. watasei* visual pigments may have spectral sensitivity close enough to their own bioluminescent light for high visual perception, as suggested for some species of lanternfishes [29]. Sensitivity of visual pigment is not determined in *D. watasei* but it seems that visual sensitivity on the reflection peaks of tapeta lucida in lanternfishes was previously suggested [26, 183]. Moreover, rhodopsin of *Diaphus* species have absorbance λmax= 483 – 490 nm [29], close to the estimated light emission of ventral body photophores (λmax= 460 – 470 nm).

a. Counterillumination in the mesopelagic zone

Coelenterazine is widespread among mesopelagic fishes as the substrate for bioluminescent reaction [32, 34, 91]. Pure extracts of *D. watasei* luciferase with coelenterazine emit λmax= 454 nm. Photophores of mesopelagic fishes are commonly supplied with pigmented filters [43, 184] that allow an adequate bioluminescent spectra for counterillumination [102, 185]. Lanternfishes are an exception, lacking pigmented filters but possessing instead a coloured inner reflector for the same purposes [18]. Reflection spectra of *D. watasei* body photophores under white light has λmax= 476 – 526 nm but the actual light reflection from luciferin-luciferase reaction was estimated with λmax= 460 - 470 nm. This range is to downwelling light penetrating in the mesopelagic zone (λmax= 472 – 486 nm, 200 – 615 m depth [17]) and as the coefficient of light

attenuation is low at 470 – 480 nm [120], the final spectral output of light emitted from the photocytes and modulated by the inner reflector allows an adequate counterillumination.

Coelenterazine-based luciferases are found in a wide diversity of animal taxa [49] that emit various wavelength peaks [30]. Curiously, luminous spectra from some of these animals are close to the spectra of mesopelagic ambient light, such as the sea pen *Philosarcus* and copepod *Gaussia* with light emissions at 470 - 475 [30]. On the other hand, coelenterazine-based luciferase from deep-sea shrimp *Oplophorus* has emission maxima at 455 nm [177], right next to *D. watasei*. Moreover, *Oplophorus* has two different bioluminescence mechanisms, secretory and photophores [186]. Luminous secretions are projected from the shrimp's mouth as a defensive response while cuticular ventral photophores are used for counterillumination [187]. Similarly, ventral photophores in lanternfishes have also camouflage purposes [40, 99] as well head photophores in *Diaphus* are proposed to be used as torches to illuminate surroundings and prey [49], and for mating [39] (See Chapter 2). For both animals, in which multifunctional bioluminescence includes counterillumination, the wavelength peaks of coelenterazine-based luciferases (454 [177]- 455 nm) do not seem to be a good match the downwelling light on the deep-sea [3]. Ventral photophores used for counterillumination are supplied with coloured tissues – pigmented filter in *Oplophorus*, reflector in *Diaphus* – to spectrally tune the light produced luciferin-luciferase reaction for counterillumination [18]. Taking into account the development of tuning structures in ventral photophores, the luciferases shortwave peaks may be related to the scenario of additional purposes for bioluminescence besides camouflage. However, the advantages of the coelenterazine-luciferases peak wavelengths around 450 nm in these animals are still unknown.

a. Diel vertical migrations and tunable light camouflage

Lanternfishes are known to be part of the mesopelagic community that perform vertical migrations (DVMs), ascending to shallow waters at dusk and returning to mesopelagic at dawn [13, 75, 76]. During DVM, fishes move along different light scenarios. Due to absorption and scattering by water molecules and particles suspended on it, downwelling light spectra changes dramatically from the ocean surface to 100 m but below these depths only slight changes are observed [17, 120]. As the majority of deep-sea fishes, myctophids developed extremely sensitive eyes designed for high photon catch by the following main ocular adaptations: large eyes and pupils with aphakic gaps [3]; tapetum lucidum [24]; pure-rod retina [25, 26]; high density of large photoreceptor cells [22, 25]; high photoreceptor – ganglion cell convergence ratio [27]; large sized retinal photoreceptor outer segments [25, 28]; and high concentration of

rhodopsin [26, 28]. Deep-sea fishes are estimated to be able to detect dim downwelling sunlight down to 1150 m depth [22] and lanternfishes eyes are also well adapted to see it [29, 74]. Lanternfish vision seems to be adequate to detect differences on downwelling light during vertical migrations.

Moonlight has very different spectral characteristics than sunlight, flat curve and not well-defined peaks with wavelength over 750 nm [169]. Mesopelagic fishes in general [188] and lanternfishes [189] seem to avoid moonlight, being reported migrate to shallower depths in moonless nights which might related to the fact that counterillumination does not seem effective at night in surface waters [168]. On the other hand, spectral peaks of moonlight below 100 m are very similar to sunlight [17], so it is assumed that below 200 m, downwelling light does not represent variations at day and night time. Vertical migrations length vary between species, but *Diaphus* do not reach surface at night, being midwater migrants [75]. Particularly for *D. watasei,* migration is performed from 2005 to 258 m [180]. Regarding temporal interval of migrations, lanternfishes usually start to ascend 1 h before dusk and reach back to the initial depths 1 h after dawn [6]. Thus, during migrations, myctophids moves between daytime and twilight downwelling. Contrarily to moonlight, twilight at surface has spectral curve has a well-defined peak at 450 nm [169]. Taking into account that twilight spectra is not reported on the mesopelagic zone and its wavelength peak at surface is within the narrow waveband range of downwelling light below 200 m (430 to 530 nm) [17, 18], it is assumed that mesopelagic ambient at twilight have spectral peaks within daytime and twilight at surface. In fact, noticing the spectral peak range between twilight at surface (450 nm [169]) and downwelling light at mesopelagic to (472 – 486 nm [17]) it is observed that the peak spectral variation of light emission in *D. watasei* ventral photophores (460 – 470 nm) fits perfectly inside it (Fig. 47). It is proposed that the inner reflector modulates the light emitted from the photocytes (450 nm) to a range of longer wavelengths according to variation of downwelling light spectra during diel vertical migrations. By allowing a constant adaptation to the diverse ambient light during migrations, reflector of lanternfishes would achieve an advantageous counterillumination at any depths that the fish migrates.

Adaptation to light during DVMs has a similar scenario for the unique rod-like cones found in pearleye fishes *Maurolicus* [190]. Even though not observed for fishes, some squids bear photophores that can modulate bioluminescent spectra with collagen iridophores [117]. In squids *Abralia, Pyroteuthis* and *Leachia*, spectral manipulation is achieved by changing platelets spacing or muscular contraction, matching spectral light scenarios encountered during DVMs [116, 191, 192]. Apart from lanternfishes, coloured inner reflectors are not reported other bioluminescent deep-sea fishes that perform DVMs that use pigmented filters to modulate light spectra for counterillumination [18, 43]. Adaptable counterillumination spectra is most

likely a specific feature of lanternfishes and the reason behind these fishes evolved a coloured reflector instead of pigmented filters in photophores. In fact, lanternfishes were shortly reported with this mechanism as [50] states solely "At least one myctophid fish also can regulate the colour of its luminescence (personal observation)." Even though it is not described the mechanism behind the observed colour regulation neither the species or the colours observed, it is quite possible using tunable iridophores. Tunable iridophores are able to control or "tune" the spectra of light reflection [145], modelling the cytoplasm thickness between platelets or the angle of the platelets to the focused light, resulting in altered light interference spectra [124, 125]. Similarly structured to inner reflector iridophores in *D. watasei* body photophores (see Chapter 2), monolayered tunable iridophores with guanine crystals are reported in copepods [159] and fishes [193] for camouflage purposes. Sapphirinid copepods are able to modulate reflection spectra by regulation of cytoplasm thickness for cuticle iridophores arranged in hexagonal interlocking [141, 154, 159], similar shape and arrangement as found on *D. watasei* (see Chapter 3). Neon tetra fishes regulate the angle of platelets inclination in skin iridophores for the same purposes, even though the iridophores arrangement and platelet shape [138] differs from the observed in the inner reflector in *D. watasei.* From the high similarity of shape and arrangement on copepods, *D. watasei* is most likely to modulate thickness of cytoplasm for bioluminescent spectra modulation. Structure and arrangement of iridophores in inner reflector of body photophores is different from other reflectors in photophores in *D. watasei*. Additionally to the spectra match of bioluminescence modulated by reflector and downwelling light during DVMs, the structure of iridophores indicates as well potential adaptable reflection.

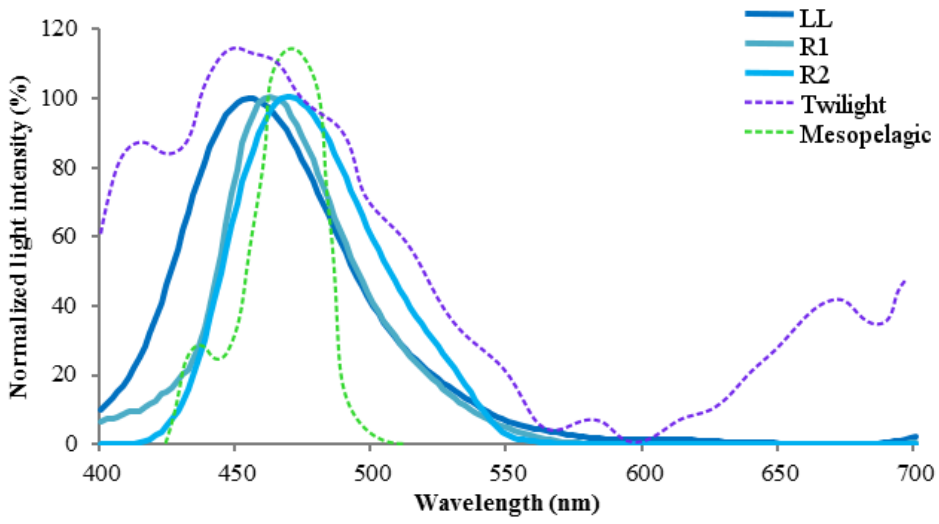

Figure 47 – Normalized spectra (%) of *Diaphus* luciferin-luciferase reaction (LL) and range (R1 – R2) of calculated reflection spectra from *D. watasei*'s inner body photophores of luciferin-luciferase reaction, compared to ambient light at mesopelagic depths and twilight at surface. Mesopelagic downwelling light at 800m adapted from [16]; Twilight at surface adapted from [169].

a. Conclusions

This chapter included fir the first time, *Diaphus* luciferase emission spectra and its modulation by the inner reflector of ventral body photophores of *D. watasei.* Spectra of light emitted after reflective modulation fits to the downwelling light on the mesopelagic zone [17] where *D watasei* inhabits [180], resulting in a successful counterillumination [120]. Based on the spectral variation of modulated emissions by the reflector fit on the range of ambient light during vertical migrations it was proposed the hypothesis of adaptable counterillumination during DVMs for lanternfishes. This can be achieved by tunability of iridophores on inner reflector of body photophores, suggested as well by the structure and arrangement of iridophores in this tissue, its divergences to other reflectors in *D. watasei* photophores (See Chapter 2 and 3) and its similarities to the tunable iridophores of sapphirinid copepods [159]. This seems exclusive to lanternfishes, as other diel migrant luminous fishes have photophores with pigment filters for counterillumination [18, 43] which would not allow spectral regulation.

Continuous research will be done on *D. watasei* photophores to confirm the tunability of inner reflector iridophores. Primarily, TEM microscopy is performed to confirm the ultrastructural colour in comparison to other reflectors in photophores of the fish. Physiological mechanism to regulate reflection spectra of tunable iridophores will be discussed in Chapter 7. SEM microscopy was performed to examine the ultrastructure on the inner reflector in body photophores of *D. watasei* and it is included in next Chapter 6.

CHAPTER 6

Functional ultrastructure of iridophores in the inner reflector of body photophores

1. Introduction

In fishes, structural colour with high intensity of reflection is achieved by guanine crystals in iridophores, such as skin in shallow water species for camouflage purposes [118, 138, 140, 141, 145, 151]. Thin film of guanine platelets (less than 1 μm thick) in multilayered platelets of high refractive index (1.83) stacked parallel to each other and spaced by cytoplasm with low refractive index (1.33) results in the physical phenomena of colour reflection by light interference [124, 125]. Spectra produced in such physiological mechanism on guanine iridophores of fish tissues reaches longer wavelengths by enhancement of thickness of cytoplasm spacing between platelets and lower angle of light incidence on the platelets surface [124, 125]. Even though guanine crystals on iridophores are widely reported in skin of shallow water species [138, 140, 147, 151], the reflectors of photophores of luminous fishes are assumed to be the same composition [117] but in fact only a few studies were made in this regard, the midshipman fish *Porichthys* [156], flashlight fish *Anomalops* [133] and pearleye fish *Maurolicus* [119].

The great majority of mesopelagic animals such as lanternfishes are bioluminescent and achieve light camouflage by counterillumination [3, 40, 50, 53]. This trend of luminous ecological purpose is related to the specific light characteristics of the mesopelagic zone, characterized by dim downwelling light of narrow blue-green spectra on regular vertical angle, allowing light signals to be perceived at long distances by predators and where preys can take advantage of light camouflage [3, 50, 54]. Apart from light intensity that is reported to be under neural control [91–95] and regulated in lanternfishes ventral photophores to match the ambient spectra [99], spectra and angle of bioluminescence is of the essence to achieve an adequate counterillumination [40, 120]. Ventral light emissions on body photophores of these fishes were observed previously [99, 100], although the angle of counterillumination was only analysed in the viperfish *Chaulodius* and the hatchetfish *Argyropelecus* [103], in the latter achieved by light guiding silver inner reflector of photophores [118]. Spectra of light emissions is commonly tuned to the downwelling light in mesopelagic animals by absorption of light emitted from photocytes in pigmented filters [18, 43, 120, 185]. Rare cases such as euphausiids [42, 114] and squids [115, 116] are reported to developed another mechanism for the same purpose by modulating light spectra on inner coloured reflectors. In fishes, similar reflectors seems to be restricted to lanternfish ventral photophores, lacking pigmented filters [18].

Relation of spectra and angle from the light projected by the blue-green inner reflector photophores of lanternfishes and its role on counterillumination is not reported. After the analyses of light angle for light camouflage related to the hexagonal interlocking arrangement of iridophores and parabolic-like shape respectively on Chapters 3 and 4 and spectral modulation

on Chapter 5 it became logical to me that the next step would be to unveil the ultrastructure behind such a complex reflective tissue. Additionally, the ultrastructure of guanine platelets in iridophores of the inner reflector is not yet reported. This final experimental chapter includes such analyses, by using a novel technique that allows the observation of ultrastructure on biological tissues by SEM microscopy on BSE mode developed by [194] and creating a spectrometry system that allows to analyse the spectra variation of iridophores according to the angle variation based on [138, 150].

2. Materials and methods

a. Photophores semi-thin sections

This chapter includes the first observation of ultrastructure of the iridophores guanine platelets in the inner reflector of lanternfishes body photophores. For this reason, using *D. watasei* as model, methods are detailed to be able to be reproduced in future studies. Specimens of *D. watasei* were collected on 25.01.2019 at Mimase fishery port in Kōchi city (高知市御畳瀬支所), Japan (see Chapter 2). Fishes were kept on ice until in a closed cooler box until reaching the Marine Biology Laboratory of Kōchi University (高知大学海洋生物学研究室). With the aid of fine forceps and mini-scissors, two VO1 body photophores of one specimen were dissected , lateral side of the sample cut in triangular shape for posterior orientation purposes. Photophores were fixed in the same way as silver tissues for measurements of spectra reflection in (Chapter 5). Post-dissection, post-fixation and embedding were performed at the Fish Biology Laboratory (魚類生物学研究室), semi-thin sections at the Experimental Preparation Room of the Department of Applied Sciences of Chubu University (実験準備応用生物学研究科中部大学), and sections SEM microscopy observation at the Institute of Science and Technology Research Analysis Centre (総合工学研究所分析計測センター), Chubu University (中部大学).

Fixed photophores in sodium cacodylate buffer were picked from 4°C and, with under stereo microscope, remove the surplus skin and muscle around the photophore with the aid of fine forceps and mini-scissors. Transversal cut performed on the middle part of the organ with a razorblade, to ensure similar sections as observed on light microscopy (see Chapter 2). One half of each photophore was placed in 10 ml glass flask with 0.1 mol/L sodium cacodylate buffer, on ice. Post-fixation and embedding were adapted from [182]. Samples were post-fixed with 1% osmium tetroxide solution for 90 minutes, washed in distilled water and dehydrated in ethanol

series: 1- 6. 15-30- 45-60-75-90% (30 min each); 7. 95% (15 min); 8-10. 100% I-II (10 min each). On a rotator (2RPM R051, TAAB Laboratories Equipment Ltd., U.K.), samples were then cleared in two series of Qi.1 (Nisshin EM Co. Lda., Japan) for 15 minutes each, followed by 1:1 Qi-1: araldite resin (Quetol 523, Nisshin EM Co. Lda, Japan) for 1 h and three in araldite resin for 1h each. Tissues were embedded in araldite resin blocks, with sample side of middle half of the photophore to the left, for posterior orientation purposes. Resin blocks were placed overnight in an oven at 37ºC (IC2405, Yamato Co. Ltd., Japan) at for 3 days at 60ºC (NIB -82, AGC Techno Glass Co. Ltd., Japan) to polymerize the resin.

Preparation of semi-sections, staining and SEM sections observation adapted from [194]. Resin blocks were shaped with the aid of an ultrasonic cutter (ZO-41,Honda Electronics Co. Ltd., Japan), ensuring the side of middle half of the photophore was facing the sectioning surface of the block and the organ perpendicular to this surface, for adequate sections on transversal angle of the sample. With the aid of the binoculars, 2000 nm semi-thin sections were cut with diamond knife (Histo H1 1176, DiATOME, U.S.A.) using a ultramicrotome (Ultracut UCT, Leica, Germany).

Sections were picked with a fine forceps and placed in ultrapure water drops on glass slide for microscopy (MAS-GP type A, Matsunami, Japan), heat with breath to unwrinkle, and placed on heating plate water to dry the water drops. Slides were stained by standard staining methodology for TEM microscopy [182, 194], washed with ultrapure water and dried with blower between solution and in the end of the staining procedure. To enhance the electron density of different protein materials [195], 0.2% tannic acid in 0.1M PB was poured on sections for 30 min. Sections were stained with EM stainer and lead staining solutions (Nisshin EM Co. Lda., Japan) for 30 and 15 minutes, respectively. Glass slides areas with stained sections were cut with a glass cuter and coated with platinum/palladium using an ion sputter (E-1010, Hitachi, Japan). Sections of photophores were observed under SEM microscope (S-4300, Hitachi, Japan) by backscattered electrons (BSE). One section was chosen by photophore, based on lowest level of deformation observed on iridophores platelets of the inner reflector. Photographs were taken for the whole organ at x90 magnification, and for 3 areas on lateral (lens reflector) side, bottom and ventral (emission) side of the organ (Fig. 48A) at x400, x1800 and x3000 magnifications.

SEM photographies were tilted at 13.8º (Fig. 48B) as it was found to be the actual horizontal angle of VO1 photophores in the surface of the fish body (see Chapter 4), allowing an accurate and realistic angle estimation of light modulated by iridophores. Photographies at x400 magnification allow high magnification to see the platelets in the iridophores while low enough to observe an area with 20 – 25 iridophores which is adequate to analyse the variation of

platelets angle along the inner reflector. From these photographs, 6 sampling areas (SAs, similar analyses of inner) were established in crescent order from the lateral to ventral periphery of the organ(Fig. 48B), 2 from each photographed area (Fig. 48A).

Angle of light emitted by the photophores and reflected vertically outside by the parabolic-like inner reflector (see Chapter 4) was estimated on photographs of the whole organ at x90 magnification from 3 replicates for each SA (Fig. 48B). Unfortunately, photocytes group for the sections of photophore 2 were detached from the connective tissue where it lays presumably during tissue sampling and dissection. Angle of light emitted by the photophores and reflected outside were only able to be calculated for photophore 1. Nevertheless, as both photophores are from the pair VO1 and symmetrical positioned in the fish body, photocytes reflection angles to outside of the organ estimated for each Sa on photophore 1 were used for both photophores. Using photographs at x400 magnification, vertical angle was measured for the inner reflector surface (3 replicates) and platelets (N=10) in iridophores on 3 iridophores per SA (Fig. 48C). Measurements of the surface and platelets angle was performed taking into account the inter-tissue artifact spaces observed from the detachment of reflector from the cup during sectioning. Angle between platelets and reflector surface per SA, was calculated by subtracting the value measured for the vertical angle of each platelet and subtracted from the average value of the vertical angle of the surface. Angle between photocytes and platelets was calculated by adding the average value of the vertical angle of photocytes light emission to outside to the vertical angle of platelets. Although platelets can be observed on the photographies at x400, the thickness is only possible under x3000 magnification. Thickness of platelets was measured from 10 platelets for each photographed area (lateral, bottom and ventral). Measured platelets were selected by most focused and less damaged. Unfortunately, due to deformation of platelets during semi-thin sections procedure, spacing between platelets were highly variable represented by many artifact spaces between the platelets, which did not allow to measure the spacing between platelets in order to estimate the wavelength of light interference reflection [124, 125, 159, 182].Measurement of angles on SEM photographies were performed using ImageJ 1.50i (National Institutes of Health, USA) and exported to Microsoft Office 2000 Excel (Microsoft Corporation, USA) for basic statistical analyses, tables and graphs.

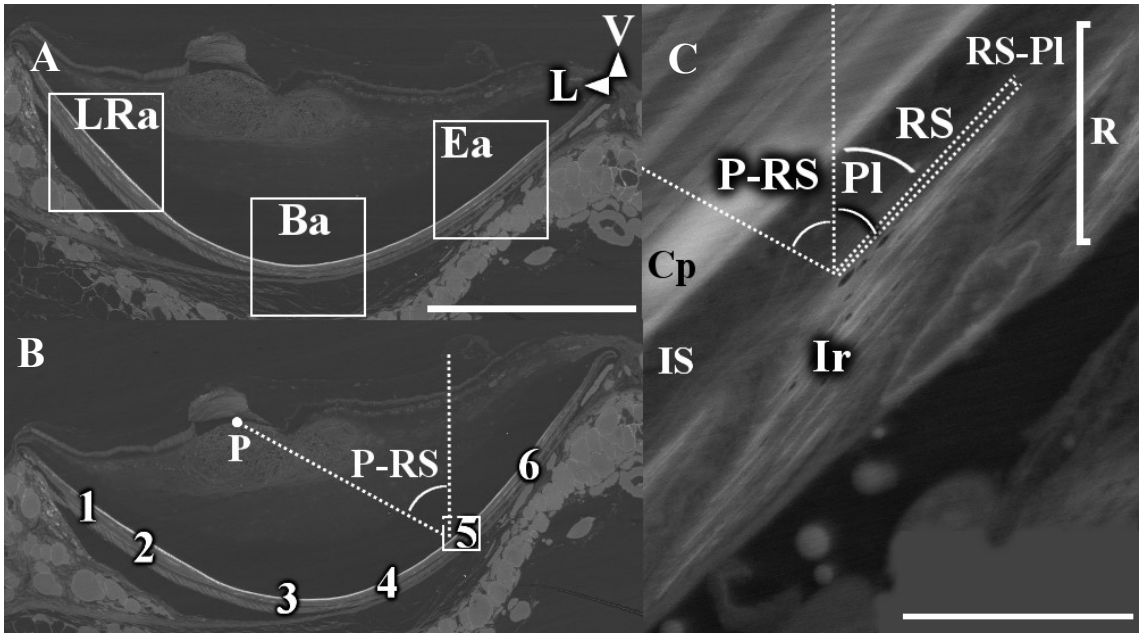

Figure 48 - Estimation of iridophore ultrastructural angles from SEM microscope photographies on *D. watasei'*sVO1 ventral body photophore (photophore 1). A) Raw image showing the 3 photographed areas (white outlined squares) of the organ. B) Tilted image with scheme of photocytes reflection angle and SAs. C) Iridophore on reflector and represented estimated angles. White outlined square on (B) indicates location of (C). LRa= Lens reflector area; Ba= Bottom area; Ea= Emission area; P= Photocytes; P-RS= Photocytes reflection angle; Cp= Cup; IS: Inter-tissue space between cup and inner reflector; Ir= Iridophore; R= Reflector; RS= reflector surface angle; Pl= Platelet angle; RS-Pl= Reflector surface-platelet angle; VO1= Ventral organ; V=Ventral; L=Lateral. Dotted white lines and curved lines represent angles. Scale bars: A-B) 500 µ m; C) 10 µ m.

b. Spectra of light interference with angle variation

Using *D. watasei* lanternfish as model, it was measured for the first time the variation of reflection spectra by light interference with angle of iridophores on fishes photophores. In this way, established spectrometry system and methodology are detailed to allow it to be reproduced in future studies. Fishes were sampled and ventral body photophores dissected from fishes in the same way as on the previous section for SEM photophores. Two VO1 and one PO3 photophores were fixed after removing the lens reflector with fine forceps and dissection and removal of photocytes, connective tissue and transparent fluid without damaging the cup and the inner reflection below it (see Chapter 2). Two experimental tests were used to analyse the wavelength of light interference with angle variation of iridophores of inner reflector of photophores. General experimental design is the same for both tests and similar to the system used in Chapter 5 for measuring the reflection spectra on silver tissues. Photophore is washed in distilled water and placed inside a chamber with distilled water, under 4x magnification of light microscope and the wavelength reflection of white light is measured on iridophores of the inner reflector positioned at different angles. Chamber consists in black rubber attached to a glass slide for microscopy (MAS-GP type A, Matsunami, Japan) with double sided tape and covered by a

coverslip (Neo No.1, Matsunami, Japan). Precise stage position can be adapted on light microscope which represents a high advantage of accuracy for SAs than the method used on fresh samples (see Chapter 5).

On the first experiment, spectra was measured on iridophores of different angles of the parabola-like reflector (see Chapter 4). Spectral reflection is measured on 6 sampling areas illuminated on the inner reflector (R.ISA) on the middle transversal plane of the organ, in crescent order from lateral (lens reflector) to the ventral (emission) side of the organ (Fig. 49 A). R.ISAs used were positioned in similar areas of the middle transversal plane of the reflector as the SAs used in angle measurements on SEM photographies the previous section. The spectral light reflection was measured under white light at 50º covering all the sample from an external light source, used one adjustable arm of dual gooseneck fibre optic illuminator with halogen light source (Olympus LG-PS 2, Japan) (Fig. 49B). 50º angle of light emission was established from preliminary tests between other non-vertical angles (data not shown), selection criteria was by highest light intensity of reflection. Constant non-vertical angle of light source for all 6 same R.ISAs, allow to correlate the variation of actual wavelength of light reflection to the vertical angle of the photocytes light emission on the reflector estimated on SEM photographs in the previous section. This ensures and approach to analyse the variation of light interference wavelength to the angle of iridophores along the parabolic-like inner reflector of body photophores.

In the second experiment, spectra of light reflection was measured using an epi-illumination light source (Nikon LV-LH 50 PC1, Japan) system of light microscopy (Fig. 49 C). Contrary to the previous experimental system, this has a vertical light source which, as described in the measurements on fresh body photophores (see Chapter 5) is only projected by the inner reflector central (bottom) area where the iridophores are perpendicular to the focused white light (R.IA, same purpose as spectral measurements in fresh photophores on Chapter 5). Spectral measurements were only performed on the bottom of the reflector with the aid of the binoculars and the live mode of spectrometer, selecting the area highest intensity of reflection. Measurement chamber was detached from the glass slide and attached to levers of different angles (10º, 20º, and 30º). The same area was measured with iridophores at 3 different angles, allowing to confirm that the wavelength variation is due in the previous test is due to angle variation of the iridophores. Epi-illumination light is focused on a 0º vertical angle, allows high accuracy for measuring angle-dependent wavelength of light interference as used in [138].

Room lights were turned off before the experiments. Lambertian optical diffuser of white polytetrafluoroethylene (WS-1, OceanOptics Inc./Ocean Insight, USA) was used as reflection standard. Each measurement was set for an averaged from 5 scans to allow high

accuracy of the reflection wavelength λmax. Nevertheless, preliminary tests were made to confirm the accuracy of this method (see Supplement 5). Spectrometry analyses were performed using OceanView 1.6.7 (OceanOptics Inc./Ocean Insight, USA) and exported to Microsoft Office 2000 Excel (Microsoft Corporation, USA) for basic statistical analyses and graphs.

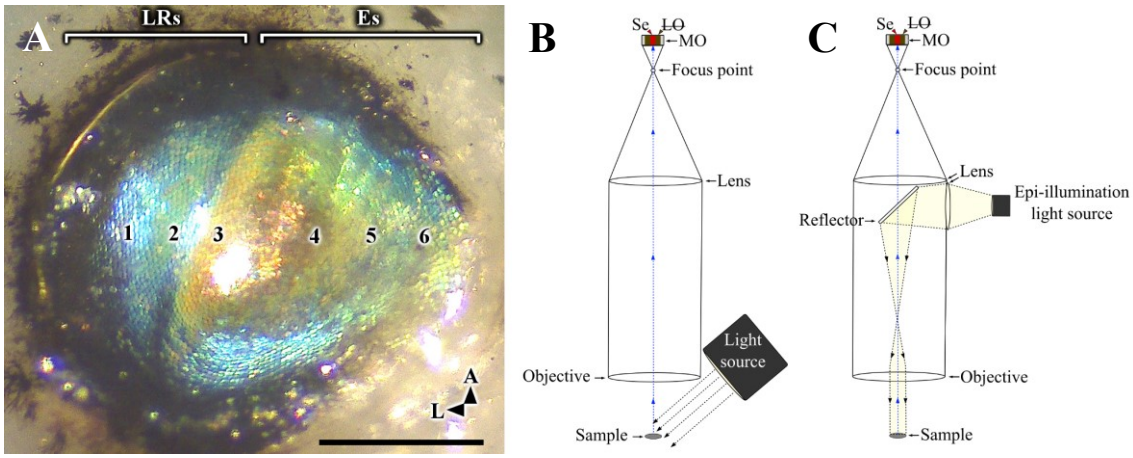

Figure 49 – Spectrometry experiments for wavelength variation with angle of iridophores on the inner reflector of *D. watasei*'s ventral photophores. A) Stereo microscope photography of ventral photophore showing the sampling areas illuminated on the inner reflector (R.ISA) (1-6) used in the experimental system represented in (B). Schematic illustration of the mechanism used for spectrometry tests for: B) Photophore curvature under 50° light; and C) Photophore on tilted angles under epi-illumination. LRs= Lens reflector side; Es= Emission side; A= Anterior; L= Lateral; Se= Spectrometer sensor; ~~LO~~= Fibre optic light source off; MO= Microscope objective. Scale bar= 500 µm.

3. Results

c. SEM microscopy

Semi-thin sections show the inclination angle and ultrastructure structure of iridophores in the inner reflector of ventral body photophores VO1. Vertical angle of platelets varies along the reflector, which can be observed from the inclination of iridophores in the inner reflector (Fig. 50). Iridophores on the peripheral areas have lower vertical angle when compared to the middle area, i.e., the bottom of the photophore. On the latter, vertical angle of iridophores seem close to right angle and platelets are parallel to the surface of the reflector (Fig. 50D). As close as the iridophores are to the peripheral area, cells follow the curvature of the reflector and platelets seem roughly parallel to the tissue surface (Fig. 50C-E). On the most peripheral area of the reflector, iridophores are inclined and the vertical angle of platelets become lower (Fig. 50B). Most peripheral area of the ventral side could only be observed in detail for photophore 2, due to the areas of photophore that were photographed for higher resolutions, it was not included in the shots for photophore 1. Artifact spaces are a consequence minor deformation of tissues

during fixation and semi-thin sections performance. It is assumed as the cause for variation of angle pattern along the inner reflector between the examined photophores.

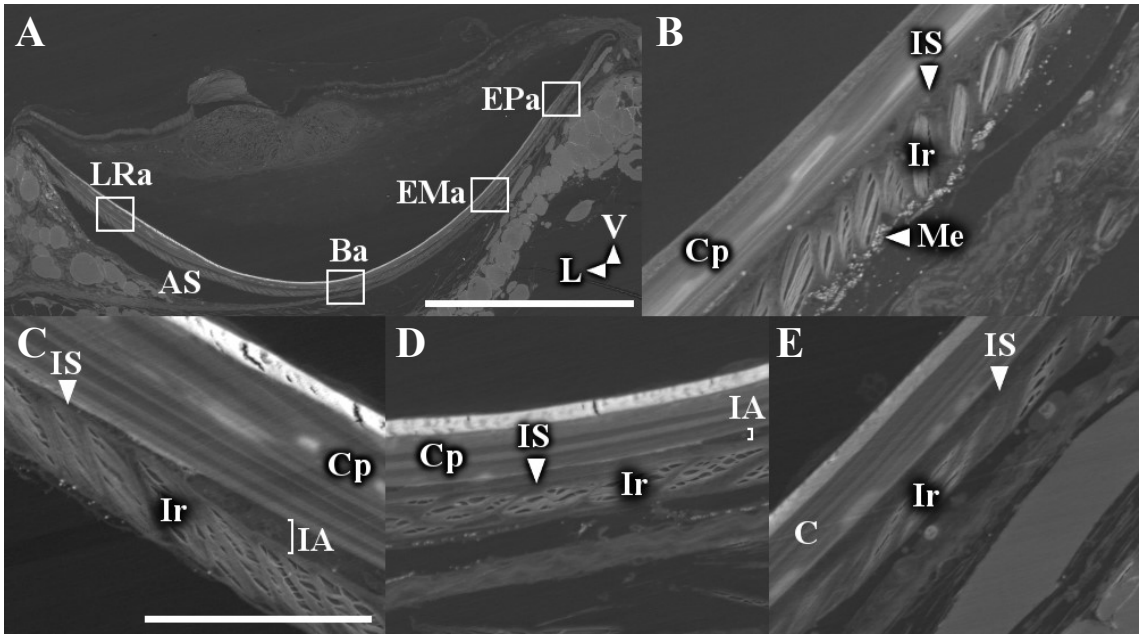

Figure 50 – SEM microscope photographies of iridophores located on areas along the inner reflector of *D. watasei'*s VO1 ventral body photophores. A) General structure of photophore (photophore 1). B) Emission-peripheral area (photophore 2). C) Lens reflector area (photophore 1). D) Bottom area (photophore 1); E) Emission-median area (photophore 1). LRa= Lens reflector area; Ba= Bottom area; EMa= Emission-median area; EPa= Emission-peripheral area; AS= Artifact space from detachment of photophore from supportive connective tissue; IS= Inter-tissue space between cup and reflector; Cp= Cup; Ir= Iridophore; IA= Inter-tissue artifact space between cup and reflector; Me= Melanophores; VO= Ventral organ. White outlined squared on (A) indicate the areas on other images. Scale bars: A) 500 µm; B-C) 50 µm.

Inside the iridophores, thin platelets are stacked in layers with cytoplasm between them (Fig. 51). Platelets thickness vary from 78 to 125 nm (95.63 ± S.D. 13.06 nm, *n*= 60). High variation of spacing between platelets is observed, including massive "holes" followed by bending of platelets (Fig. 51B). These features are assumed to be caused by minor tissue deformation during thin-sections are responsible for angle variations per SA on observed photophores.

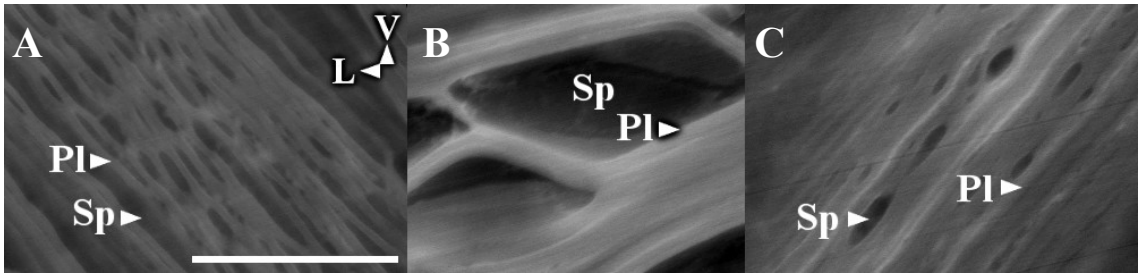

Figure 51 – SEM microscope photographies of guanine platelets in iridophores along the inner reflector of *D. watasei'*s VO1 ventral body photophore (photophore 1): A) Lens reflector area; B) Bottom area; C) Emission area. Pl= Platelet; Sp= Inter-platelet artifact space; VO= Ventral organ;V= Ventral; L= Lateral. Scale bar= 2.5 µm.

Vertical angle of the reflector surface (Fig. 52A) varies between 35.22 – 90.24º on examined photophores, lower variation on photophore 1, 37.10 – 88.59º (59.77 ± S.D. 15.32º, *n*= 6), than in photophore 2, 35.22 – 90.42º (54.59 ± S.D. 16.23º, *n*= 6). Regarding the vertical angle of platelets (Fig. 52B), varies between 10.49 – 87.61º for both photophores, lower on photophore 1, 31.22 – 87.61º (54.14 ± S.D. 17.00º, *n*= 6), than in photophore 2, 10.49 – 83.30º (46.17 ± S.D.19.13º, *n*= 6). Angle between reflector surface and platelets (Fig. 52C) varies from -7.11º to 27.58º on examined photophores, lower variation on photophore 1, -7.11 – 18.56º (5.48 ± S.D. 5.28º, *n*= 6) than on photophore 2, -3.27 – 27.58º (8.42 ± S.D. 7.67º, *n*= 6). High S.D. compared to averages on this parameter is due to the low numerical values of the first and angle variation platelets due to minor deformations under sectioning procedure.

Same pattern of vertical angle variation for the reflector surface and for platelets, is observed in both organs of higher angles in the middle area, diminishing closer to the periphery, in accordance with observed on the sections photographies (for more detailed values of averages and standard deviation, see Supplement 6). Although, closer to the peripheral areas the platelets angle reaches lower minimum values than the tissue surface. This is in accordance to the parallel angle between reflector surface and platelets on the middle area, becoming non-parallel closer to the peripheries. Higher variation, lower minimum values (vertical angles of surface and platelets) and higher maximum values (angle between reflector surface and platelets) are observed on photophore 2 are related to the peripheral area of ventral side on photophore 2 being measured on the most area of the reflector and slightly less peripheral on photophore 1.

Photogenic area was not observed in sections of photophore 2, presumably due to detachment during dissection and sample preparation of fresh photophore. Vertical angle between photocytes and reflector surface in photophore 1 (Fig. 53A) enhances from the bottom to the periphery, varying between 12.58 – 84.88º (48.85º ± S.D. 22.48º, *n*= 6).

Angle between photocytes and platelets (Fig. 53B), varies between 77.36 – 118.39º, lower variation on photophore 1, 77.36 – 118.39º (102.86 ± S.D. 11.67º, *n*= 6) than photophore 2, 79.59 – 107.69º (95.02 ± S.D. 7.00º, *n*= 6). Pattern of angle variation between photocytes and platelets per SAs is similar between photophores, although not on the periphery. This is due to the peripheral area of ventral side on photophore 2 being measured on the most area of the reflector and slightly less peripheral on photophore 1 Angle between photocytes and platelets varies in a similar pattern as the vertical angle between photocytes and reflector surface, but with much higher variation on the latter, for both examined photophores.

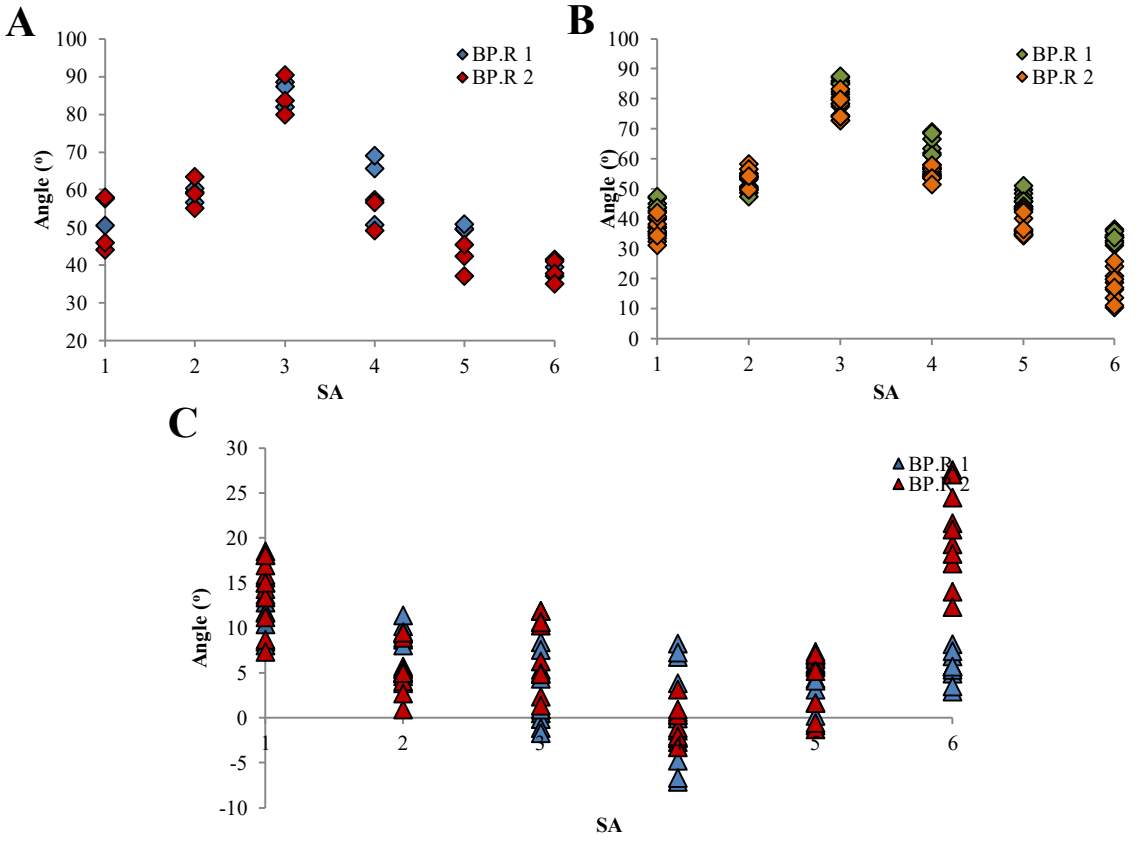

Figure 52 - Distribution plots of measured and calculated parameters for estimation of reflection angles of platelets on the inner reflector of *D. watasei*'s ventral body photophore observed under SEM microscopy: A) Reflector surface angle; B) Platelets angle; C) Reflector surface-platelets angle; BP.R=Inner reflector of body photophore.

Regarding the emission area of the photophore (SAs 3 to 6), i.e., not covered by lens reflector, a angles between the platelets and reflector surface is, on SAs 3 – 6 for photophore 1 is between -7.11 – 8.39º (3.16 ± S.D. 4.04º), and on SAs 3 – 5 for photophore 2 is between -3.27 – 11.90º (3.70 ± S.D. 4.70º). On SAs 3 to 6, it was found on both analysed photophores a higher variation for the angles of photocytes – reflector surface in relation to the angles of photocytes – platelets. Angle of photocytes – reflector surface angle on photophore 1 is 12.58 – 84.88º (51.67 ± S.D. 25.44º, *n*= 4). Angle of photocytes – platelets on photophore 1 is 94.49 – 118. 39º (107.83 ± S.D. 6.84º, *n*= 4) and photophore 2 is 89.71 – 107.69º (98.56 ± S.D.4.54º, *n*= 4).

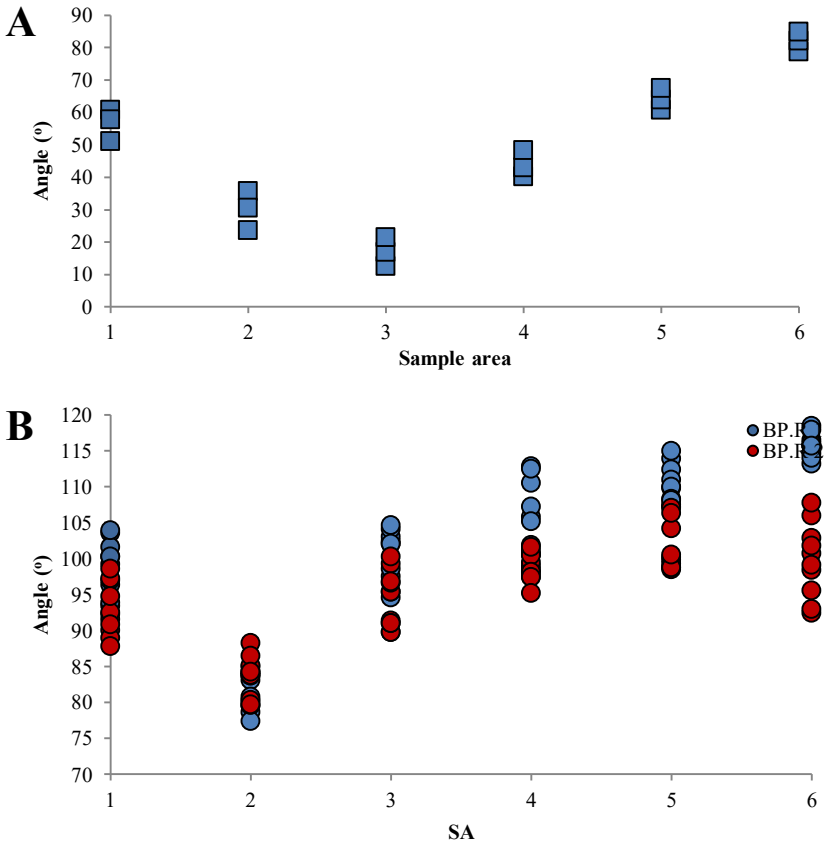

Figure 53 – Distribution plots of measured and calculated parameters for estimation of reflection angles of light from photocytes on platelets on inner reflector of *D. watasei*'s ventral body photophore observed under SEM microscopy: A) Photocytes angle; B) Photocytes-platelets angle. BP.R= Inner reflector of body photophore.

a. Spectra variation per sample are

Cumulative light intensity is different for each measured photophore, higher average and variation on photophore 1 and lower average and variation on photophore 3 (Fig. 54, for detailed values of average and standard variation see Supplement 7). Variation of cumulative light intensity for photophore 1 is between $5.01x10^4$ – $7.04x10^5$ RLUs ($3.61x10^5$. ± S.D. $2.73x10^5$ RLUs, n= 6), for photophore 2 between $4.40x10^4$ – $7.05x10^5$ RLUs ($3.44x10^5$ ± S.D. $2.53x10^5$ RLUs, n= 6), and for photophore 3 between $5.41x10^4$ – $4.99x10^5$ RLUs ($2.55x10^5$ ± S.D .$1.70x10^5$ RLUs, n= 6). Minimum intensity is reached on R.ISA 4 for all photophores and maximum on R.ISA 5 for photophores 1 and 3, and R.ISA 1 for photophore 2.

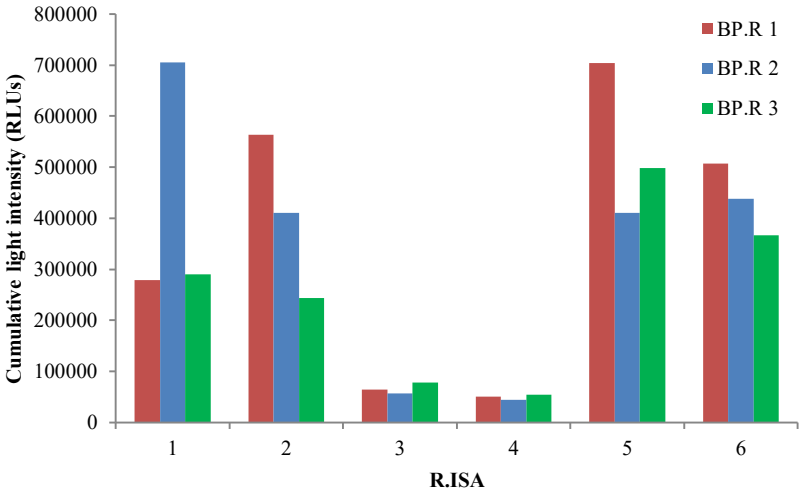

Figure 54 – Histogram of cumulative reflection light intensity of inner reflector of *D. watasei*'s ventral body photophore, 3 photophores, per 6 R.ISA. BP.R= Inner reflector of body photophore; R.ISA= Sampling area

Full width at half maximum (FWHM) is dependent on the photophore, higher average and variation on photophore 1 and lower variation on photophore 2 (Fig. 55 - 56). Variation of FWHM for photophore 1 is between 98 – 312 nm (205 ± S.D. 88nm), for photophore 2 between 132 – 198 nm (162 ± S.D. 27 nm), and for photophore 3 between 110 – 224 nm (162 ± S.D. 52 nm). Minimum values of FWHM are reached on R.ISA 6 for photophore 1 and R.ISA 1 for photophore 3, and maximum values on R.ISA 4 for all photophores.

Note that minimum values of cumulative light intensity are all in R.ISA located on the middle of the photophore and maximum on the peripheral areas, and that shorter wavelengths λmax and minimum values of FWHM are all in R.ISA located on the periphery of the photophore while longer wavelengths λmax and maximum values of FWHM on the middle areas.

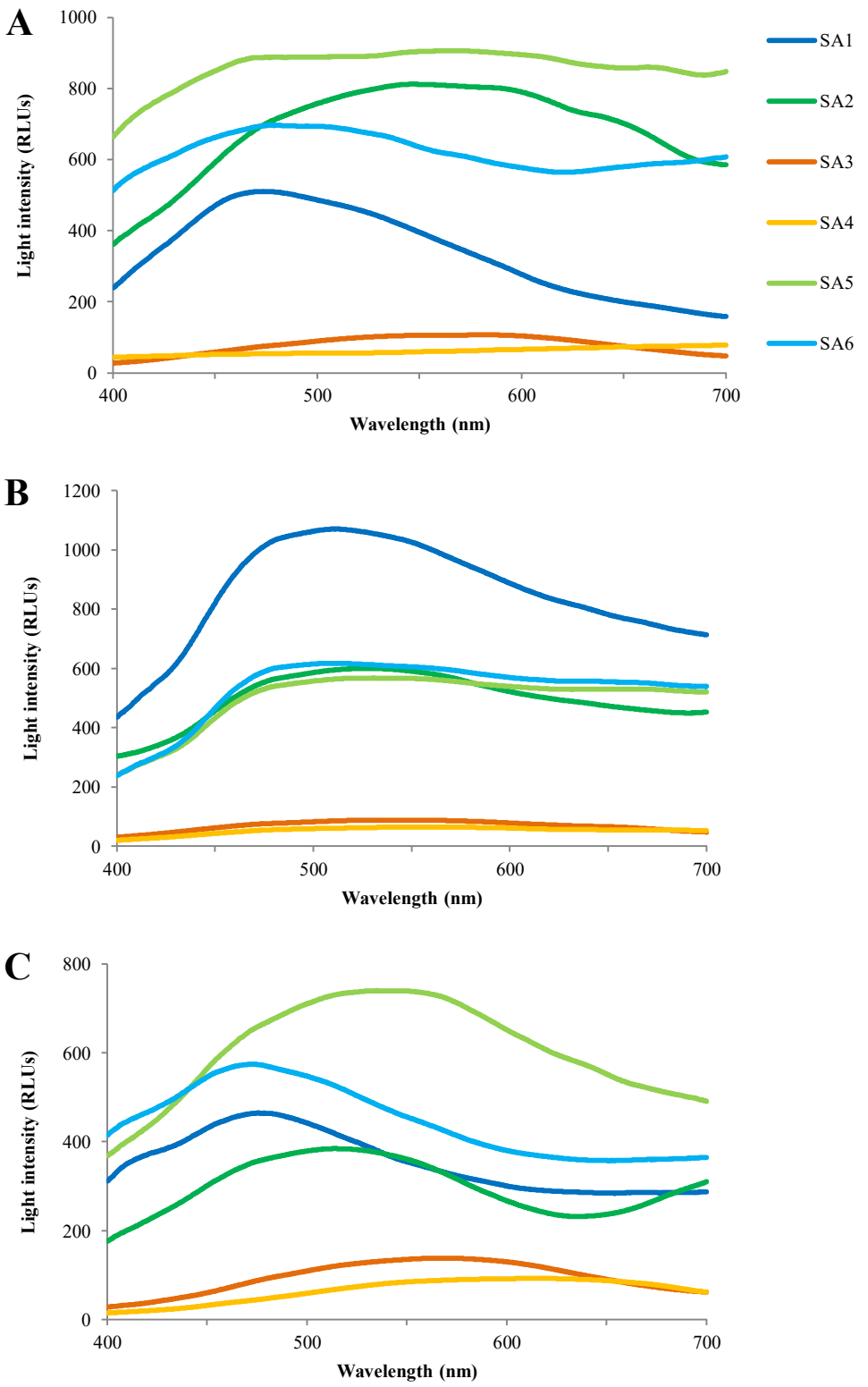

Figure 55 – Raw data of reflection spectra at 50º from inner reflector of *D. watasei*'s ventral body photophore per 6 SAs on: A) Photophore 1; B) Photophore 2; C) Photophore 3. RLUs= Relative light units.

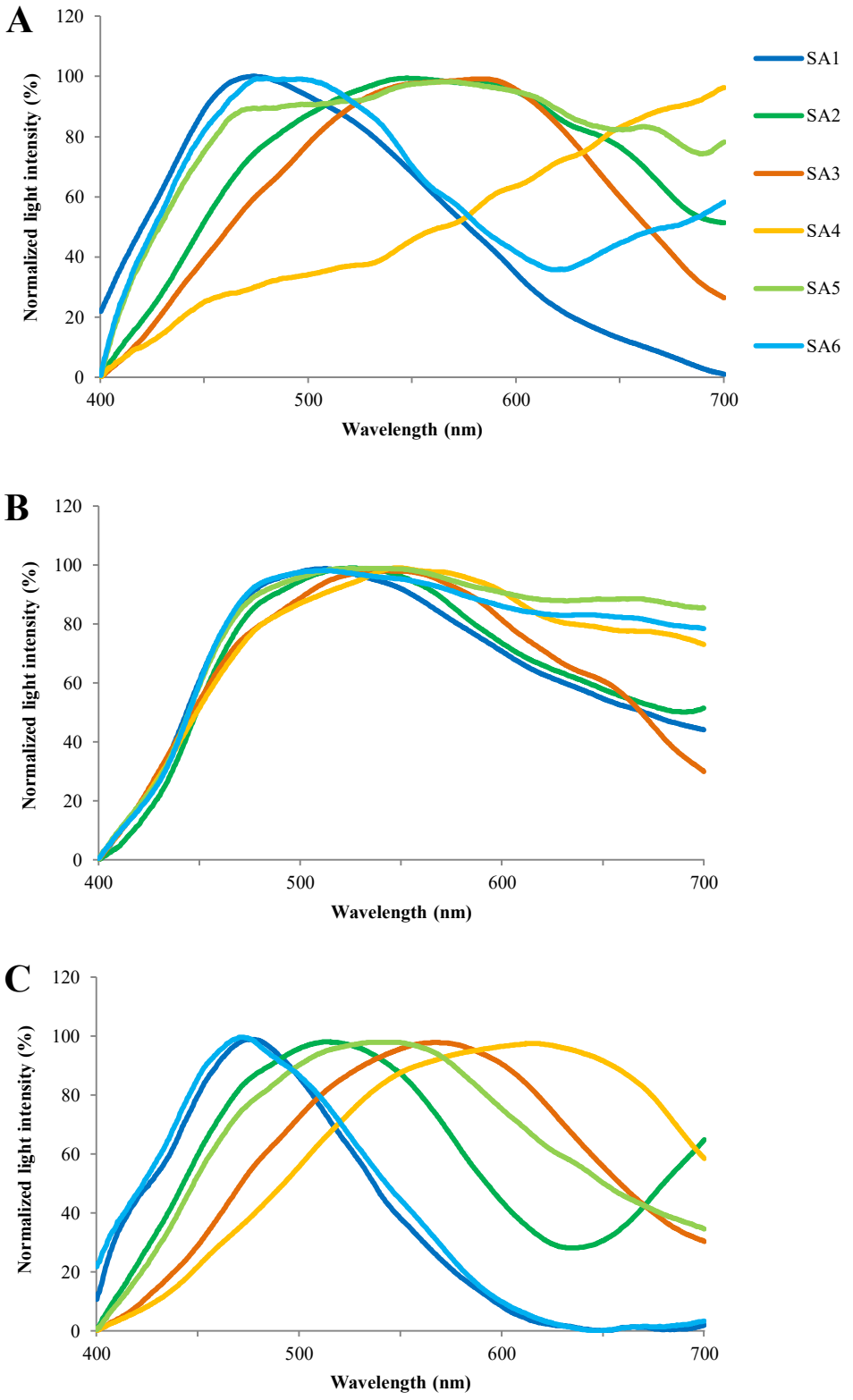

Figure 56 – Normalized (%) reflection spectra at 50 ° from inner reflector of *D. watasei*'s ventral body photophore per 6 SA on: A) Photophore 1; B) Photophore 2; C) Photophore 3. RLUs= Relative light units.

b. Spectra variation per tilting angle

Reflection spectra was measured under epi-illumination on the same area of the photophore tilted at angles of 10, 20 and 30º. Reflection light intensity is highly dependent on the photophore, higher average and variation on photophore 2 and lower variation on photophore 1 (Fig. 57 – 58, for detailed values of average and standard deviation, see Supplement 8). Variation of light intensity for photophore 1 is between 57.06 – 69.36 RLUs (63.28 ± S.D. 6.15 RLUs), photophore 2 between 155.80 – 263.40 RLUs (195.35± S.D. 59.19 RLUs), and photophore 3 109.16 – 172.06 RLUs (149.39 ± S.D. 34.94 RLUs). Minimum values of light intensity are reached at 10º for photophore 1 and 2, and at 30º for photophore 3. Maximum values of light intensity were inverse, at 30º for photophore 1 and 2, and at 10º for photophore 3.

Peaks of reflection spectra are different among photophores, higher average and variation on photophore 3, lower average on photophore 2 and variation on photophore 1 (Fig. 57 – 58). Variation of wavelength λmax for photophore 1 is between 578 – 604 nm (587 ± S.D. 15 nm), for photophore 2 between 528 – 571 nm (546 ± S.D. 22 nm), and for photophore 3 between 567 – 619 nm (594 ± S.D. 26 nm). Shorter wavelengths λmax are always reached at 30º and longer wavelengths at 10º.

FWHM values vary between photophores, higher average on photophore 1 and variation on photophore 2, lower average on photophore 2 and variation on photophore 1 (Fig. 57 – 58). Variation of FWHM for photophore 1 is 186 – 208 nm (196 ± S.D. 11 nm), for photophore 2 between 145 – 217 nm (176 ± S.D. 38 nm), and photophore 3 between 155 – 211 nm (189 ± S.D. 29 nm). Minimum values of FWHM light intensity are reached at 20º for photophore , and at 30º for photophore 2 and 3. Maximum values for all photophores were observed at 10º.

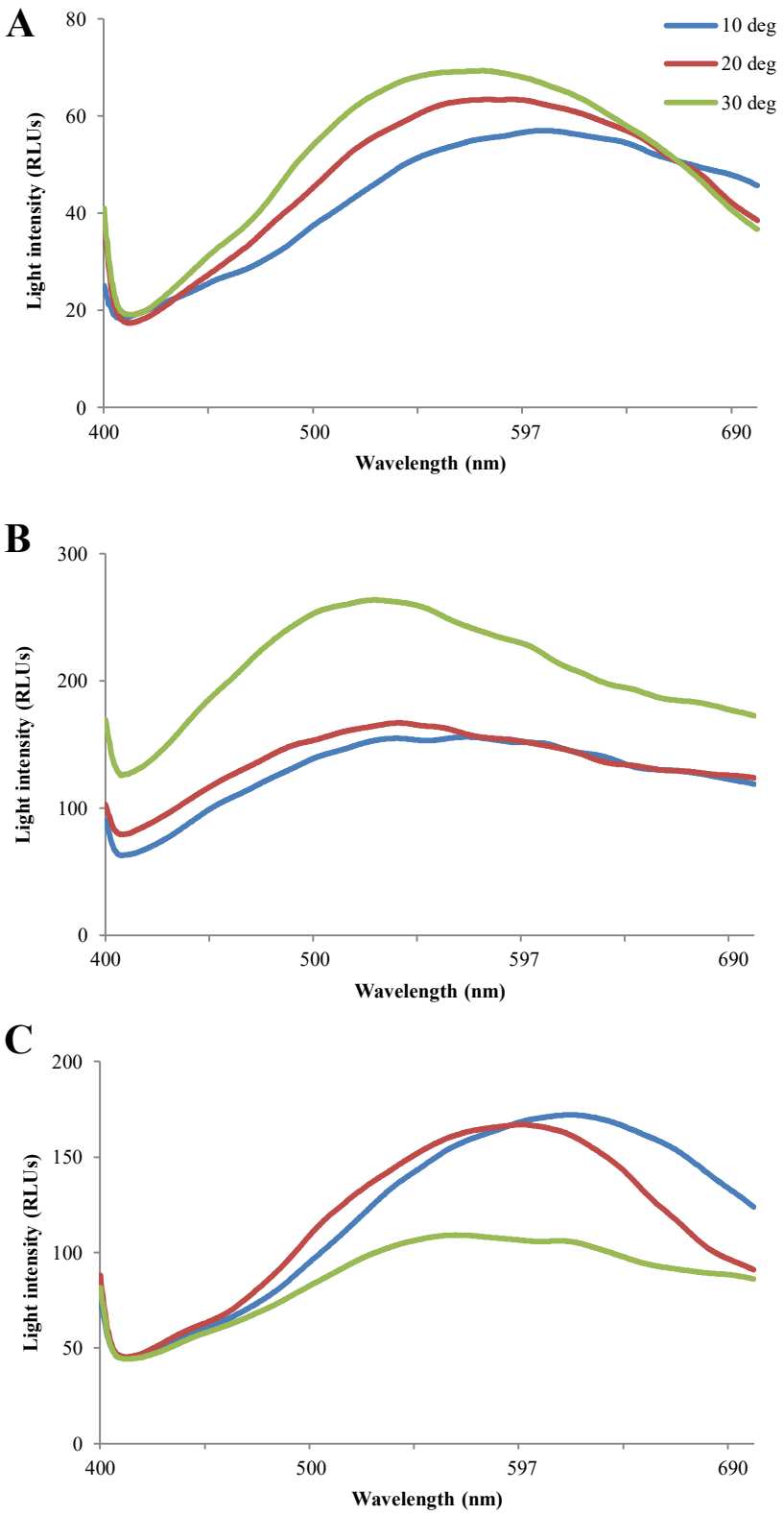

Figure 57 – Raw data for reflection spectra of central area of inner reflector of *D. watasei*'s ventral body photophore under tilted angles of 10º, 20º and 30º for A-C) Photophores 1 – 3. 10-30= 10 - 30º. deg= Degrees (º); RLUs= Relative light units.

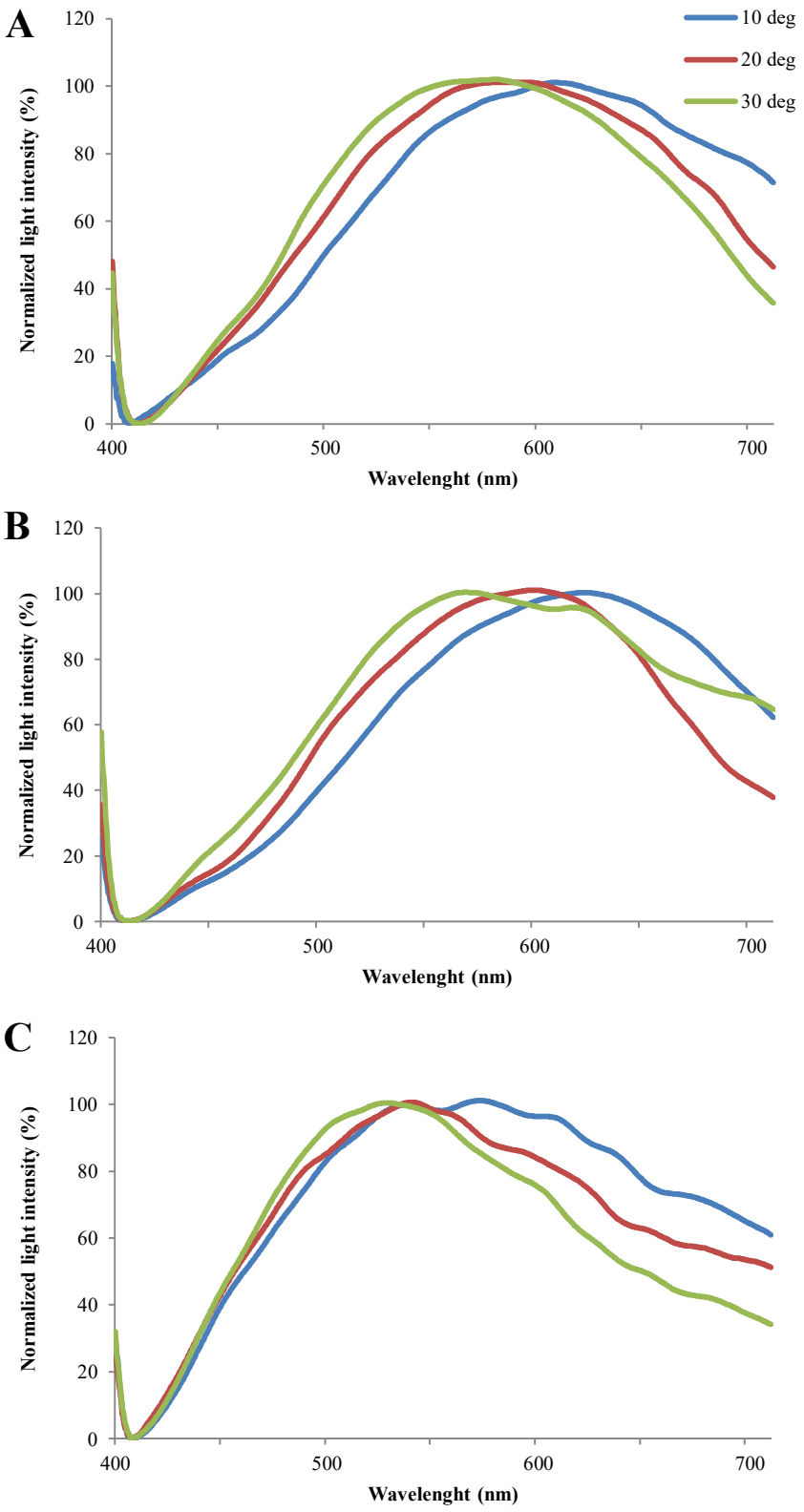

Figure 58 – Normalized data (%) for reflection spectra of central area of inner reflector of *D. watasei*'s ventral body photophore under tilted angles of 10º, 20º and 30º for A-C) Photophores 1 – 3. 10-30= 10 - 30º. deg= Degrees (º); RLUs= Relative light units.

4. Discussion

c. Light interference and angle-dependent spectra

Iridophores in the inner reflector of *D. watasei* ventral body photophores are constituted by thin platelets (96 nm), in the range of observed range of average thickness in coloured skin of fish (70 – 100 nm) [147], indicating that the observed platelets are guanine crystals. This is supported by the guanine identified in this reflective tissue (see Chapter 3). Observed arrangement of parallel guanine platelets in layered stacks was previously described to be responsible for light interference in fish iridophores [118, 124, 125] which suggests that this mechanism is in the basis of the examined reflection spectra (see Chapter 5). Unfortunately, due to section deformation of iridophores and higher magnification limitations of SEM microscope the thickness of the cytoplasm thickness could not be determined.

Spectral variation under epi-illumination when photophores were tilted 10 – 30^{o} vary from 15 to 26 nm per photophore (λmax= 528 – 619 nm). Reflection spectra by light interference and respective variation per angle was estimated for guanine iridophores, assuming no alteration of cytoplasm thickness between different angles [124]. Longer wavelengths than 528 nm in the visible spectra, are obtained for angles variation up to 24^{o}, which is close to the observed in this study. Some variability is expected for these spectral measurements, as the angle of photophore accommodation in the chamber used for the analyses are assumed to have some degree of variation between different samples. Results of angle-dependent wavelength in the inner reflector of *D. watasei* ventral photophores are also in accordance with the observed in the jewel beetle *Chrysochroa* [150]. Then, it is assumed that the theoretical principles in [125, 196] of angle-dependent wavelength for light interference are applicable to the iridophores of the inner reflector of *D. watasei* ventral photophores for further discussion.

Reflection spectra measured without photophore tilting is noticeable, at first sight, the divergence of wavelength λmax to the measurements on fresh tissues (Chapter 5), which is explained essentially by fixation and experimental design. Longer wavelengths are expected in the blue-green inner reflector of the photophore after fixation in glutaraldehyde due to slight dislocation of platelets during fixation, which would alter the angle and spacing between them and, consequently, wavelength of light interference [124]. as reported for the structural colour on scales of guanine iridophores in herring *Clupea* to change from blue to green after glutaraldehyde fixation [197]. Additionally, reflection spectra on fresh photophores was measured using a system similar to epi-illumination, with angle close to 0, between light source

and the spectrometer sensor while on the non-tilt experiment, was measured with 50º angle between light source and the spectrometer sensor (Fig. 59A). The first system only allows light to be measured on the middle area of the organ where the platelets are parallel to the vertical angle of focused light, while allowing measure reflection along all the reflector. On the downside, for the first system, light is only focused on a small area of the reflector (100 µm) while on the second one the light source is focused on all the organ, where some small degree of light contamination from other angles can occur. Differences between the methods are clear when one notice that while the middle is the only area of the reflector that can be measured with the first system, it is the areas for which the cumulative light intensity is lower in the second system. Highest cumulative light intensity area on the reflector was chosen in R.IA for fresh tissue spectral measurements, suggesting it to reflect the right angle of photocytes – reflector surface on that area (Fig. 59A) which will be taken into account for discussion of spectrometry angles for the second system.

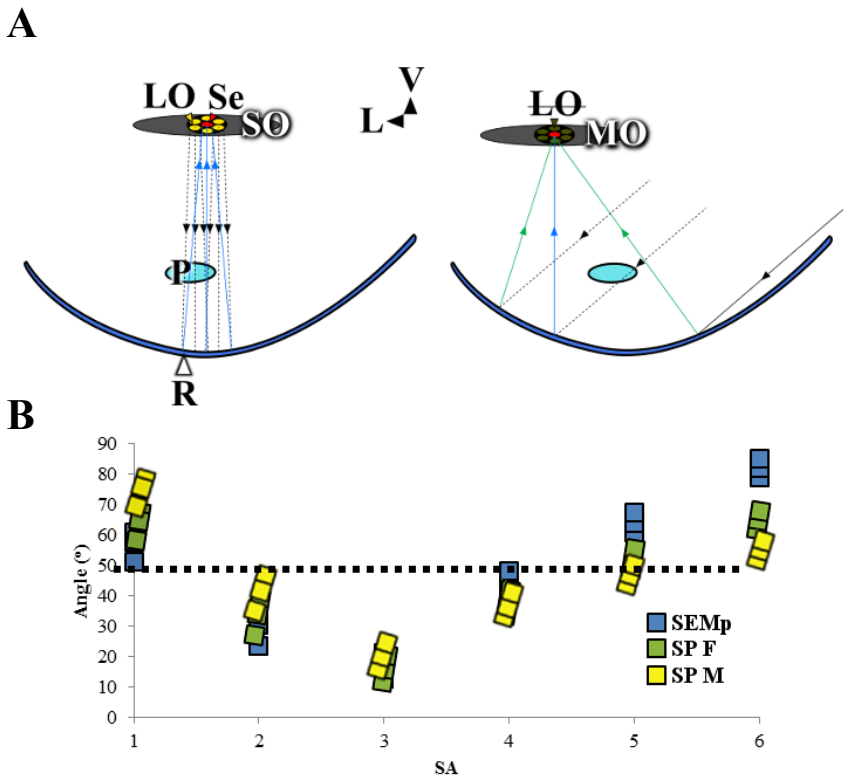

Figure 59 – Schematic illustration of spectrometry systems for measuring light reflection of *D. watasei* ventral photophores and photophore angle between SEM microscope photographies and spectrometry tests. A) Spectrometry system used on fresh photophores on R.IA (left) and non-tilted fixed samples at 50º on R.ISAs (right). B) Angle of photocytes – reflector surface for SEM microscope photographies (SAs) and theoretical range of photophore angle on chamber for spectrometry tests at 50º (R.IAs). LO= Fibre optic light source on; SO= Stereo microscope objective; Se= Spectrometer sensor; P= Photocytes; R= Inner reflector; ~~LO~~= Fibre optic light source off; MO= Microscope objective; SEMp= SEM microscopy photographies; SP F= Spectrometry testes flat photophore angle; SP M= Spectrometry tests maximum photophore angle; V= Ventral; L= Lateral; R.IA= Illuminated central area of the inner reflector; R.ISA= Sampling area illuminated on the inner reflector;. Dashed black lines (A) represent the light emission from the light source in the bifurcate fibre cable probe (left) and vertical 50º light source (right) and black arrow heads light direction. Blue line represents the light angle projected from the photocytes by the inner reflector

and blue arrow heads the light direction. Green lines represents light angle from examples of contaminated reflection and green arrow heads the light direction. Dotted black line (B) delineates SAs focused by 50º angle.

In these spectral tests for 3 photophores, λmax vary in a range of 253 nm (475 to 728 nm). On SEM sections of photophore 1, the angle of photocytes – surface reflector was estimated to vary in a range of 71º (13 to 85º). According to [124], angle variation of 72º corresponds to a range of 250 nm in the visible spectra, which indicates that the angle of photocytes – surface reflector on SEM sections is well represented by the spectral measurements. To determine the correspondence of the 50º angle (light source – spectrometer probe) in the spectral experiments to the photocytes – reflector surface in SEM, one might first take into account the photophore angle. Angle of the photophore in SEM photographs was corrected to the actual one that it originally lays on the body surface. In the reflection spectrometry tests, the position of the photophore in the experimental chamber is assumed to be flatter or even slightly tilted in the opposite inclination (Fig. 59B). In the spectrometry tests positioned photophore, the 50º angle of photocytes – reflector surface will be positioned in the R.ISAs/SAs 2, 5 and 6. However, light from the photocytes is projected in R.ISA/SA 2 to the lens reflector, which avoids it to be directly emitted outside on the lateral side of the organ [87] (see Chapter 4). As the mechanism of light reflection that project light outside the organ from the lens reflector area is still not fully understood, only the area that allow direct reflection of light outside from the photocytes is discussed, i.e. R.ISAs/SAs 5 and 6. Moreover, looking at the cumulative light intensity for the emission side of the photophore (R.ISAs 3-6), R.ISAs 5 and 6 reflect higher intensity for the 3 photophores, which was the principle taken into account for R.IA selection on measurement of light reflection in fresh tissues (See Chapter 5). Reflection spectra λmax obtained for R.ISAs5 and 6 for 3 photophores is between 475 and 546 nm which is in the range of the reflection measured on fresh tissues under white light (476 – 525 nm, see Chapter 5). This indicates that, on spectrometry tests, actual angle of photocytes – reflector surface is achieved on the R.ISAs/SAs 5 and 6 and the wavelength variation between R.ISA/ is related to the variation of angle inclination of iridophores along the inner reflector SAs. Additionally, in the 3 tested photophores, reflection wavelength λmax has the same pattern, longer wavelengths on R.ISAs 3-4 (539 – 728 nm), gradually becoming shorter to the peripheral R.ISA 6 (475 – 512 nm). On SEM, photocytes – reflector surface angle varies in the opposite way, from SA 3 – 4 (13 – 48º) to SA 6 (78 – 84º). Longer reflection spectra λmax on R.ISA/SA with lower angle of photocytes – reflector surface and *vice versa* is in agreement with the theoretical calculations for angle variation on light interference iridophores [124, 125]. Therefore, for angle-dependent light interference on the emission side of inner reflector of *D. watasei* ventral photophores, the experimental reflection spectra measurements (R.ISA) are explained by the theoretical estimations based on the ultrastructure of guanine platelets (SA).

d. Parabolic reflector and platelets angle

Inner reflector of *D. watasei* ventral photophores is parabola-like shaped with hexagonal arrangement of iridophores to ensure a ventral angle of light emission for an adequate counterillumination (see Chapter 4). However, it was assumed that platelets are parallel to the reflector surface, as it is required for the tissue to project light from photocytes as predicted by the theoretical model of reflection on parabolic mirrors [171]. In this chapter, the angle between guanine platelets and the reflector surface was estimated on both analysed photophores. For the area of the photophore that is not covered by the lens reflector and emits light directly from the photocytes, excluding most peripheral SA of photophore 2 (see the last paragraph), the platelets are found to be close to parallel angle to the tissue surface (average, photophores1, 2= 3.16 º, 3.79º). Observed angles of platelets inclination are adequate for the parabola-like reflector to project light on a ventral angle for an adequate match to downwelling light and a successful counterillumination.

According to [124, 125], maintaining the spacing between platelets, when the focus angle of light on the iridophore enhances, reflected spectra from light interference alters to shorter wavelengths. Angle of light emitted from the photocytes and projected outside by the reflector varies along the photophore 1 (SA 3 to 6= 12. 58 – 84.88º). On the side of the organ that is not covered by the lens reflector and emits light directly from the photocytes to the outside, this angle differences result in a highly variable spectra between the middle and the peripheral area, as observed under white light at 50º (475 - 728 nm). Photocytes light emission spectra from the photocytes is quite limited (λmax= 454 nm; FWHM= 61 nm) when compared to the white light source used (λmax= 570 nm, ; FWHM= 470 nm; data not included), and the same angle of light emitted does not focus in all the organ as in the 50º spectrometry experiment but only focused on an area of 100 μm (diameter of photophores, see Chapter 2). Even taking this into account, the spectra variation of light projected from iridophores reflecting in such various angles [124, 150] along one photophore it should not be precise enough to narrow down to the range of spectral peaks of downwelling light in mesopelagic (λmax= 472 – 484 nm [17]) to allow a successful counterillumination [120]. Taking into account that an inadequate counterillumination is more likely to make the fish an easier prey than to conceal in from the predators [20, 40], it is expected some mechanism of angle compensation to ensure and appropriate and constant spectra of bioluminescence from the ventral photophores of *D. watasei.*

Going one step back, even though the angle between platelets and the reflector is parallel enough to maintain the inner reflector of photophores functioning according to the

principles of the parabolic mirrors, there is a clear tendency for this parallelism to be disrupted as close as it gets to the peripheral areas of the organ as estimated, up to 28º (SA6, photophore 2). Examining the ventral side of the photophore that is not covered with the lens reflector and emits light directly to outside, it is found an alteration difference from the angle between photocytes and the reflector surface to the angle between the photogenic cells and the actual reflecting platelets in the iridophores. Between SAs 3 and 6, comparing to the angle photocytes – reflector surface (photophore 1= 51.67 ± S.D. 25.44º, *n*= 4), the angle of photocytes-platelets (photophore 1= 107.83 ± S.D. 6.84º; photophore 2= 98.56 ± S.D.4.54º, *n*= 4) has lower variation in angles up to 5 times and average values close to right angle. This allows the light emitted from the photocytes to be reflected outside by the platelets in a regular angle close to 90º, ensuring an emission at the same vertical angle by the parabola-like shape of the reflector [171]. Simultaneously, by maintaining a regular angle of the platelets to the focused light, light interference of the platelets produces homogenous spectra of light reflection [124, 125]. Vertical angle and regular wavelength allow a successful counterillumination on mesopelagic depths [120]. Inclined iridophores of guanine crystals on tapeta lucida in crustaceans, bivalves and sharks are reported for similar light purposes on altering reflection angle of light in the eye [126–129]. In the tapeta, the inclination of peripheral platelets has the purpose to maintain a perpendicular angle to the focused light in order to reflect back the photons on the same exact angle received by the platelets to the photoreceptors. For the photophore, the biophysical purpose of the inclination of these peripheral platelets might be to correct the parabola-like shape of the inner reflector (see Chapter 4) to function as a perfect parabolic mirror [171];. This mechanism would allow an adequate match of angle and spectra to the downwelling light for counterillumination [20, 40, 120]. Nevertheless, one cannot discard the hypothesis that the cytoplasm thickness between the guanine platelets varies along the reflector to correct the wavelength variation produced by the angle variation [124, 125, 138, 141] of photocytes – surface reflector, which might function in synergy with the angle correction by the non-parallel platelets.

e. Conclusions

This chapter includes the first clear observations of the layered platelets in iridophores of the inner reflector on lanternfishes ventral photophores. In semi-thin sections under SEM microscopy of *D. watasei* ventral photophores, platelets were identified as guanine crystals by its arrangement [130, 139, 140] and thickness [147]. Parallel arrangement of multilayered in iridophores with cytoplasmic spacing confirms the structural colour of reflection observed on the tissue is due to light interference of guanine platelets [125].

The first analysis of ultrastructure and spectrometry to study angle-dependent wavelength on reflectors of photophores in fishes is included as well. Angle-dependent light interference [124] was confirmed on tilted (10, 20 and 30º) ventral photophores of *D. watasei* by spectrometry under epi-illumination microscope. Variation of light reflection spectra along the emission area of inner reflector at 50º is according to the estimation of platelets angle [124]on SEM microscope photographies.

On *D. watasei* ventral photophores, the angle of platelets is roughly parallel to the to the parabolic-like inner reflector surface allowing it to function as a parabolic mirror [171], providing an adequate angle on ventral direction for counterillumination [40, 120]. Angle between photocytes and platelets is close to 90º, to allow light to be projected outside the organ on ventral angle by parabolic reflection [171] and on the same wavelength [124] for an appropriate counterillumination [40, 120]. Ventral photophores of lanternfishes seems to be provided with a reflective system based on the inner reflector designed for adequate angle [171] and spectra [124, 125], not only tissue level but also cellular (iridophores) and intracellular (platelets), to allow ventral angle and homogenous spectra for successful counterillumination [40, 120].

This study is currently being continued on performing of thin-sections for TEM analyses of the cytoplasmic thickness along the reflector for wavelength estimation along the inner reflector of *D. watasei* ventral photophores. It is also under preparation a spectrometry system that allow to measure reflection the spectra of individual iridophore while tilting photophore angle without moving the photophore position, while detect the reflection angle as well.

CHAPTER 7

General discussion

1. Multifunctional bioluminescence in mesopelagic zone

f. Head photophores

Mesopelagic zone has been claim for some time as the primary domain of bioluminescence in the planet, in terms of species diversity and abundance, as well as luminous systems complexity [50]. Although not clearly examined, this scenario is highly probable since the great majority of luminous organisms are marine and pelagic [49], and the most bioluminescent marine organisms were reported in the mesopelagic [170]. Such high biodiversity of luminescent organisms is due to the light parameters of the mesopelagic zone that make light signals specially advantageous in this environment [50, 54]. This truly twilight zone is penetrated only by dim light and without any visual obstacles, allowing luminous signals to be easily seen at large distances [20, 50, 54].

Diaphus watasei took advantage of the light scenario were inhabits and developed diverse photophores to achieve multifunctional ecological roles. This was observed by the adaptation of inner structure of the light organs and the main tissues with active function on light emissions: 1. Area of photocytes for different intensity of light emissions; 2. Lens thickness and composition for various dioptric levels of light angle control; 3. Angle and organization of guanine platelets in inner reflector for light spectra and angle control; 4. Accessory reflectors for angle limitation of light emission.

Observed histological sections of *D. watasei* 's head photophores (Ant, Dn, Vn) exhibit higher photocytes area, frontal lenses and back reflectors for simultaneous frontal emissions of highest light intensity estimated in *D. watasei*, working as "light torch" in a very adequate way to the proposed function of illumination of prey and surroundings [49]. Silver inner reflectors of guanine crystals allow high intensity reflection in a broadband spectral reflection [118, 141] and non-dioptric lenses [198–200] are related to ecological bioluminescent roles that are related to light intensity but do not require spectral or angle precision of light emissions, such as counterillumination [40]. Lateral reflectors and lenses in Ant and Vn allow also light emissions on lateral directions, most likely for secondary functions besides illumination. Although there is no clear evidence in *D. watasei,* Vn is reported as sexually dimorphic among *Diaphus* [39], ventral-lateral flashes would allow light signals for sexual purposes These observations are in accordance with the sexually dimorphic caudal photophores in other species of lanternfishes were reported to have bright emotions for intraspecific sexual signalling [96, 98]. Luminous purposes are not reported for Ant, the photophore with highest individual light intensity which emits dorsal-laterally. Based on a different direction than Vn and intensity, it might be for light signals to fulfil other intraspecific communication signal, such as schooling or recognition, as in

other luminous marine animals [49]. Multifunctional luminous purposes in head photophores are assumed to be allowed due to, as reported in luminous patches and caudal organs in lanternfishes, emit bright lights under different physiological control than body photophores [94, 96, 98, 112]. It seems a similar case as in the deep-sea dragonfishes [18, 39] and shallow-water nocturnal flashlight fishes [137], which sub-ocular photophores allow multifunctional light emissions for illumination and intraspecific communication.

a. Body photophores

Besides allowing luminous signals to be easily seen at large distances [20, 50, 54], other light characteristics of the mesopelagic zone are adequate for bioluminescent camouflage, which explains why so many species inhabit here developed ventral photophores for counterillumination [16, 54]. Most light is absorbed on shallow-waters, reaching the mesopelagic zone just a narrow wavelength of blue-green [3, 16], highly directional on a vertical angle [3, 16, 54]. Ventral photophores of lanternfishes are neutrally controlled [91–95, 100] ensuring an adequate regulation of bioluminescent intensity under different ambient light levels as previously reported [99, 201]. Additionally to intensity, to achieve successful camouflage by counterillumination, light emissions of *D. watasei* require to match the angle and spectra of downwelling light [18, 20, 40, 103, 120].

Comparing to head photophores, body organs have photocytes area up to 10x smaller, allowing lower light emissions [96] to match the dim downwelling light on mesopelagic zone [17] for an adequate counterillumination [40]. Observed histological sections of *D. watasei*'s branchiostegal, and ventral and lateral body photophores hare much more complex, relatively to head photophores. Variation of organ inner structure, namely for dioptric lenses, coloured and accessory reflectors, correlate to the position of light organ in the fish body, achieving an adequate spectral and angular for successful counterillumination [18, 40, 87, 97, 108]. Observed histological sections of structural coloured iridophores with guanine crystals [124, 125, 141, 202] ensure spectral modulation of photocytes light emissions by the inner reflector [18, 90, 202] to match the downwelling light for counterillumination [40, 120]. Thicker [198–200] lenses with oblique collagen layers [142–144], and inclined iridophores [126–129] of the inner reflector on branchiostegal and lateral photophores; and functional inner reflector only in the dorsal side of lateral organs [199, 203] seem to "compensate" the non-ventral position of these organs to ensure light emissions on ventral direction, matching the vertical downwelling light angle on mesopelagic depths [3, 19, 103] for a successful counterillumination [20, 40, 103, 120].

Histological sections of ventral body photophores of *D. watasei* revealed an inner structure designed for precise light emission on a ventral angle. While the parabola-like inner reflector with focus point located on the top of photocytes projects light ventrally [171], accessory lens reflectors in ventral and body photophores avoid light leaking on lateral angles [87] projecting it to the inner reflector on the emission side of the photophore passing through the photocytes, ensuring all light is directed outside the organ on a ventral angle. On semi-thin sections under SEM microscopy, platelets were identified in the inner reflector of *D. watasei*'s body photophores as guanine crystals by its arrangement [130, 139, 140] and thickness [147]. Platelets were observed in the inner reflector to be positioned in parallel to the tissue surface, allowing it to function as theoretically determined for parabolic mirrors [171]. Unique hexagonal interlocking arrangement of these iridophores was found to project a constant angle of light along all the reflector [163] with high energetic efficiency. The result is a complex system of light reflection where the main role is performed by the inner reflector, designed precisely to ensure precise ventral light emissions that matches the downwelling sunlight in deep-sea for a successful counterillumination [20, 40, 103]. This is supported by the reported downward light emissions on body photophores of lanternfishes *Myctpohum* [99] and *Tarletonbeania* [100] and ventral angle analysed in other mesopelagic fishes [103].

Spectra of the bioluminescent reflection was obtained by mixing purified luciferase luciferase extracts from *D. watasei* ventral photophores with coelenterazine and reflection spectra was measured from the inner reflector of fresh photophores. It was found that the spectra of light emitted by the photocytes (454 nm) is modulated by the inner reflector (460 – 470 nm) to match the downwelling light on the mesopelagic zone (472 – 486 nm) [17] where *D watasei* inhabits [180], resulting in a successful counterillumination [120]. The ultrastructure of the iridophores was analysed in semi-thin sections under SEM microscopy, to analyse the biophysical mechanism behind the apparent structural colour of the photophores. Guanine platelets were observed in multilayered stacks, parallel to each other with cytoplasmic spacing in between. This arrangement produces light interference of guanine platelets [118, 124, 125, 138, 159] which provides the reflection colour observed on this tissue. Besides the cellular structure organization of the iridophores, the wavelength of light interference is also dependent on the angle from which the light is focused on the platelets [125, 150, 196]. Light reflection was measured in fixed photophores, on the middle area of the organ under epi-illumination at tilting angles (10, 20, 30^{o}), and from the middle to peripheral area of the organ with light source at 50^{o}. From SEM microscope photographies, light angle between photocytes and guanine platelets was estimated, on the ventral side of the organ that is not covered by the lens reflector and emits light directly outside. Angle-dependent light interference [124] was confirmed under epi-illumination microscope and the estimated angle [124] between photocytes and platelets on

SEM photographies is in accordance with the variation of light reflection spectra at 50º. Inclination angle of platelets in the reflector was estimated to maintain an angle close to 90º to the photocytes, allowing light from the photogenic cells to be reflected outside in the same wavelength and angle [124, 125].It was found that inner reflector of the ventral photophores of *D. watasei* seem to be accurately designed down to the intracellular level, to adequate angle [171] and spectra [124, 125], for successful counterillumination [40, 120] in the mesopelagic realm [17, 19].

2. Counterillumination and diel vertical migrations

Lanternfishes are diel vertical migrators, ascending to shallow waters at dusk to feed on zooplankton and returning to mesopelagic depths at dawn [13, 75, 76]. During this dislocation on the pelagic realm, light scenario changes dramatically, which turns disadvantageous any counterillumination tuned to mesopelagic [3, 18, 20, 50, 168]. Lanternfishes have highly sensitive eyes [3, 22, 24–28] adapted to perceive downwelling light and bioluminescence [29, 74, 109], indicating that these fishes can notice the difference between their bioluminescence and the light scenarios differences during diel vertical migrations (DVMs). *D. watasei* reaches minimum depths of 258 m [180], where the downwelling light penetrates the ocean in the same vertical angle as in the mesopelagic depths below [3, 19, 103], indicating that the angle of counterillumination light [40, 103] does not need to be regulated during migrations. Intensity of sunlight at midday in the ocean enhances up to $1x10^4$ times from 600 to 200 m, which is up to $1x10^6$ times more intense than at night (100m) [17], not representing a problem for the neutrally controlled photophores of lanternfishes [91–95, 100] that can regulate the intensity output of light emission [99, 201].

Regarding light spectra, absorption and scattering of water molecules and suspended particles filter the downwelling light wavelengths from the ocean surface to 100 m, while below these depths only slight changes are observed [17, 120]. Spectral peaks of moonlight below 100 m are very similar to sunlight [17], but as migrations of lanternfishes time span is from 1h before dusk to 1 h after dawn [6], besides downwelling sunlight at mesopelagic depths, *D. watasei* encounters twilight spectra along the way. Variability of estimated wavelength of *Diaphus* luciferase light (λmax= 454 nm) that is modulated by the inner reflector of ventral body photophores (λmax= 460 – 470 nm) was found to fit in the spectra range of downwelling light from twilight at surface (λmax= 450 nm [169]) and sunlight at mesopelagic depths (λmax = 472 – 486 nm [17]). This lead to a to an hypothesis for spectral adaptation by inner reflector light interference of counterillumination during DVMs in lanternfishes, supported by similar

mechanism reported for counterillumination spectral regulation during DVMs [116, 191, 192] and bioluminescence colour change observed in a lanternfish [50].

Modulation of light reflection spectra can be achieved by tunable iridophores [145]. Tunable guanine iridophores with similar structure to *D.watasei*'s inner reflector are reported in the skin of neon tetra fishes [138] and cuticle of sapphirinid copepods [159], for camouflage purposes. In copepods, reflected wavelength of light interference is controlled by changing the thickness of inter-platelets cytoplasmic layers [159]. Due to similar crystal morphology and hexagonal interlocking arrangement of iridophores reported on tunable iridophores of copepods [141, 154, 159] as found in *D. watasei*, it is probable for a tunability mechanism alike to be found for the lanternfish inner reflector. Osmoregulation is reported as the responsible mechanism for the alterations of inter-platelet cytoplasmic thickness, precisely examined and described in the *Dorytheuthis* squid [204]. Enhancing the ionic concentration of buffer solution makes intracellular water to flow outside of iridophore cell, diminishing the cytoplasm thickness between the plates, and *vice versa.* Reduction of cytoplasm thickness between platelets produces shortwave alteration of light interference spectra [124, 125]. Structural colour alteration by osmolarity changes is reported for guanine iridophores in skins of chameleons [153], lizards [182], fishes [146] and suggested for the sapphirinid copepods cuticle [159]. Namely in fishes, osmoregulation of iridophores was analysed on the neon tetra *Paracheirodon* [138, 151, 205], the sprat *Clupea sprattus*[147], the herring. *C. harengus* [197], the whiptail *Pentapodus* [206] and the blue damselfish *Chrysiptera* [207].

Preliminary tests for osmoregulation on inner reflector of *D. chrysorhynchus* ventral photophores were performed, not included in the main body of this thesis due to high variability data without clear patterns and low number of samples in adequate physiological conditions. Nevertheless, data from these tests are included for discussion purposes as preliminary confirmation of structural colour control by osmolarity in *Diaphus* lanternfishes. Hypertonic and isotonic solutions were prepared according to [138, 205] and the criteria for samples selection was based on physiological conditions and level of response on osmolarity alterations. Samples were submerged in osmolarity solutions (5 x volume of the sample) for 30 – 40 minutes, and reflection spectra measured from fresh, kept at 4ºC overnight and – 80ºC defrosted photophores (for spectrometry procedures, see Chapters 5 for fresh and overnight samples, and 6 for defrosted ones). Even though not all the samples respond to osmolarity alterations, i.e., reflection colour is visibly altered by different osmolarity, general tendency is for the structural colour to change for shorter wavelengths in hypertonic solution, relatively to isotonic solutions or without any solution added (fresh samples) (Fig. 60A). Similar tendencies are observed in reflection spectra for fresh samples and defrosted samples (Fig. 60B-C), latter ones with less clear curves. High variability in intensity and spectral curve shapes is observed in samples on

both conditions and no clear pattern is determined following osmolarity of solutions. Nevertheless, in samples that respond to osmolarity such as the presented ones, wavelength peaks always change to shorter wavelengths in hypertonic solutions, as according to previous reports in fishes skin [138, 147, 151, 197]. These results are supported by the fact that in samples with good physiological conditions the colour alteration by osmolarity is reversible, and any other guanine reflective tissues exhibit any visible structural colour alteration whatsoever, when submitted to different osmolarity solutions (data not shown). The reasons for the observed reflection spectra alterations by osmolarity only in some photophores and high variability of light intensity in different osmolarity solutions is still not yet understood in fresh samples. Low level and high variability of response to osmolarity in defrosted samples it is likely to be due to the physiological conditions of dead cells. Physiological conditions and damage of cells may be responsible for the variability observed on fresh and overnight samples, even though the reason for the sample kept overnight at 4°C be highly responsive to osmolarity than fresh samples is still not understood. It is likely that light interference in the inner reflector of *Diaphus* lanternfishes is controlled by osmoregulation but examination of higher number of fresh samples are required in order to optimize the methodological procedures and obtain conclusive results.

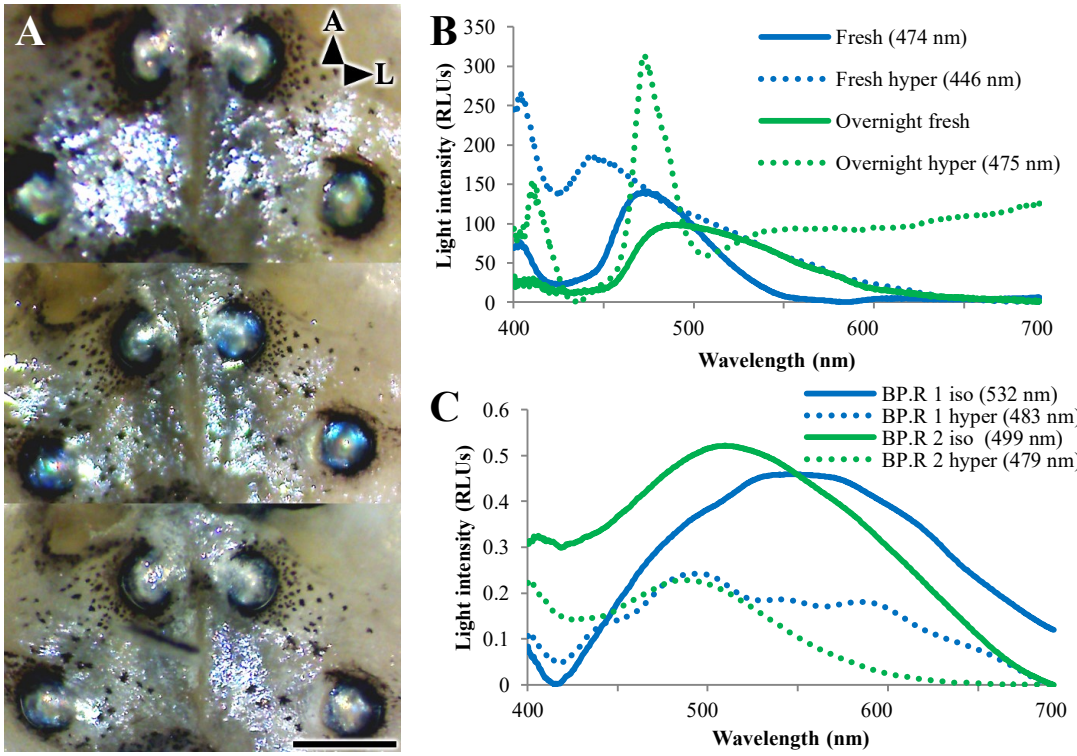

Figure 60 – Preliminary tests on osmoregulation of inner reflector in *D. chrysorhyncus*'s ventral body photophores. A) Photography under stereo microscope (ventral view) of sample under isotonic (upper), hypertonic (middle), distilled water (lower). Reflection spectra of: B) Fresh samples and kept overnight at 4°C; and C) Defrosted samples.. λmax values (B ,C) are presented between brackets. Hyper= Hypertonic; Iso= Isotonic; BP.R= Inner reflector of body photophore; A= Anterior; L= Lateral; RLUs= Relative light units. Scale bar= 1 m.

3. Conclusions

Facing the evolutionary efforts to achieve such complex organs with different organ and tissues structures, and tissues origins exclusively in photophores with counterillumination purposes, seems to indicate this camouflage [40, 50, 54, 120] represents a huge ecological advantage for mesopelagic fishes and with higher importance for its survival than other bioluminescent roles, as the ones performed by head photophores [39, 49].

Besides the inner structure of the reflector in body photophores, iridophores shape and arrangement have a critical role to ensure an adequate and regular angle, as well maximum intensity of light reflection for counterillumination in the mesopelagic realm [16, 103]. Light reflection performance and energetic efficiency of the iridophores hexagonal arrangement in the inner reflector is one step ahead to understand the reflective mechanism of lanternfish photophores. Parabolic-like inner reflector with platelets parallel to the tissue surface [171] while slightly tilted for regular wavelength [124, 125, 150] by angle-dependent correction [126–129], focus-point on the photocytes [174] and accessory lens reflector [87] as lateral shutter and light guide, if not the most, complex and accurate system of reflectors in light organs of fishes, comparatively to other luminous species [117]. Structure of lanternfish ventral photophores do not only ensure an adequate spectra and angle for camouflage [18, 20, 40, 50, 103, 120], but likely to control the light emission spectra by osmoregulation [118, 124, 138, 141, 146, 151, 159, 208] to the changing scenarios of downwelling light [17, 19] while performing DVMs [6, 75, 180].

Other diel migrant luminous fishes have photophores with pigment filters for counterillumination [18, 43] which would not allow spectral regulation. In these cases, a silver inner reflector is also required to ensure all the light produced by the photocytes is emitted outside the organ [39, 117]. Aside from some cephalopods [115, 116], myctophids are the only bioluminescent animals exclusively using complex reflective systems in photophores for angle and spectral match to downwelling light on counterillumination [18, 40, 103] with the additional feature of wavelength adaptation during DVMs. Complexity of reflective system in *D. watasei* ventral photophores seems to be far beyond what is yet comprehended and expected. Bioluminescence arose in lanternfishes around 80 million years ago [55], lanternfish photophores were engineered and refined by natural selection for a long way until achieving this highly complex and accurate mechanism of light modulation to fulfil a specific purpose crucial for their survival. Advantages of the unique mechanism in lanternfish photophores might explain the high species diversification of this family, comparatively to the general bioluminescent fishes [55].

4. Novel data and applications

Chapter 2

Reported different structure and tissues origin, in photophores of lanternfishes, for the same ecological purpose, namely, branchiostegal, ventral and body photophores for counterillumination. Additionally, is determined that these divergences are correlated to the position of light organs on the fish body and lateral photophores of body are also for counterillumination

Chapter 3

First UV confirmations of guanine (confirmed by FTIR and XRD[209]) and morphological and statistical examination of "perfect" hexagonal shaped guanine crystals from inner reflector of lanternfish photophores. Additionally, biophysical approach of light reflection on hexagonal interlocked guanine iridophores on light organs of bioluminescent animals.

Chapter 4

Established and described a biophysical approach of parabolic reflectors in luminous fish photophores for counterillumination, using lanternfish *D. watasei* as model [209].

Chapter 5

Reported *Diaphus* luciferase emission spectra and its modulation by the inner reflector of ventral body photophores of *D. watasei* [209]. Insights of DVM adapted spectra in counterillumination of fishes and exclusively to lanternfishes .

Chapter 6

Includes the first clear observations of the layered platelets in iridophores of the inner reflector on lanternfishes ventral photophores. Analysis of ultrastructure and spectrometry to study angle-dependent wavelength on reflectors of photophores in fishes is included as well.

Applications

Photophores of *D. watasei* have the same basic inner structure, but minor alterations in photophore area and reflector structure provide diverse output signals for specific purposes between head and body photophores. Additionally, dioptric lenses thickness and iridophores distribution and angle in the reflector seem to produce high changes in the angle of light emissions. Minor structural changes for diverse reflective purposes should be useful in the design of multipurpose light devices, essentially on a millimetres scale, such as the photophores.

Hexagonal interlocking arrangement of nanometres iridophores in the inner reflector of body photophores ensures high energetic performance by reducing the size and number of platelets per area while maximize a regular intensity of light reflection on a precise direction. This microstructure of multilayered iridophores have biomimetic potential to enhance performance of nano-reflectors allowing high and regular light intensity in a precise direction across a surface while ensuring low energetic costs.

Giant telescopes parabolic mirrors function solely with a similar structure [172], as the inner reflector of lanternfish photophores. Curiously, in photophores this reflector represents only a part of its reflective system. Complex reflection system of the photophores can be used to enhance performance of telescopes and other reflective devices with high accuracy of light reflection.

Modulation of reflection wavelength of light interference by tunable iridophores allows multiple spectra emission from the same light source on the inner reflector of photophores. Moreover, the platelets inclination in the tissue ensures a regular and precise reflection spectra and angle. This structure should have high interest for biomimetics ensuring multi-coloured light emissions from a regular white light, instead of using a different coloured light for each spectral purpose. It can be used to enhance performance of multi-coloured lights while minimizing energetic costs minimization, such as in traffic signals or on/off green/red lights in everyday devices.

5. References

1. Herring P (2002) The biology of the deep ocean. Oxford University Press, Oxford

2. Sutton TT (2013) Vertical ecology of the pelagic ocean: Classical patterns and new perspectives. J Fish Biol 83:1508–1527. DOI:10.1111/jfb.12263

3. Warrant EJ, Locket NA (2004) Vision in the deep sea. Biol Rev Camb Philos Soc 79:671–712. DOI:10.1017/S1464793103006420

4. Robinson C, Steinberg DK, Anderson TR, *et al* (2010) Mesopelagic zone ecology and biogeochemistry - a synthesis. Deep Res Part II Top Stud Oceanogr 57:1504–1518. DOI:10.1016/j.dsr2.2010.02.018

5. Priede IG, Bergstad OA, Miller PI, *et al* (2013) Does presence of a mid-ocean ridge enhance biomass and biodiversity ? PLoS One 8:1–10. DOI:10.1371/journal.pone.0061550

6. Catul V, Gauns M, Karuppasamy PK (2011) A review on mesopelagic fishes belonging to family Myctophidae. Rev Fish Biol Fish 21:339–354. DOI:10.1007/s11160-010-9176-4

7. Elia MD, Warren JD, Rodriguez-pinto I, *et al* (2016) Diel variation in the vertical distribution of deep-water scattering layers in the Gulf of Mexico. Deep Res Part I Oceanogr Res Pap 115:91–102. DOI:10.1016/j.dsr.2016.05.014

8. Clarke TA (1987) The distribution of vertically migrating fishes across the Central Equatorial Pacific T. Biol Oceanogr 4:47–81. DOI:10.1080/01965581.1987.10749484

9. Benoit-bird KJ, Mcmanus MA (2012) Bottom-up regulation of a pelagic community through spatial aggregations. Biol Lett 8:813–816

10. Benoit-bird KJ, Zirbel MJ, Mcmanus MA (2008) Diel variation of zooplankton distributions in Hawaiian waters favors horizontal diel migration by midwater micronekton. Mar Ecol Prog Ser 367:109–123. DOI:10.3354/meps07571

11. Benoit-Bird KJ, Au WWL (2006) Extreme diel horizontal migrations by a tropical nearshore resident micronekton community. Mar Ecol Prog Ser 319:1–14. DOI:10.3354/meps319001

12. Frank M, Widder A (2002) Effects of a decrease in downwelling irradiance on the daytime vertical distribution patterns of zooplankton and micronekton. Mar Biol

140:1181–1193. DOI:10.1007/s00227-002-0788-7

13. Roe HSJ, Badcock J (1984) The diel migrations and distributions within a mesopelagic community in the North East Atlantic. 5. Vertical migrations and feeding of fish. Prog Oceanogr 13:389–424

14. Bianchi D, Mislan KAS (2016) Global patterns of diel vertical migration times and velocities from acoustic data. Limnol Oceanogr 61:353–364. DOI:10.1002/lno.10219

15. Bergstad OA, Wik ÅD, Hildre Ø (2003) Predator-prey relationships and food sources of the Skagerrak deep-water fish assemblage. J Northwest Atl Fish Sci 31:165–180

16. Johnsen S (2014) Hide and seek in the open sea: pelagic camouflage and visual countermeasures. Ann Rev Mar Sci 6:369–92. DOI:10.1146/annurev-marine-010213-135018

17. Kampa EM (1970) Underwater daylight and moonlight measurements in the Eastern North Atlantic. J Mar Biol Assoc United Kingdom 50:397–420. DOI:10.1017/S0025315400004604

18. Denton EJ, Herring PJ, Widder EA, *et al* (1985) The roles of filters in the photophores of oceanic animals and their relation to vision in the oceanic environment. Proc R Soc B Biol Sci 225:63–97. DOI:10.1098/rspb.1985.0051

19. Jerlov NG (1968) Radiance. In: Jerlov NG (ed) Optical oceanography. Elsevier, Amesterdam, pp 107–114

20. Nilsson D, Warrant E, Johnsen S (2014) Computational visual ecology in the pelagic realm. Philos Trans R Soc Lond B Biol Sci 369:20130038. DOI:10.1098/rstb.2013.0038

21. Gagnon YL, Sutton TT, Johnsen S (2013) Visual acuity in pelagic fishes and mollusks. Vision Res 92:1–9. DOI:10.1016/j.visres.2013.08.007

22. Denton EJ, Warren FJ (1957) The photosensitive pigments in the retinae of deep-sea fish. J Mar Biol Assoc United Kingdom 36:651–662. DOI:10.1017/S0025315400025911

23. Herring PJ (2000) Species abundance, sexual encounter and bioluminescent signalling in the deep sea. Philos Trans R Soc Lond B Biol Sci 355:1273–1276. DOI:10.1098/rstb.2000.0682

24. Douglas RH, Partridge JC, Marshall NJ (1998) The eyes of deep-sea fish I: lens pigmentation, tapeta and visual pigments. Prog Retin Eye Res 17:597–636.

DOI:10.1016/S1350-9462(98)00002-0

25. Pankhurst NW (1987) Intra- and interspecific changes in retinal morphology among mesopelagic and demersal teleosts from the slope waters of New Zealand. Environ Biol Fishes 19:269–280. DOI:10.1007/BF00003228

26. O'Day WT, Fernandez HR (1976) Vision in the lanternfish *Stenobrachius leucopsarus* (Myctophidae). Mar Biol 37:187–195. DOI:10.1007/BF00389128

27. McNulty JA, Nafpaktitis BG (1977) Morphology of the pineal complex in seven species of lanternfishes (Pisces: Myctophidae). Am J Anat 150:509–529

28. Partridge JC, Shand J, Archer SN, *et al* (1989) Interspecific variation in the visual pigments of deep-sea fishes. J Comp Physiol A 164:513–529. DOI:10.1007/BF00610445

29. Turner JR, White EM, Collins M a., *et al* (2009) Vision in lanternfish (Myctophidae): adaptations for viewing bioluminescence in the deep-sea. Deep Res Part I Oceanogr Res Pap 56:1003–1017. DOI:10.1016/j.dsr.2009.01.007

30. Shimomura O (2006) Bioluminescence: Chemical principles and methods. World Scientific Publishing Co.

31. Tsarkova AS, Kaskova ZM, Yampolsky I V. (2016) A Tale of two luciferins: fungal and earthworm new bioluminescent systems. Acc Chem Res 49:2372–2380. DOI:10.1021/acs.accounts.6b00322

32. Thompson EM, Rees J (1995) Origins of luciferins: ecology of bioluminescence in marine fishes. In: Hochachka P, Mommsen T (eds) Biochemistry and molecular biology of fishes. Elsevier Science, Amsterdam

33. Campbell AK, Herring PJ (1990) Imidazolopyrazine bioluminescence in copepods and other marine organisms. Mar Biol 104:219–225

34. Shimomura O, Inoue S, Johnson FH, Haneda Y (1980) Widespread occurrence of coelenterazine in marine bioluminescence. Comp Biochem Physiol - Part B Biochem 65:435–437. DOI:10.1016/0305-0491(80)90044-9

35. Renwart M, Mallefet J (2013) First study of the chemistry of the luminous system in a deep-sea shark , *Etmopterus spinax* Linnaeus, 1758 (Chondrichthyes: Etmopteridae). J Exp Mar Bio Ecol 448:214–219. DOI:10.1016/j.jembe.2013.07.010

36. Mensinger AF, Case JF (1991) Bioluminescence maintenance in juvenile *Porichthys*

notatus. Biol Bull 181:118–188

37. Mallefet J, Shimomura O (1995) Presence of coelenterazine in mesopelagic fishes from the Strait of Messina. Marine 124:381–385

38. Haneda Y, Johnson FH (1962) The photogenic organs of *Parapriacanthus beryciformes* Franz and other fish with the indirect ypype of luminescent system'. J Morphol 110:187–198. DOI:10.1002/jmor.1051100206

39. Herring PJ, Morin JG (1978) Bioluminescence in fishes. In: Herring PJ (ed) Bioluminescence in action. Academic Press, London, pp 273–329

40. Clarke WD (1963) Function of bioluminescence in mesopelagic organisms. Nature 198:1244–1246. DOI:10.1038/1981244a0

41. Cavallaro M, Mammola CL, Verdiglione R (2004) Structural and ultrastructural comparison of photophores of two species of deep-sea fishes: *Argyropelecus hemigymnus* and *Maurolicus muelleri*. J Fish Biol 64:1552–1567. DOI:10.1111/j.0022-1112.2004.00410.x

42. Bassot J-M On the comparative morphology of some luminous organs. In: Johnson FH, Haneda Y (eds) Bioluminescence in progress. Princeton University Press, Princeton

43. Haneda Y (1952) Some luminous fishes from the genera *Yarrella* and *Polyipnus*. Pacific Sci 4:13–16

44. O'Day WT (1973) Luminescent silhouetting in stomiatoid fishes. Contrib Sci from Nat Hist Museum Los Angeles 246:1–8

45. Best ACG, Bone Q (1976) On the integument and photophores of the alepocephalid fishes *Xenodermichthys* and *Photostylus*. J Mar Biol Assoc United Kingdom 56:227–236. DOI:10.1017/S0025315400020567

46. Claes JM, Mallefet J (2015) Comparative control of luminescence in sharks: new insights from the slendertail lanternshark (*Etmopterus molleri*). J Exp Mar Bio Ecol 467:87–94. DOI:10.1016/j.jembe.2015.03.008

47. Baguet F (1975) Excitation and control of isolated photophores of luminous fishes. Prog Neurobiol 5:97–125

48. Case JF, Strause LG (1978) Neurally controlled luminescent systems. In: Herring PJ (ed) Bioluminescence in action. Academic Press, pp 331–336

49. Haddock SHD, Moline MA, Case JF (2010) Bioluminescence in the sea. Ann Rev Mar Sci 2:443–493. DOI:10.1146/annurev-marine-120308-081028

50. Young RE (1983) Oceanic bioluminescence: an overview of general functions. Bull Mar Sci 33:829–845

51. Nicol JAC (1978) Bioluminescence and vision. In: Herring PJ (ed) Bioluminescence in action. Academic Press, pp 367–408

52. Morin JG (1983) Coastal bioluminiscence: patterns and functions. Bull Mar Sci 33:787–817

53. Widder EA (2010) Bioluminescence in the ocean: origins of biological, chemical, and ecological diversity. Science 328:704–708. DOI:10.1126/science.1174269

54. Widder EA (2001) Marine bioluminescence. Biosci Explain 1:1–9

55. Davis MP, Holcroft NI, Wiley EO, *et al* (2014) Species-specific bioluminescence facilitates speciation in the deep sea. Mar Biol 161:1139–1148. DOI:10.1007/s00227-014-2406-x

56. Poulsen JY, Byrkjedal I, Willassen E, *et al* (2013) Mitogenomic sequences and evidence from unique gene rearrangements corroborate evolutionary relationships of myctophiformes (Neoteleostei). BMC Evol Biol 13:111. DOI:10.1186/1471-2148-13-111

57. Moser HG, Ahlstrom EH (1974) Role of larval stages in systematic investigations of marine teleosts myctophidae a case study. Fish Bull 72:391–413

58. Vipin PM, Ravi R, Fernandez TJ, *et al* (2012) Distribution of myctophid resources in the Indian Ocean. 423–436. DOI:10.1007/s11160-011-9244-4

59. Sassa C, Kawaguchi K (2004) Larval feeding habits of *Diaphus garmani* and *Myctophum asperum* (Pisces : Myctophidae) in the transition region of the western North Pacific. 278:279–290

60. Kinzer J, Schultz K (1985) Vertical distribution and feeding patterns of midwater fish in the central equatorial Atlantic. I. Myctophidae. Mar Biol 85:313–322

61. Gjøsæter J (1984) Mesopelagic fish, a large potential resource in the Arabian Sea. Deep Res Part I Oceanogr Res Pap 31:1019–1035. DOI:10.1016/0198-0149(84)90054-2

62. Dalpadado P (1988) Reproductive biology of the lanternfish *Benthosema pterotum* from

the Indian Ocean. Mar Biol 98:307–316

63. Moser HG, Ahlstrom EH (1972) Development of the lanternfish, *Scopelopsis multipunctatus* Brauer 1906, with a discussion of its phylogenetic position in the family myctophidae and its role in a proposed mechanism for the evolution of photophore patterns in lanternfishes. Fish Bull 70:541–564

64. Sassa C, Kawaguchi K, Hirota Y, Ishida M (2007) Distribution depth of the transforming stage larvae of myctophid fishes in the subtropical – tropical waters of the western North Pacific. 54:2181–2193. DOI:10.1016/j.dsr.2007.09.006

65. Kawaguchi K, Mauchline J (1982) Biology of myctophid fishes (family Myctophidae) in the Rockall Trough, Northeastern Atlantic Ocean. Biol Oceanogr 1:337–373. DOI:10.1080/01965581.1982.10749447

66. Childress JJ, Taylor SM, Cailliet GM, Price MH (1980) Patterns of growth, energy utilization and reproduction in some meso- and bathypelagic fishes off Southern California. Mar Biol 61:27–40. DOI:10.1007/BF00410339

67. Gjøsæter J, Kawaguchi K (1980) A review of the world's resources of mesopelagic fish. FAO Fish Tech Pap 193:1–51

68. Hulley PA (1994) Lanternfishes. In: Paxton JR, Cottrill P, Bowmaker JK (eds) Encycopledia of fishes. Academic Press, San Diego, p 127.128

69. Alwis A de, Gjøsæter J (1988) Some aspects of the feeding ecology of myctophids in the waters off Central East Africa. Flødevigen Rapp 1:17–53

70. Noord JE Van, Olson RJ, Redfern J, Kaufmann RS (2013) Diet and prey selectivity in three surface- migrating myctophids in the eastern tropical Pacific. Ichthyol Res 60:287–290. DOI:10.1007/s10228-013-0350-2

71. Noord JE Van (2013) Diet of five species of the family Myctophidae caught off the Mariana Islands. Ichthyol Res 60:89–92. DOI:10.1007/s10228-012-0315-x

72. Pusch C, Schnack-schiel S, Mizdalski E, Westernhagen H Von (2004) Feeding ecology of three myctophid species at the Great Meteor Seamount (North-east Atlantic). Arch Fish Mar Res 51:251–271

73. Martin RP, Davis MP (2016) Patterns of phenotypic variation in the mouth size of lanternfishes (Teleostei: Myctophiformes). Copeia 104:795–807. DOI:10.1643/ci-15-345

74. Busserolles F De, Marshall NJ (2017) Seeing in the deep-sea: visual adaptations in lanternfishes. 372:20160070. DOI:10.1098/rstb.2016.0070

75. Watanabe H, Moku M, Kawaguchi K, *et al* (1999) Diel vertical migration of myctophid fishes (Family myctophidae) in the transitional waters of the western North Pacific. Fish Oceanogr 8:115–127. DOI:10.1046/j.1365-2419.1999.00103.x

76. Clarke TA (1973) Some aspects of the ecology of lanternfishes (Myctophidae) in the Pacific Ocean near Hawaii. Fish Bull 71:401–434

77. Macpherson E, Roel BA (2010) Trophic relationships in the demersal fish community off Namibia. South African J Mar Sci 37–41. DOI:10.2989/025776187784522432

78. Trueman CN, Johnston G, Hea BO, Mackenzie KM (2014) Trophic interactions of fish communities at midwater depths enhance long-term carbon storage and benthic production on continental slopes. Proc R Soc B Biol Sci 281:20140669

79. Saunders RA, Collins MA, Ward P, *et al* (2015) Trophodynamics of Protomyctophum (Myctophidae) in the Scotia Sea (Southern Ocean). J fish 87:1031–1058. DOI:10.1111/jfb.12776

80. Anderson TR, Martin AP, Lampitt RS, *et al* (2019) Quantifying carbon fluxes from primary production to mesopelagic fish using a simple food web model. ICES J Mar Sci 76:690–701. DOI:10.1093/icesjms/fsx234

81. Evans BI, Fernald RD (1990) Metamorphosis and fish vision. J Neurobiol 21:1037–1052. DOI:10.1002/neu.480210709

82. Evans B, Browman HI (2004) Variation in the development of the fish retina. Am Fish Soc Symp 10:146–166

83. Wagner HJ, Fröhlich E, Negishi K, Collin SP (1998) The eyes of deep-sea fish II. Functional morphology of the retina. Prog Retin Eye Res 17:637–685. DOI:10.1016/S1350-9462(98)00003-2

84. Moser HG (1996) The early stages of fishes in the California current region. Atlas number 33. California Cooperative Oceanic Fishery Investigations, La Jolla

85. Suntsov A V, Widder EA, Sutton TT (2008) Bioluminescence. In: Finn RN, Kapoor BG (eds) Fish larval physiology. Enfield: Science Publishers, New Hampshire, pp 51–88

86. Kubodera T, Koyama Y, Mori K (2007) Observations of wild hunting behaviour and

bioluminescence of a large deep-sea, eight-armed squid, *Taningia danae*. Proc Biol Sci 274:1029–1034. DOI:10.1098/rspb.2006.0236

87. Fraser-Brunner A (1948) A classification of the fishes of the family Myctophidae. Proc Zool Soc London 118:1019–1108

88. Moser HG, Ahlstrom EH, Paxton JR (1984) Myctophidae: development. Ontog Syst fishes based an Int Symp Dedic to Mem Elbert Halvor Ahlstrom 72:218–239

89. Duchatelet L, Hermans C, Duhamel G, *et al* (2019) Coelenterazine detection in five myctophid species from the Kerguelen Plateau. Kerguelen Plateau Mar Ecosyst + Fish Proc Second Symp 31–41

90. Herring PJ (1987) Trophic and physiological studies over the North West African slope and in the eastern North Atlantic. Discov Cruises Reports 200:56

91. Krönström J, Mallefet J (2010) Evidence for a widespread involvement of NO in control of photogenesis in bioluminescent fish. Acta Zool 91:474–483. DOI:10.1111/j.1463-6395.2009.00438.x

92. Anctil M (1979) Physiological control of bioluminescence. Photochem. Photobiol. 30:777–780

93. Nicol JAC (1959) The regulation of light emission in animals. Biol Rev 1–40. DOI:10.1111/j.1469-185X.1960.tb01321.x

94. Anctil M, Case JF (1977) The caudal luminous organs of lanternfishes: general innervation and ultrastructure. Am J Anat 149:1–22

95. Lawry JV (2016) The trigeminofacial innervation of the cephalic lateral line organs and photophores of the lantern fish *Tarletonbeania crenularis* (Myctophidae). 1:1–4. DOI:10.1080/10236247209386904

96. Edwards AS, Herring PJ (1977) Observations on the comparative morphology and operation of the photogenic tissues of myctophid fishes. Mar Biol 41:59–70. DOI:10.1007/BF00390582

97. O'Day WT (1972) The histology and fine structure of some bioluminescent organs in deep-sea fishes (PhD thesis). University of Southern California, Los Angeles

98. Barnes AT, Case JF (1974) The luminescence of lanternfish (Myctophidae): spontaneous activity and responses to mechanical, electrical, and chemical stimulation. J Exp Mar Bio

Ecol 15:203–221

99. Young RE, Roper CFE, Walters JF (1979) Eyes and extraocular photoreceptors in midwater cephalopods and fishes: their roles in detecting downwelling light for counterillumination. Mar Biol 51:371–380. DOI:10.1007/BF00389215

100. Anctil M, Gruchy CG (1970) Stimulation and photography of bioluminescence in lanternfishes (Myctophidae). J Fish Res Board Canada 20:826–829

101. Herring PJ (1983) The spectral characteristics of luminous marine organisms. Proc R Soc B Biol Sci 220:183–217. DOI:10.1098/rspb.1983.0095

102. Widder EA, Latz MI, Case JF (1983) Marine bioluminescence spectra measured with an optical multichannel detection system. Biol Bull 165:797–810. DOI:doi: 10.2307/1541479

103. Denton EJ, Gilpin-Brown JB, Wright PG (1972) The angular distribution of the light produced by some mesopelagic fish in relation to their camouflage. Proc R Soc B Biol Sci 182:145–158. DOI:10.1098/rspb.1972.0071

104. Cavallaro M, Mammola CL, Verdiglione R (2004) Structural and ultrastructural comparison of photophores of two species of deep-sea fishes: *Argyrpelecus hemigymnus* and *Maurolicus muelleri*. J Fish Biol 64:1552–1567. DOI:10.1111/j.0022-1112.2004.00410.x

105. Cavallaro M, Battaglia P, Laur R, *et al* (2015) The morphology of photophores in the garrick , cyclothone braueri (Family: Gonostomatidae): an ultrastructure study. Acta Zool 96:1–5. DOI:10.1111/azo.12076

106. Cavallaro M, Battaglia P, Guerrera MC, *et al* (2019) Structure and ultrastructure study on photophores of the Madeira lanternfish, *Ceratoscopelus maderensis* (Lowe, 1839), Pisces: Myctophidae. Acta Zool 100:89–95. DOI:10.1111/azo.12236

107. Cavallaro M, Montalbano G, Guerrera MC, *et al* (2015) Preliminary data on the structure of the small lantern fish photophores, *Diaphus holti* Tåning, 1918 (Family: Myctophidae). Biol Mar Mediterr 22:221–222

108. Lawry JV (1973) Dioptric modifications of the scales overlying the photophores of the lantern fish, *Tarletonbeania crenularis* (Myctophidae). J Anat 114:55–63

109. Lawry JV (1974) Lantern fish compare downwelling light and bioluminescence. Nature 24:155–157

110. Nicol JAC (1960) Spectral composition of the light of the lantern-fish, *Myctophum punctatum*. J Mar Biol Assoc United Kingdom 39:27–32

111. Herring PJ (2007) Sex with the lights on ? A review of bioluminescent sexual dimorphism in the sea. J Mar Biol Assoc United Kingdom 87:829–842. DOI:10.1017/S0025315407056433

112. Anadón E (1957) Anatomía e histologia de las placas luminosas caudales de *Lampadena nitida* (Taaning). Boletií la Real Soc Española Hist Nat Sección Biológica 55:129–144

113. Haneda Y (1949) Luminous organs of fish which emit light indirectly. Pacific Sci 4:214–227

114. Herring PJ, Locket NA (1978) The luminescence and photophores of euphausiid crustaceans. J Zool 186:431–462. DOI:10.1111/j.1469-7998.1978.tb03932.x

115. Arnold JM, Young RE, King M V (1974) Ultrastructure of a cephalopod photophore. II. Iridophores as reflectors and transmitters. Biol Bull 147:522–534. DOI:10.2307/1540737

116. Butcher S, Dilly PN, Herring PJ (1982) The comparative morphology of the photophores of the squid *Pyroteuthis margaritifera* (Cephalopoda: Enoploteuthidae). J Zool 196:133–150. DOI:10.1111/j.1469-7998.1982.tb03497.x

117. Herring PJ (2000) Bioluminescent signals and the role of reflectors. J Opt A Pure Appl 2:R29–R38. DOI:10.1088/1464-4258/2/6/202

118. Denton EJ (1970) Review lecture: on the organization of reflecting surfaces in some marine animals. 258:285–313. DOI:10.1098/rstb.1970.0037

119. Barraud J, Bassot J-M, Favard P (1959) Identification radiocristallographique et aspects cytologiques de la guanine dans le reflécteur des photophores chez *Maurolicus pennanti* (Téléostéen Maurolicidae) Walbaum. Comptes rendus l'Académie des Sci 249:2633–2635

120. Johnsen S, Widder EA, Mobley CD (2004) Propagation and perception of bioluminescence: factors affecting counterillumination as a cryptic strategy. Biol Bull 207:1–16

121. Aksnes DL, Dupont N, Staby A, *et al* (2009) Coastal water darkening and implications for mesopelagic regime shifts in Norwegian fjords. 387:39–49. DOI:10.3354/meps08120

122. Pedrotti FL, Pedrotti LM, Pedrotti LS (2014) Geometrical optics. In: Pedrotti FL,

Pedrotti LM, Pedrotti LS (eds) Introduction to optics, 3rd ed. Pearson Education Limited, Harlow, pp 17–52

123. Saleh BEA, Teich MC (1991) Ray optics. In: Saleh BEA, Teich MC (eds) Fundamentals of Photonics. John Wiley & Sons, New York, pp 1–40

124. Land MF (1972) The physics and biology of animal reflectors. Prog Biophys Mol Biol 24:75–106

125. Huxley BYAF (1968) A theoretical treatment of the reflexion of light by multilayer structures. J Exp Biol 48:227–245

126. Land MF (2009) Biological optics: deep reflections. Curr Biol 19:78–80. DOI:10.1016/j.cub.2008.11.038

127. Land MF (1965) Image formation by a concave refloctor in the eye of the scallop *Pecten maximus*. 179:138–153

128. Herring PJ (1994) Reflective systems in aquatic animals. Comp Biochem Physiol - A Physiol 109:513–546. DOI:10.1016/0300-9629(94)90192-9

129. Denton EJ, Nicol JAC (1964) The chorioidal tapeta of some cartilaginous fishes (Chondrichthyes). J Mar Biol Assoc United Kingdom 44:219–258. DOI:10.1017/S0025315400024760

130. Gur D, Leshem B, Oron D, *et al* (2014) The structural basis for enhanced silver reflectance in koi fish scale and skin. J Am Chem Soc 136:177236–17242. DOI:10.1021/ja509340c

131. McKenzie DR, Yin Y, McFall WD (1995) Silvery fish skin as an example of a chaotic reflector. Proc R Soc London 451:579–584. DOI:10.1098/rspa.1974.0120

132. Munk O (1999) The escal photophore of ceratioids (Pisces; Ceratioidei) - a review of structure and function. Acta Zool 80:265–284. DOI:10.1046/j.1463-6395.1999.00023.x

133. Watson M, Thurston EL, Nicol JAC (1978) Reflectors in the light organ of *Anomalops* (Anomalopidae, Teleostei). Proc R Soc London - Biol Sci 202:339–351. DOI:10.1098/rspb.1978.0071

134. Poulsen JY, Sado T, Hahn C, *et al* (2016) Preservation obscures pelagic deep-sea fish diversity: doubling the number of sole-bearing opisthoproctids and resurrection of the genus *Monacoa* (Opisthoproctidae, Argentiniformes). PLoS One 11: e01597:

DOI:10.1371/journal.pone.0159762

135. Aksnes DL, Giske J (1993) A theoretical model of aquatic visual feeding. Ecol Modell 67:233–250. DOI:10.1016/0304-3800(93)90007-F

136. Bernal A, Olivar MP, Maynou F, *et al* (2015) Diet and feeding strategies of mesopelagic fishes in the western Mediterranean. Prog Oceanogr 135:1–17. DOI:10.1016/j.pocean.2015.03.005

137. Morin JG, Harrington A, Nealson K, *et al* (1975) Light for all reasons: versatility in the behavioral repertoire of the flashlight fish. Science 190:74–76. DOI:10.1126/science.190.4209.74

138. Yoshioka S, Matsuhana B, Tanaka S, *et al* (2011) Mechanism of variable structural colour in the neon tetra: quantitative evaluation of the Venetian blind model. J R Soc Interface 8:56–66. DOI:10.1098/rsif.2010.0253

139. Kawaguti S (1965) Electron microscopy on iridophores in the scale of the blue wrasse. Proc Jpn Acad 41:610–613

140. Kawaguti S, Kamishima Y (1966) Electron microscopy on the blue back of a clupeoid fish, *Harengula zunasi*. Proc Jpn Acad 42:389–393

141. Gur D, Palmer BA, Weiner S, Addadi L (2017) Light manipulation by guanine crystals in organisms: biogenic scatterers, mirrors, multilayer reflectors and photonic crystals. Adv Funct Mater 27:1603514. DOI:10.1002/adfm.201603514

142. Locket NA (2000) On the lens pad of *Benthalbella infans, a scopelarchid*, a scopelarchid deep-sea teleost. Philos Trans R Soc B Biol Sci 355:1167–1169. DOI:10.1098/rstb.2000.0660

143. Locket NA (1977) Adaptations to the deep-sea environment. In: Handbook of sensory physiology. The visual system in vertebrates. Springer-Verlag, Berlin, pp 67–192

144. Collin SP, Hoskins R V, Partridge JC (1998) Seven retinal specializations in the tubular eye of the Scopelarchus michaelsarsi : a case study in visual iptimization. Brain Behav Evol 51:291–314. DOI:10.1159/000006544

145. Sköld HN, Aspengren S, Cheney KL, Wallin M (2016) Fish chromatophores - from molecular motors to animal behavior. Int Rev Cell Mol Biol 321:171–219. DOI:10.1016/bs.ircmb.2015.09.005

146. Fujii R (2000) The regulation of motile activity in fish chromatophores. Pigment Cell Res 13:300–319. DOI:10.1034/j.1600-0749.2000.130502.x

147. Denton EJ, Land MF (1971) Mechanism of reflexion in silvery layers of fish and cephalopods. Proc R Soc London - Biol Sci 178:43–61. DOI:10.1098/rspb.1971.0051

148. Hirsch A, Gur D, Polishchuk I, *et al* (2015) "Guanigma": The Revised Structure of Biogenic Anhydrous Guanine. Chem Mater 27:8289–8297. DOI:10.1021/acs.chemmater.5b03549

149. Gur D, Politi Y, Sivan B, *et al* (2013) Guanine-based photonic crystals in fish scales form from an amorphous precursor. Angew Chemie - Int Ed 52:388–391. DOI:10.1002/anie.201205336

150. Yoshioka S, Kinoshita S, Iida H, Hariyama T (2012) Phase-adjusting layers in the multilayer reflector of a jewel beetle. J Phys Soc Japan 81:1–7. DOI:10.1143/JPSJ.81.054801

151. Lythgoe JN, Shand J (1982) Changes in spectral reflexions from the iridophores of the neon tetra. J Physiol 325:23–34

152. Levy-Lior A, Shimoni E, Schwartz O, *et al* (2010) Guanine-Based biogenic photonic-crystal arrays in fish and spiders. Adv Funct Mater 20:320–329. DOI:10.1002/adfm.200901437

153. Teyssier J, Saenko SV, Van Der Marel D, Milinkovitch MC (2015) Photonic crystals cause active colour change in chameleons. Nat Commun 6:1–7. DOI:10.1038/ncomms7368

154. Hirsch A, Palmer BA, Elad N, *et al* (2017) Biologically controlled morphology and twinning in guanine crystals. Angew Chemie 129:9548–9552. DOI:10.1002/ange.201704801

155. Funt N, Palmer BA, Weiner S, Addadi L (2017) Koi fish-scale iridophore cells orient guanine crystals to maximize light reflection. Chempluschem 82:914–923. DOI:10.1002/cplu.201700151

156. Nicol JAC (1957) Observations on photophores and luminescence in the teleost Porichthys. 98:179–188. DOI:10.1017/S002531540000574

157. Ohshima H (1911) Some observations on the luminous organs of fishes. J Coll Sci Imp Univ Tokyo 27:1–25

158. Emery C (1884) Intorno alle macchie spendeti della pelle nei pesci del genere *Scopelus*. Mitth aus der Zool Stn zu Neapel 5:471–482

159. Gur D, Leshem B, Farstey V, *et al* (2016) Light-induced color change in the sapphirinid copepods: tunable photonic crystals. Adv Funct Mater 26:1393–1399. DOI:10.1002/adfm.201504339

160. Somiya H (1980) Fishes with eye shine: functional morphology of guanine type tapetum lucidum. Mar Ecol Prog Ser 2:9–26. DOI:10.3354/meps002009

161. Somiya H (1989) Guanine-type retinal tapetum of three species of mormyrid fishes. Japanese J Ichthyol 36:220–226. DOI:10.1007/BF02914325

162. Takei S, Somiya H (2002) Guanine-type retinal tapetum and ganglion cell topography in the retina of a carangid fish, *Kaiwarinus equula*. Proc R Soc B Biol Sci 269:75–82. DOI:10.1098/rspb.2001.1849

163. Hales TC (2001) The honeycomb conjecture. Discrete Comput Geom 25:1–22. DOI:10.1007/s00454-001-0021-3

164. Nicol JAC, Arnott HJ, Best ACG (1973) Tapeta lucida in bony fishes (Actinopterygii): a survey. Can J Zool 51:69–81. DOI:10.1139/z73-012

165. Best ACG, Nicol JAC (1980) Eyeshine in fishes: a review of ocular reflectors. Can J Zool 58:945–956

166. Cavallaro M, Mammola CL, Verdiglione R (2004) Structural and ultrastructural comparison of photophores of two species of deep-sea fishes: Argyropelecus hemigymnus and Maurolicus muelleri. J Fish Biol 64:1552–1567. DOI:10.1111/j.0022-1112.2004.00410.x

167. Herring PJ, Munk O (1994) The escal light gland of the deep-sea anglerfish *Haplophryne mollis* (Pisces: Ceratioidei) with observations on luminescence control. J Mar Biol Assoc United Kingdom 74:747–763

168. Young RE, Kampa EM, Maynard SD, *et al* (1980) Counterillumination and the upper depth limits of midwater animals. Deep Sea Res Part A Oceanogr Res Pap 27:671–691. DOI:10.1016/0198-0149(80)90022-9

169. Palmer G, Johnsen S (2015) Downwelling spectral irradiance during evening twilight as a function of the lunar phase. Appl Opt 54:B85–B92

170. Martini S, Haddock SHD (2017) Quantification of bioluminescence from the surface to the deep sea demonstrates its predominance as an ecological trait. Sci Rep 7:45750. DOI:10.1038/srep45750

171. Williams RC (1987) A proof of the reflective property of the parabola. Am Math Mon 94:667–668

172. Mast TS, Nelson JE (1982) Figure control for a fully segmented telescope mirror. Appl Opt 21:2631. DOI:10.1364/ao.21.002631

173. Ayoub AB (2003) The eccentricity of a conic section. Coll Math J 34:116–121

174. Bendt P, Rabl A (1981) Optical analysis of point focus parabolic radiation concentrators. Appl Opt 20:674–683

175. Nicol JAC (1969) Bioluminescence. In: Hoar WS, Randall DJ (eds) Fish physiology. Reproduction and growth: bioluminescence, pigments and poisons., 3rd ed. Academic Press, pp 355–400

176. McFall-Ngai M, Morin JG (1991) Camouflage by disruptive illumination in leiognathids, a family of shallow-water bioluminescent fishes. J Exp Biol 156:119–137

177. Satoshi I, Watanabe K, Nakamura H, Shimomura O (2000) Secretional luciferase of the luminous shrimp *Oplophorus gracilirostris*: cDNA cloning of a novel imidazopyrazinone luciferase 1. FEBS 481:19–25

178. Matthews JC, Hori K, Cormier MJ (1977) Purification and properties of *Renilla reniformis* luciferase. Biochemistry 16:85–92

179. Markova S V, Golz S, Frank LA, *et al* (2004) Cloning and expression of cDNA for a luciferase from the marine copepod *Metridia longa*. J Biol Chem 279:3212–3217

180. Shinohara G, Nakae M, Ueda Y (1996) Annotated checklist of deep-sea Ffshes of the sea of Japan. Memories Natl Sci Musem 29:153–185

181. Tsuji FI, Haneda Y (1971) Luminescent system in a myctophid fish, *Diaphus elucens* Brauer. Nature 233:623–624

182. Saenko S V, Teyssier J, van der Marel D, Milinkovitch MC (2013) Precise colocalization of interacting structural and pigmentary elements generates extensive color pattern variation in Phelsuma lizards. BMC Biol 11:. DOI:10.1186/1741-7007-11-105

183. Warrant E (2004) Vision in the dimmest habitats on Earth. J Comp Physiol A Neuroethol Sensory, Neural, Behav Physiol 190:765–789. DOI:10.1007/s00359-004-0546-z

184. Haneda Y (1985) Pisces. In: Haneda Y (ed) Luminous organisms. Kouseisha-kouseikaku, Tokyo

185. Herring PJ (1981) Red fluorescence of fish and cephalopod photophores. In: DeLuca MA, Mcelroy WD (eds) Bioluminescence and chemiluminescence : basic chemistry and analytical application. Academic Press, New York

186. Herring PJ (1976) Bioluminescence in decapod crustacea. J Mar Biol Assoc United Kingdom 56:1029–1047

187. Herring PJ (1985) Bioluminescence in the crustacea. J Crustac Biol 5:557–573. DOI:10.2307/1548235

188. Hernández-León S, Almeida C, Yebra L, *et al* (2001) Zooplankton abundance in subtropical waters: is there a lunar cycle? Sci Mar 65:59–63. DOI:10.3989/scimar.2001.65s159

189. Linkowski T (1996) Lunar rhythms of vertical migrations coded in otolith microstructure of North Atlantic lanternfishes , genus Hygophum. Mar Biol 124:495–508

190. de Busserolles F, Cortesi F, Helvik JV, *et al* (2017) Pushing the limits of photoreception in twilight conditions : The rod-like cone retina of the deep-sea pearlsides. 3:eaao4709. DOI:10.1126/sciadv.aao4709

191. Latz MI, Frank TM, Case JF (1988) Spectral composition of bioluminescence of epipelagic organisms from the Sargasso Sea. Mar Biol 98:441–446. DOI:10.1007/BF00391120

192. Young RE, Arnold JM (1982) The functional morphology of a ventral photophore from the mesopelagic squid, *Abralia trigonura*. Malacologia 23:135–163

193. Gur D, Palmer BA, Leshem B, *et al* (2015) The mechanism of color change in the neon tetra fish: a light-induced tunable photonic crystal array. Angew Chemie - Int Ed 54:12426–12430. DOI:10.1002/anie.201502268

194. Koga D, Kusumi S, Shodo R, *et al* (2015) High-resolution imaging by scanning electron microscopy of semithin sections in correlation with light microscopy. Microscopy 64:387–394. DOI:10.1093/jmicro/dfv042

195. Roholl PJM, Leene W, Kapsenberg ML, Vos JG (1981) The use of tannic acid fixation for the electron microscope visualization of fluorochrome-labelled antibodies attached to cell surface antigens. J Immunol Methods 42:285–289. DOI:10.1016/0022-1759(81)90157-5

196. Land MF, Nilsson D-E (2006) General purpose and special purpose visual systems. Invertebr Vis 167–210

197. Bone Q, Denton EJ (1971) The osmotic effect of electron microscope fixatives. J Cell Biol 49:571–581. DOI:10.1083/jcb.49.3.571

198. Fernald R (1987) Aquatic adaptations in fish eyes. In: Atema J, Fay RR, N PA, Tavolga WN (eds) Sensory biology of aquatic animals. Springer-Verlag, New York

199. Pedrotti LS (2009) Basic Geometrical Optics. In: Roychoudhuri C (ed) Fundamentals of Photonics. pp 73–116

200. Land MF (2012) The evolution of lenses. Ophthalmic Physiol Opt 32:449–460. DOI:10.1111/j.1475-1313.2012.00941.x

201. Young RE, Roper CFE (1977) Intensity regulation of bioluminescence during countershading in living midwater animals. Fish Bull 75:239–252

202. Young RE, Mencher FM (1980) Bioluminescence in mesopelagic squid: diel color change during counterillumination. Science 208:1286–1288. DOI:10.1126/science.208.4449.1286

203. Han F (2017) Geometric optics. In: A modern course in university physics. Optics, thermal lhysics, modern physics. pp 1–64

204. DeMartini DG, Krogstad DV, Morse DE (2013) Membrane invaginations facilitate reversible water flux driving tunable iridescence in a dynamic biophotonic system. Proc Natl Acad Sci U S A 110:2552–2556. DOI:10.1073/pnas.1217260110

205. Hiroshi N, Noriko O, Ryozo F (1990) Light-reflecting properties of the iridophores of the neon tetra, Paracheirodon innesi. Comp Biochem Physiol - Part A Physiol 95:337–341. DOI:10.1016/0300-9629(90)90229-L

206. Mäthger LM, Denton EJ, Marshall NJ, Hanlon RT (2009) Mechanisms and behavioural functions of structural coloration in cephalopods. J R Soc Interface 6 suppl 2:S149–S163. DOI:10.1098/rsif.2008.0366.focus

207. Oshima N, Fujii R (1987) Motile mechanism of blue damselfish (*Chrysiptera cyanea*) iridophores. Cell Motil Cytoskeleton 8:85–90

208. Lythgoe JN, Shand J (1989) The structural basis for iridescent colour changes in dermal and corneal iridophores in fish. J Exp Biol 141:313–325

209. Paitio J, Yano D, Muneyama E, *et al* (2019) Reflector of the body photophore in lanternfish is mechanistically tuned to project the biochemical emission in photocytes for counterillumination. Biochem Biophys Res Commun (in press). DOI:10.1016/j.bbrc.2019.10.197

SUPPLEMENTARY DATA

1. Supplement 1

Table 1 – Average and standard deviation for morphometric measurements of *D. watasei* photophores from histological sections. Br= Branchiostegal organ; PVO= Subpectoral organ; VLO= Supraventral organ; SAO= Supranal organ; PO= Pectoral organ; VO= Ventral organ; Ant= Antorbital organ; Dn= Dorsonasal organ; Vn= Ventronasal organ; S.D.= Standard deviation; n.a.= not applicable, n.d.= no data.

Morphometric parameter	Photophore	**Br1.1**	**Br1.2**	**Br1.3**	**PVO2**	**VLO**	**SAO2**	**PO3**	**VO1**	**VO2**	**Ant**	**Dn**	**Vn**
Organ diameter	Average	763.70	794.42	722.11	1252.54	502.58	1002.87	1412.94	1429.68	879.78	736.94	910.95	2556.47
(µm)	S.D.	3.61	3.44	14.92	8.21	4.60	6.06	11.07	16.13	3.48	15.47	16.60	25.25
Photocyte area	Average	11540.98	11518.46	11503.72	9737.67	2140.67	7467.78	9259.50	5824.79	3055.33	130543.62	129937.80	217407.16
(μm^2)	S.D.	274.50	340.78	416.00	56.86	38.28	233.25	366.32	227.19	197.16	2704.10	5947.72	2794.69
Lens reflector length	Average	n.a.	n.a.	n.a.	361.76	n.d.	n.d.	n.d.	522.70	525.76	n.a.	n.a.	n.a.
(µm)	S.D.	n.a.	n.a.	n.a.	4.60	n.d.	n.d.	n.d.	2.83	6.41	n.a.	n.a.	n.a.

	SA		1	2	3	4	5	6	7	8	9	10
Reflector thickness (µm)	Average	**Br1.1**	12.97	16.24	16.02	17.62	15.33	19.39	17.85	14.26	11.13	8.62
		Br1.2	10.68	12.64	16.61	15.82	14.96	17.84	15.93	16.10	11.89	7.48
		Br1.3	12.96	13.55	15.60	17.55	19.25	18.58	16.67	15.86	12.44	8.19
		PVO2	11.10	7.58	5.86	4.24	6.12	5.31	3.87	2.65	2.19	1.65
		VLO	6.12	7.25	4.10	1.82	1.69	0.96	1.20	1.84	1.30	1.38
		SAO2	17.60	20.22	15.24	6.28	3.99	3.77	2.49	2.78	2.47	2.14
		PO3	14.12	11.15	8.17	5.14	3.64	4.45	2.03	4.36	8.46	14.04
		VO1	9.57	7.89	6.30	5.74	4.84	4.95	5.27	6.11	6.07	7.17
		VO2	13.75	8.36	4.26	7.10	6.81	5.15	5.42	5.48	5.12	8.40
		Ant	43.70	65.66	94.54	123.61	100.81	100.45	66.65	47.26	24.13	11.56
		Dn	17.34	15.02	29.89	127.88	141.68	87.36	41.80	40.56	42.64	23.21
		Vn	21.24	25.24	37.18	39.04	98.36	101.62	127.52	64.94	55.79	19.85
	S.D.	**Br1.1**	0.61	1.05	0.89	1.28	0.92	0.87	0.86	0.52	1.75	0.23

Br1.2	1.14	0.41	1.37	1.90	2.43	2.59	2.37	2.06	1.07	2.17
Br1.3	0.34	1.35	0.95	1.21	1.04	2.36	2.24	2.44	2.77	1.49
PVO2	2.10	2.50	1.92	0.24	1.24	1.74	0.50	0.24	0.35	0.27
VLO	1.03	1.19	0.63	0.47	0.48	0.64	0.00	0.22	0.17	0.28
SAO2	3.43	1.81	1.26	0.23	0.51	0.77	0.36	0.32	0.33	0.41
PO3	0.48	0.81	0.67	0.17	0.61	1.07	0.46	0.22	0.97	1.27
VO1	0.80	0.71	0.34	0.75	0.33	0.26	0.76	0.23	0.51	0.68
VO2	0.41	0.93	0.40	1.40	0.40	1.49	0.36	0.31	0.87	0.73
Ant	3.31	5.28	10.46	2.93	5.71	3.25	7.97	10.30	9.88	2.75
Dn	4.61	2.02	4.32	6.42	11.10	11.64	8.61	1.41	3.94	3.99
Vn	2.05	2.15	3.50	2.89	7.42	3.31	7.10	4.58	1.44	1.56

	SA		1	2	3	4	5
Lens thickness (μm)	Average	**Br1.1**	103.12	69.83	42.86	35.64	23.09
		Br1.2	90.62	79.18	45.69	25.20	17.14
		Br1.3	88.71	51.27	48.35	34.60	17.10
		PVO2	15.83	32.73	87.27	70.57	28.16
		VO1	38.96	43.24	59.55	51.34	32.11
	S.D.	**Br1.1**	4.64	2.27	1.69	5.30	1.65
		Br1.2	7.25	5.45	3.84	2.48	2.16
		Br1.3	9.78	3.89	6.46	3.68	8.41
		PVO2	1.01	1.82	5.45	5.46	3.24
		VO1	0.58	0.69	3.18	3.72	1.82

2. Supplement 2

Table 2 – Average and standard deviation of length, width and length/width ratio of iridophores platelets on reflective tissues in *Diaphus watasei* and *D.* sp. LR= Lens reflector of body photophores; HP.R= Inner reflector of head photophore; BP.R= Inner reflector of body photophore; L/W= Length/width; N= Number of platelets; S.D.= Standard deviation.

	Raw data			Treated data (N= 50)	
Tissue		**Average**	**S.D.**	**Average**	**S.D.**
		D. watasei			
LR (N=154)	Length (µm)	20.27	6.93	17.87	4.43
LR (N=154)	Width (µm)	6.67	3.48	5.71	1.22
LR (N=154)	L/W ratio	3.29	1.00	3.18	0.70
Iris (N=270)	Length (µm)	43.42	12.01	42.93	8.77
Iris (N=270)	Width (µm)	8.73	3.10	8.25	2.02
Iris (N=270)	L/W ratio	5.26	1.51	5.42	1.39
Skin (N= 125)	Length (µm)	21.58	4.81	21.27	4.44
Skin (N= 125)	Width (µm)	7.16	1.59	7.27	1.36
Skin (N= 125)	L/W ratio	3.08	0.68	2.96	0.55
HP.R (N=230)	Length (µm)	45.38	10.14	44.64	8.84
HP.R (N=230)	Width (µm)	14.08	3.80	13.80	3.10
HP.R (N=230)	L/W ratio	3.33	0.74	3.31	0.61
BP.R (N= 152)	Length (µm)	31.08	3.42	31.12	3.49
BP.R (N= 152)	Width (µm)	21.59	2.35	21.55	2.36
BP.R (N= 152)	L/W ratio	1.45	0.15	1.45	0.14
T (N= 105)	Length (µm)	50.02	14.96	48.47	14.06
T (N= 105)	Width (µm)	8.83	2.63	8.66	2.25
T (N= 105)	L/W ratio	5.81	1.43	5.73	1.45
		D. sp			
BP.R (N= 145)	Length (µm)	21.14	3.25	20.46	3.81
BP.R (N= 145)	Width (µm)	15.04	2.44	14.64	2.79

BP.R (N= 145)	L/W ratio	1.41	0.15	1.41	0.16
T (N=112)	Length (µm)	42.06	14.21	40.90	14.72
T (N=112)	Width (µm)	9.56	4.37	7.73	3.09
T (N=112)	L/W ratio	4.77	1.47	5.63	1.90

3. Supplement 3

FTIR and XRD analyses were performed for platelets from *D.watasei* of body photophores and commercial anhydrous guanine powder (Fujifilm Wako Pure Chemicals, Japan), used as positive control. FTIR an XRD spectral peaks of platelets perfectly matched the anhydrous guanine (Fig. 61) which proves that iridophores of the inner reflector of *D. watasei* body photophores are composed by guanine platelets. For more details, see [209]

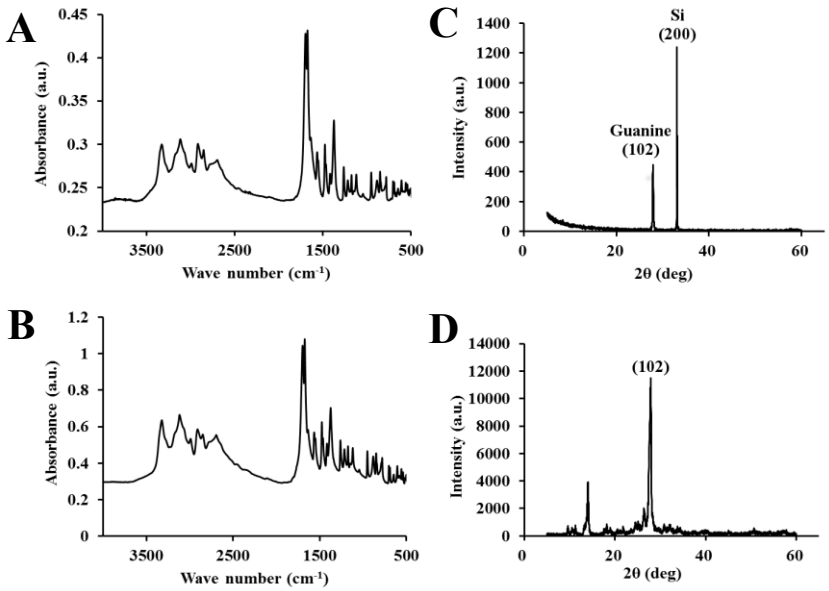

Figure 61 – FTIR spectra of platelets from the inner reflector of A) *D. watasei* body photophores, and B) commercial anhydrous guanine powder. XRD spectra of platelets in C) photophore and D) guanine powder. FTIR= Fourier transform infrared spectrometry; XRD= X-ray diffraction.

4. Supplement 4

Table 3 – Average and standard deviation of sampled points on inner reflector of *D. watasei*'s ventral body photophores from histological sections. SA.P= Sample points; S.D.= Standard deviation.

SA.P	PO3				VO1				VO2			
	Horizontal position (µm)		Vertical position (µm)		Horizontal position (µm)		Vertical position (µm)		Horizontal position (µm)		Vertical position (µm)	
	Average	S.D.	Average	S.D.	Average	S.D.	Average	S.D.	Average	S.D.	Average	S.D.
1	65.44	2.69	229.89	1.54	91.67	2.33	220.00	1.45	140.44	2.78	155.89	1.39
2	91.67	5.93	207.00	6.43	116.11	6.83	201.78	5.87	170.89	6.30	132.33	6.96
3	124.56	12.55	183.67	9.96	148.78	9.67	185.78	7.90	205.56	6.41	122.33	2.40
4	160.33	9.17	167.00	4.67	183.67	19.97	172.22	11.11	243.78	12.81	118.56	0.39
5	193.44	8.68	152.78	3.15	222.11	17.77	160.89	3.02	281.78	7.31	117.89	1.02
6	241.22	20.49	141.00	3.71	259.67	26.71	153.11	5.23	317.33	2.31	120.78	1.02
7	289.44	18.04	135.00	1.15	309.44	16.94	146.67	2.52	383.56	74.99	128.11	12.32
8	342.11	12.10	136.11	1.54	364.11	23.22	142.22	1.35	481.56	13.09	149.00	8.67
9	403.89	25.73	141.22	3.15	419.44	32.72	139.33	2.96	509.11	9.90	167.22	7.13
10	449.00	23.35	150.11	3.42	458.67	38.34	140.00	4.36	537.78	12.30	186.78	8.34
11	494.78	17.82	164.78	8.88	501.44	38.38	145.56	7.65	572.67	6.36	214.78	2.69
12	534.56	9.48	188.33	8.67	559.89	44.94	172.67	22.28	600.44	6.84	237.89	6.19
13	569.22	5.98	214.33	3.53	604.78	18.57	202.44	15.69	626.44	5.18	263.22	5.55
14	599.44	3.08	247.22	6.30	633.67	19.92	224.00	15.92	648.44	5.18	285.67	8.08
15	626.33	3.33	280.33	4.37	661.44	17.99	250.22	16.69	674.00	7.02	308.56	7.78
16	651.22	7.31	307.89	8.39	685.00	16.90	278.00	20.28	694.89	7.13	336.56	11.28
17	677.67	10.73	340.11	12.58	699.89	13.88	308.00	25.70	714.89	5.00	367.67	11.02
18	702.11	11.00	372.78	14.79	716.33	8.29	344.89	11.51	732.22	4.68	392.56	10.01
19	722.33	8.67	397.89	11.48	726.56	7.27	367.33	12.73	749.78	6.19	419.22	7.37
20	742.56	4.44	423.89	1.02	738.78	1.50	392.11	5.59	775.78	3.29	457.67	5.21

5. Supplement 5

In order to estimate the accuracy of the methodology used for spectral reflection, preliminary tests were performed with illuminated area of inner reflector for spectrometry analyses (R.IA) subsampling on 3 ventral body photophores, one from a different specimen Between subsamples, photophore position was dislocated from under the stereo microscope objective and repositioned. All spectral measurements were made from the highest reflection area.

Variation of light reflection intensity and spectra was observed between subsamples for all photophores testes (Figure 62). Variation of spectra and intensity confirms that subsamples are not biased or repeated. Each photophore has different reflection spectra but variation of is low (up to 7.48 nm) between subsamples (Table 4). Variations of λmax up to 2 nm are assumed as noise from readings of spectrometer sensor. Low error between subsamples confirms the accuracy methodology is adequate to allow one measurement to be representative of each photophore, which validates the results on Chapter 5.

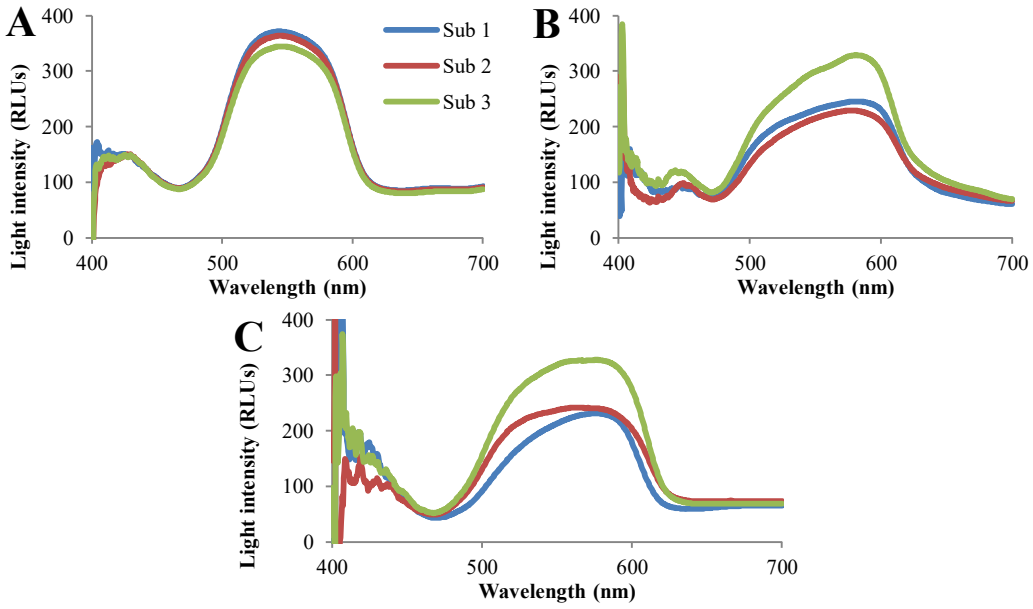

Figure 62 – Reflection spectra of subsamples for each tested *D. watasei*'s inner reflector of ventral body photophore: A) Photophore 1; B) Photophore 2; C) Photophore 3. Sub= Subsample. RLU= Relative light units.

Table 4 – Average and standard deviation of light reflection λmax spectra and intensity per subsamples of tested *D. watasei*'s inner reflector of photophores. LI= Light intensity; RLUs= Relative light units; Wl= wavelength.

	Photophore 1		Photophore 2		Photophore 3	
	LI (RLUs)	Wl (nm)	LI (RLUs)	Wl (nm)	LI (RLUs)	Wl (nm)
Subsample 1	372	484	232	516	245	521
Subsample 2	364	486	242	504	229	518
Subsample 3	345	485	328	517	329	521
Average	360	485	267	512	268	520
Standard deviation	13.87	1.02	52.84	7.48	53.37	1.88

6. Supplement 6

Table 5 - Measured and calculated parameters for estimation of reflection angles of platelets of *D. watasei*'s inner reflector of VO1 ventral body photophores observed under SEM microscopy. RS= Inner reflector surface angle; Pl= Platelet angle; RS-Pl= Inner reflector surface-platelet angle; P-RS= Photocytes– inner reflector surface angle; P-Pl= Photocytes-platelet angle; Min= Minimum; Max= Maximum; Av= Average; S.D.= Standard deviation.

SA		Photophore 1					Photophore 2			
		RS (º)	Pl (º)	RS-Pl (º)	P-RS (º)	P-Pl (º)	RS (º)	Pl (º)	RS-Pl (º)	P-Pl (º)
1	Min	50.58	36.87	8.04	51	93.37	44.13	31.23	7.34	87.73
	Max	57.94	47.39	18.56	60.8	103.89	58.00	42.00	18.12	98.51
	Av	55.43	42.38	13.05	56.5	98.88	49.35	35.88	13.47	92.38
	S.D.	4.20	3.70	3.70	5.02	3.70	7.54	3.47	3.47	3.47
2	Min	56.77	47.45	3.86	23.6	77.36	55.11	49.68	0.92	79.59
	Max	60.38	55.01	11.42	35.6	84.92	63.44	58.30	9.54	88.21
	Av	58.87	51.68	7.19	29.9	81.59	59.22	53.58	5.64	83.49
	S.D.	1.88	2.66	2.66	6.01	2.66	4.16	2.88	2.88	2.88
3	Min	81.93	77.56	-1.66	12.6	94.49	79.96	72.78	1.38	89.71
	Max	88.59	87.61	8.39	21.3	104.54	90.42	83.30	11.90	100.23
	Av	85.95	83.43	2.52	16.9	100.36	84.68	77.15	7.53	94.08
	S.D.	3.54	3.63	3.63	4.38	3.63	5.31	4.01	4.01	4.01
4	Min	50.79	53.55	-7.11	40.2	97.38	49.21	51.34	-3.27	95.17
	Max	69.10	68.96	8.30	48.3	112.80	57.45	57.75	3.14	101.58
	Av	61.85	61.17	0.68	43.8	105.01	54.48	55.36	-0.89	99.20
	S.D.	9.73	5.77	5.77	4.08	5.77	4.57	2.01	2.01	2.01
5	Min	49.52	43.15	-0.84	60.7	107.14	37.22	34.42	-1.28	98.40
	Max	50.88	50.91	6.92	67.4	114.89	45.49	43.03	7.32	107.01
	Av	50.07	46.26	3.81	64	110.24	41.74	37.29	4.46	101.27
	S.D.	0.72	2.71	2.71	3.35	2.71	4.19	3.26	3.26	3.26
6	Min	37.10	31.22	2.94	78.8	113.14	35.22	10.49	12.30	92.41
	Max	41.58	36.47	8.19	84.9	118.39	41.12	25.77	27.58	107.69
	Av	39.41	33.78	5.63	81.9	115.70	38.07	17.77	20.30	99.70
	S.D.	2.24	1.62	1.62	3.05	1.62	2.96	5.13	5.13	5.13

7. Supplement 7

Table 6 – Cumulative and λmax reflection intensity, λmax reflection spectra and FWHM of reflection spectra at 50° of photophores from SAs of inner reflector of *D. watasei* VO1 ventral body photophores. RLUs= Relative light units; R. ISA= Sample area; S.D.= Standard deviation; λmax= Wavelength maximum; FWHM= Full width at half maximum.

Cumulative intensity (RLUs)			
R.ISA	Photophore 1	Photophore 2	Photophore 3
1	279138.10	704705.60	290084.40
2	562853.60	410012.70	243999.24
3	64489.13	57196.47	78195.62
4	50089.94	43968.61	54126.60
5	704319.50	410941.70	498775.50
6	507283.40	437453.60	365890.70
Average	3.61E+05	3.44E+05	2.55E+05
S. D.	2.73E+05	2.53E+05	1.70E+05

λmax light intensity (RLUs)			
R.ISA	Photophore 1	Photophore 2	Photophore 3
1	511	1070	465
2	812	600	385
3	107	88	138
4	80	65	93
5	906	568	740
6	696	618	575
Average	518.76	501.50	399.11
S. D.	354.91	377.48	250.42

λmax wavelength (nm)			
R.ISA	Photophore 1	Photophore 2	Photophore 3
1	475	510	476
2	546	527	514
3	580	539	566
4	728	548	613
5	568	530	535
6	476	512	475
Average	562.17	527.67	529.83
S. D.	92.88	14.87	53.68

FWHM (nm)			
R.ISA	Photophore 1	Photophore 2	Photophore 3
1	112	132	110
2	194	156	142
3	234	184	190
4	312	198	244
5	280	170	174
6	98	134	110
Average	205.00	162.33	161.67
S. D.	87.33	26.70	51.88

8. Supplement 8

Table 7 - λmax reflection intensity and spectra, FWHM of reflection from central area of *D. watasei* body photophores inner reflector under tilting angles of 10º, 20º and 30º. RLUs= Relative light units; S.D.= Standard deviation; λmax= Wavelength maximum; FWHM= Full width at half maximum.

λmax light intensity (RLUs)			
Tilt angle (º)	Photophore 1	Photophore 2	Photophore 3
10	57.06	155.8	172.06
20	63.43	166.84	166.96
30	69.36	263.4	109.16
Average	63.283	195.347	149.393
S.D.	6.151	59.194	34.936

λmax wavelength (nm)			
Tilt angle (º)	Photophore 1	Photophore 2	Photophore 3
10	604	571	619
20	580	540	597
30	578	528	567
Average	587	546	594
S.D.	14.51	21.98	25.94

FWHM (nm)			
Tilt angle (º)	Photophore 1	Photophore 2	Photophore 3
10	208	217	211
20	186	165	199
30	194	145	155
Average	196	176	189
S.D.	11.22	37.57	29.48